NMR Studies on supramolecular aggregates in solution and the solid state

Dissertation zur Erlangung des Grades

Doktor der Naturwissenschaften

am Fachbereich Chemie und Pharmazie
der Johannes Gutenberg-Universität Mainz
vorgelegt von

Chulsoon Moon
geboren in Busan, Republic of Korea

Mainz 2008

Tag der mündlichen Prüfung: 13.02.2008

Contents

Abbreviations and Acronyms

ADC	*a*nalogue *d*igital *c*onverter
BABA	*ba*ck-to-*ba*ck
BPP-LED	*bi*polar *p*usle *l*ongitudinal *e*ddy current *d*elay
Bu	1-n-*bu*tyl-5-phenyl-barbituric acid
CIS	*c*omplexation *i*nduced *s*hifts
COSY	*co*rrelation *s*pectroscop*y*
CSA	*c*hemical *s*hift *a*nisotropy
CP	*c*ross-*p*olarization
CW	*c*ontinuous-*w*ave
DAC	2,6-*di*a*c*etamidopyridine
DAP	2,6-*di*a*m*ino*p*yridine
DD	*d*ipolar *d*ecoupling
DFT	*d*ensity *f*unctional *t*heory
DLS	*d*ynamic *l*ight *s*cattering
DOSY	*d*iffusion *o*rdered *s*pectroscop*y*
DQ	*d*ouble-*q*uantum
DQC	*d*ouble-*q*uantum *c*oherence
DSC	*d*ifferential *s*canning *c*alorimetry
FID	*f*ree *i*nduction *d*ecay
FT	*f*ourier *t*ransformation
FWHH	*f*ull *w*idth at *h*alf *h*eight
HETCOR	*h*eteronuclear *c*orrelation
HMQC	*h*eteronuclear *m*ultiple-*q*uantum
HMBC	*h*eteronuclear *m*ultiple-*b*ond
INEPT	*i*nsensitive *n*uclei *e*nhanced by *p*olarization *t*ransfer
LAB	*lab*oratory frame
LC	*l*iquid *c*hromatography
ledbpgp2s	led with bipolar gradient pusle pair, 2 spoil gradients
MAS	*m*agic-*a*ngle *s*pinning
MQ	*m*ultiple-*q*uantum
MQC	*m*ultiple-*q*uantum *c*oherence
NiDMe	1,3-*di*m*e*thyl-5-(4-*ni*trophenyl)-barbituric acid
NiBu	1-*n*-*bu*tyl-5-(4-*ni*trophenyl)-barbituric acid
NICS	*n*uclear *i*ndependent *c*hemical *s*hift

NMR	*n*uclear *m*agnetic *r*esonance
NOESY	*n*uclear *o*verhauser *e*nhancement *s*pectroscop*y*
PAS	*p*rincipal *a*xes *s*ystem
PFG	*p*ulse *f*ield *g*radient
PS	*p*roton *s*ponge
REDOR	*r*otational *e*cho, *d*ouble *r*esonance
REPT	*r*ecoupled *p*olarization *t*ransfer
RF	*r*adio *f*requency
SB	*s*ide*b*and(s)
SQ	*s*ingle-*q*uantum
TOCSY	*to*tal *c*orrelation *s*pectroscop*y*
TPPM	*t*wo-*p*ulse *p*hase-*m*odulated
ZQC	*z*ero *q*uantum *c*oherence

Chapter 1

Introduction

The concept of supramolecular chemistry was introduced in 1978 by Jean-Marie Lehn [Lehn 02] and since then it has been developed into a rapidly growing and highly interdisciplinary field of science covering the chemical, physical, and biological features of the chemical species. Different from molecular chemistry which has established its power over the covalent bond, supramolecular chemistry aims at developing highly complex chemical systems from components interacting via non-covalent intermolecular forces such as hydrogen bonding, electrostatic, and donor-acceptor interactions [Steed 00]. Such non-covalent molecular interactions form the basis of highly specific processes such as recognition, transport, and regulation, etc. that occur in biological and chemical systems. Especially, recognition directed self-assembly is of major interest in supramolecular design and engineering. To gain deeper insight into the spatial arrangement of their components and the nature of the intermolecular bonds that hold these components together, many powerful physical methods (IR, UV, X-ray diffraction, mass spectrometry, NMR, etc.) are available. Quite often, supramoleuclar structures suffer from a lack of long-range order and crystallinity due to the comparatively weak interactions that determine their structure, e.g hydrogen bonding and pi-stacking. Thus, solid state NMR techniques play a major role to understand molecular structure and dynamics in amorphous solid systems, not requiring long-range order to provide structural information.

One of the characteristic features of NMR spectroscopy is based on its high selectivity. Thus, it is desirable to exploit this technique for studying structure and dynamics of large supramolecular systems without isotopic enrichment. The observed resonance frequencies are not only isotope specific but also influenced by local fields, in particular by the distribution of electron density around the investigated nucleus.

For example, in principle, ^{1}H NMR spectroscopy has the advantage of directly probing the hydrogen bonded protons themselves. However, ^{1}H NMR spectroscopy of rigid solids is complicated by the homonuclear ^{1}H -^{1}H dipolar interactions, leading to substantial homogeneous broadening of the resonances. A number of ingenious methods have been developed to gain sufficient spectral resolution in solid state NMR. Among them, by the magic-angle spinning (MAS) technique [Andrew 58, Lowe 59], where the sample is rapidly rotated around an axis inclined at the magic angle (54.7°), mimicking solution state NMR (where the anisotropic interactions are averaged to zero), sufficient line-narrowing can be achieved.

Over the past decade, much progress has been made in the area of high resolution magic-angle spinning (MAS) solid state NMR spectroscopy and in recent years, noncovalent interactions in supramolecular systems have been studied by a variety of high-resolution ^{1}H and heteronuclear solid state NMR techniques [Schnell 01, Brown 07]. The resolved isotropic chemical shift constitutes a major source for the elucidation of structure and dynamics in solid materials. In particular, protons involved in hydrogen bonding, which has been described as the "masterkey interaction in supramolecular chemistry", typically exhibit well-resolved ^{1}H chemical shifts, mainly between 8 and 20 ppm, thereby providing valuable structural information. Moreover, when studying supramolecular host-guest complexes, changes of the observed chemical shifts of incorporated guest molecules provide significant evidence for an inclusion by possible hosts. Depending on the local geometry of the host, different induced shielding effects by e.g. aromatic moieties within the host may affect the guest molecules, and possibly allow for molecular recognition studies. In that respect, the recently introduced concept of nucleus-independent chemical shift (NICS) maps offer rather qualitative means to both facilitate an interpretation of experimental chemical shifts and locate guest molecules within the respective host.

Barbituric acids are well known for forming strongly hydrogen-bonded complexes with a variety of adenine derivatives which is one of the two purine nucleobases used in forming nucleotides of the nucleic acids DNA and RNA. The prototropic tautomerism of this material facilitates an adjustment to complementary bases containing a DDA(A = hydrogen bond acceptor site, D = hydrogen bond donor site) or ADA sequences, thereby yielding strongly hydrogen-bonded complexes. In this contribution Chapter 4 deals with the solid-state structure of the enolizable chromophor, **1-n-butyl-5-(4-nitrophenyl)-barbituric acid (NiBu)** that features adjustable hydrogen-bonding properties. Furthermore, the molecular assemblies

of **NiBu** with three different strength of bases (**Proton sponge**, adenine mimetic **2,6-diaminopyridine (DAP)** and **2,6-diacetamidopyridine (DAC)**) are studied in Chapter 4.

Diffusion NMR spectroscopy gives information over such interactions and has become the method of choice for measuring the diffusion coefficient, thereby reflecting the effective size and shape of a molecular species. Chapter 5 deals with the investigation of supramolecular aggregates in solution by means of DOSY NMR techniques. The underlying principles of DOSY NMR experiment are discussed briefly and more importantly two applications demonstrating the potential of this method are focused on.

Calix[n]arenes have gained a rather prominent position, both as host materials and as platforms to design specific receptors. In particular, tetra urea calix[4]arenes, substituted on their wide rim by four urea residues, form dimeric capsules in aprotic, apolar solvents that are stabilized by a seam of hydrogen bonds between the urea functions. This dimerization may be used to build up linear polymers from building blocks, in which two tetraurea units are covalently linked via their narrow rims. Though the dynamic nature and reversibility of capture, storage and preferably transport of guest species in their respective host materials has been comprehensively studied in solution, rather little is known about dimeric compounds in solids. In this respect, several different capsular contents(benzene, benzene-d_6, fluorobenzene, fluorobenzene-d_5, 1,4-difluorobenzene, and cobaltocenium) of tetra urea calix[4]arenes are studied by solid state NMR spectroscopy. In the solid state, the study of the interaction between tetra urea calix[4]arenes and guest is simplified by the fact that the guests molecule remains complexed and positioned within the cavity, thus allowing a more direct investigation of the host-guest interactions. This will be discussed in Chapter 6.

Chapter 2

Fundamentals in NMR spectroscopy

The first detection of radio frequency signals generated by the nuclei of atoms in bulk materials was done in 1945, by Bloch and his colleagues [Bloch 46] in California, and by Purcell and his colleagues [Purcell 46] in Harvard independently. For their discovery, Bloch and Purcell were awarded the Nobel Prize for Physics in 1952. Since that time, the development of NMR techniques has been rapid. The first commercial high-resolution proton NMR spectrometer was produced in 1953. In the years since then through the enormous advances in NMR theory and the instrumental developments, nuclear magnetic resonance (NMR) spectroscopy had become recognized as one of the most important developing tools for chemical structural analysis and dynamics of a variety of materials. In numerous fields, NMR finds applications (chemistry, physics, biology, medicine, materials science and geology) [Breitmaier 93, Cavanagh 96, Evans 95, Emsley 85, Brown 01, Percec 02].

Especially, nowadays high resolution liquid state NMR is of unique importance in organic chemistry to determine the structures of molecules. Based on the information from ^{1}H and ^{13}C spectra in liquid state, and through various 2D techniques such as COSY, TOCSY, NOESY, HMQC, and HMBC, the connectivities between proton and carbon can be assigned in organic materials [Claridge 99] . Meanwhile in the last thirty years, solid state NMR spectroscopy has advanced rapidly and is being used to study the structure and dynamics of a variety of solid systems ranging from catalysis and glasses to polymers and proteins. It was rarely possible to obtain sufficient resolution in , e.g., proton NMR spectra of complex solid materials, until in the 1950s, Andrew and Lowe introduced a technique where the sample is rapidly spun about an axis tilted with respect to the static magnetic field by the magic angle 54.7 $^{\circ}$ [Andrew 58, Lowe 59].

Different kinds of chemical and physical studies can be performed and unique

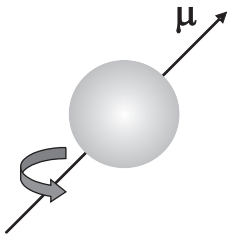

Figure 2.1: *A nucleus carries charge and when spinning possesses a magnetic moment, μ.*

anisotropic nuclear spin interactions, which vanish in solution- state can be obtained from solids. Thus chemical shift anisotropy, dipole-dipole coupling, and quadrupole coupling can be used to give quantitative information on molecular structure, conformation and dynamics. In the last decades, numerous solid-state NMR techniques have been developed and a lot of research are still dedicated to the improvement of existing methods and the development of entirely new ones. This is due to the overload of information available from solid-state NMR spectra, out of which the relevant or interesting pieces are often difficult to extract.

There are many NMR textbooks and reviews which should be consulted for greater detail of NMR [Abragam 61, Slichter 96, Mehring 83]. In this Chapter the brief underlying principles of NMR, which are essential for the understanding of the NMR methods used in this study will be described.

2.1 NMR Phenomenon and Interactions

The nuclei of all atoms may be characterized by a nuclear spin quantum number, $I \geq 1/2$. The property of nuclear spin is fundamental to the NMR phenomenon. Each nucleus with a non-zero spin possesses a magnetic moment μ, which is given by

$$\mu = \gamma \hbar I \tag{2.1}$$

where $\hbar = h/2\pi$ is Planck's constant, and the γ is the *magnetogyric ratio* which is constant for any given nuclide and may be viewed as a measure of how strongly magnetic this is. The behavior of a spin system is well described quantum mechanically by the time-dependent Schrödinger equation

$$\frac{\mathrm{d}}{\mathrm{d}t}|\Psi(t)\rangle = \frac{-i}{\hbar}\hat{\mathcal{H}}|\Psi(t)\rangle\,. \tag{2.2}$$

The evolution of the state $|\Psi(t)\rangle$ is determined by the Hamilton operator $\hat{\mathcal{H}}$ which describes the energy of the system. For a nucleus in a static magnetic field the majority of the spin interactions can be expressed in terms of the nuclear spin Hamiltonian

$$\begin{aligned} \hat{\mathcal{H}} &= \hat{\mathcal{H}}_{external} + \hat{\mathcal{H}}_{internal} && (2.3) \\ &= \hat{\mathcal{H}}_z + \hat{\mathcal{H}}_{rf} + \hat{\mathcal{H}}_Q + \hat{\mathcal{H}}_{DD} + \hat{\mathcal{H}}_{cs} + \hat{\mathcal{H}}_J && (2.4) \end{aligned}$$

where $\hat{\mathcal{H}}_z$ is the Zeeman interaction with the external magnetic field, and $\hat{\mathcal{H}}_{rf}$ is the radio frequency interaction, which are both externally applied. $\hat{\mathcal{H}}_{DD}$ is the direct dipole-dipole coupling between spins, $\hat{\mathcal{H}}_{cs}$ the chemical shift interaction, $\hat{\mathcal{H}}_Q$ the quadrupolar coupling and $\hat{\mathcal{H}}_J$ the J-coupling, which is usually an isotropic indirect spin-spin coupling via electrons. All of these are internal spin interactions and therefore intrinsic to the material being studied. It is interesting to note that for NMR the external interactions are usually much larger than the internal interactions, or the nuclear spins are more strongly coupled to the external apparatus than to their own molecular environment. This is in contrast to most other forms of spectroscopy, where the behavior of the system is set by the molecular structure itself and the information is gained by a relatively weak external perturbation [Levitt 01].

2.1.1 Zeeman-Interactions

The strongest interaction, and inherently most important to NMR, is the Zeeman interaction which is the interaction of nuclear spin I with an external static magnetic field B_0 for nuclei with spin quantum number $I \neq 0$. The Zeemann interaction causes a splitting of the degenerated $(2I+1)$ energy levels, which are defined by the magnetic nuclear spin quantum number $m_I = -I, -I+1, \cdots +I$. For a spin-1/2 nucleus such as the proton, there are 2 possible spin states denoted +1/2 and -1/2, whilst for $I = 1$, for example deuterium, the states are +1, 0 and -1 (Fig. 2.2) and so on.

If the external magnetic field is oriented along the z-axis, only the z-component of the corresponding Hamiltonian deviates from zero. The break down of this degeneracy enables the absorption and emission of energy in the form of electromagnetic radiation.

$$\hat{\mathcal{H}}_Z = -\gamma\hbar\hat{I}_Z B_0 \qquad (2.5)$$

The *eigenvalues* of $\hat{\mathcal{H}}$ are the energies associated with the different possible states

of the spin. The eigenvalues are obtained by operating $\hat{\mathcal{H}}$ on the spin wave functions:

$$\hat{\mathcal{H}}|I,m\rangle = E_{I,m}|I,m\rangle \tag{2.6}$$

where $E_{I,m}$ is the energy of the eigenstate $|I,m\rangle$. The quantum number m can take $2I+1$ values. From solving the Schrödinger equation with the Hamiltonian above, one obtains the energy levels

$$E_m = -m\hbar\gamma B_0 \tag{2.7}$$

For $I = 1/2$ the energy splitting between the two level is ΔE = -$\gamma\hbar B_0$ = $\hbar\omega_L$, where ω_L is the so-called Larmor frequency. For example, a proton in a 7T magnetic field has a Larmor frequency of 300MHz, whereas in a 16.4T magnetic it has 700MHz.

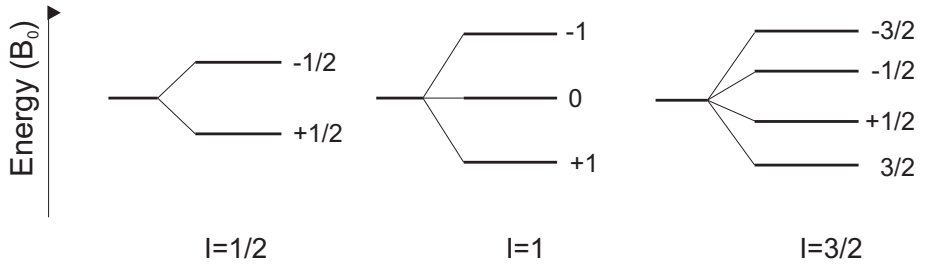

Figure 2.2: *Energy level diagram showing the breakdown of nuclear spin degeneracy upon the application of a magnetic field*

In the case of a strong external magnetic field B_0, the Zeeman interaction by far exceeds most other interactions listed in Eq.(2.4), i.e. $\|H_{external}\| \gg \|H_{internal}\|$. This allows the weaker internal NMR interactions to be treated as perturbations of the strong Zeeman interactions. The secular approximation leads to some components of the internal spin interactions being masked by Zeeman interactions, thus simplifying the internal interaction Hamiltonian, $\hat{\mathcal{H}}_{internal}$.

2.1.2 The effect of the radio frequency field (B_1)

One of the reasons for the great success of Fourier-transform (FT) NMR spectroscopy lies in the fact, that radio frequency (RF) pulses affect the spin system in a well-defined manner, which in turn allows for a defined manipulation of the system. The radio frequency corresponds to the transition frequency between Zeeman energy levels. For the description of pulsed NMR, a transition into a rotating frame of reference, which

rotates with the Larmor frequency ω_L around B_0 is convenient. A B_1 field oscillating with ω_L, which is applied perpendicular to the B_0 field, is static in the rotating frame.

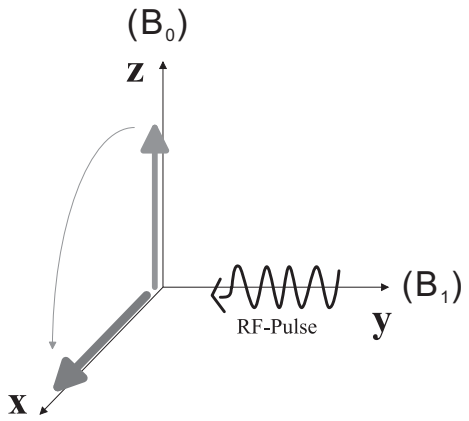

Figure 2.3: *The vector model showing the effect of 90 °y pulse*

The applied B_1 makes the spins precess around the B_1 direction. Hence, in the rotating frame, the effect of a pulse of the length t is a rotation of the initial z-magnetization in the xy-plane at the Larmor frequency. The vector diagram which explains the effect of a 90°_y pulse is presented in Fig. 2.3. Strictly speaking, the vector model only applies to uncoupled spins, and it is only quantum mechanics which can give complete understanding of pulsed-NMR. However, even with its limitations, the vector model gives us an excellent start toward understanding RF pulses. For a more complete description the reader is referred to a number of excellent text books explaining quantum mechanical description in great detail, for example [Slichter 96, Schmidt-Rohr 94].

2.1.3 Quadrupolar interaction

Nuclei with a spin $I \geq 1$ exhibit a nuclear electric moment, which interacts with the local electric field gradient generated by the surrounding electron clouds in the molecules. Thus, a nucleus with a spin greater than 1/2 not only interacts with the applied magnetic field and all local magnetic fields, but also with any electric field gradients present at the nucleus. This interaction affects the nuclear spins energy levels. The basic form of the quadrupole Hamiltonian describing the interaction between a nuclear electric quadrupole moment and an electric field gradient is

$$\hat{\mathcal{H}}_Q = \frac{eQ}{2I(2I-1)\hbar}\hat{I}\cdot V\cdot\hat{I} \tag{2.8}$$

for a spin I, where V is the electric field gradient at the nucleus, $\hat{I}$ is the nuclear spin vector and Q is the nuclear quadrupole moment. In this thesis, in case of deuteron (^{2}H : $I = 1$) the quadrupolar splitting is around 125kHz, which is sufficiently lower than the Larmor frequency so that the *secular* approximation is (which is a first-order perturbation theory) remains valid. The NMR spectra of deuteron are however dominated by the quadrupolar interactions. If θ and ϕ are the polar orientation of the B_0-field with respect to a defined principle axis system (PAS) of the quadrupolar coupling tensor, the quadrupolar frequency is given by

$$\omega = \omega_0 \pm \delta(3\cos^2\theta - 1 - \eta_Q \sin^2\theta \cos 2\phi) \tag{2.9}$$

Here, $\delta = \frac{3e^2qQ}{4\hbar}$, where $\frac{e^2qQ}{\hbar}$ is the quadrupole coupling constant, and ω_0 is the Zeeman frequency. The quantity η is the asymmetry parameter and is usually zero for C-D bonds, meaning that the electric field gradient tensor is axially symmetric. In addition, an axis of the electric field gradient tensor is along the C-D bond direction. The polar angles θ and ϕ specify the orientation of the magnetic field with respect to the principal axis system of th electric field gradient tensor. If η is taken zero, the NMR frequency of the two transitions are given by:

$$\omega = \omega_0 \pm \delta(3\cos^2\theta - 1) \tag{2.10}$$

This means that the frequencies of the NMR lines depend on the angle θ that the C-D bond makes with the external magnetic field. In the solid state, where fast motions are absent, the orientation dependence of the quadrupolar coupling leads to the well known Pake-pattern [Pake 48] as it is shown in Fig. 2.4.

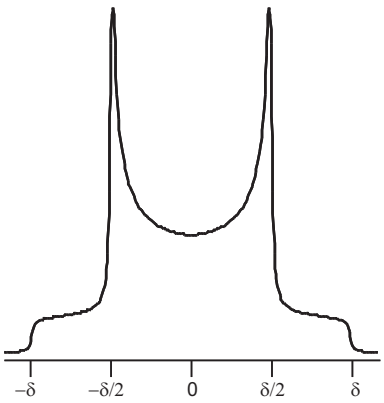

Figure 2.4: *Pake pattern.*

Molecular motion leads to a characteristic narrowing of the Pake-pattern. This

is commonly utilized in ^{2}H NMR spectroscopy, where a line shape analysis of the motionally averaged pattern yields information on the geometry and the timescale of dynamic processes [Macho 01].

2.1.4 Chemical shielding

Much of the chemical information in NMR spectra arises from chemical shifts due to the local magnetic fields generated at the nucleus by the circulation of the surrounding electrons induced by the applied field. This has lead to NMR becoming one of the most important and powerful structure elucidation techniques especially in organic synthesis field. If the resulting magnetic fields oppose the applied field (B_0) the effect is to shield the nucleus from it, and vice versa. The nucleus then experiences an effective field given by

$$B_{eff} = B_0(1-\sigma) \tag{2.11}$$

where σ, the nuclear magnetic shielding tensor and the chemical shift Hamiltonian is given by

$$\hat{H}_{CS} = \gamma\hbar\hat{I}\cdot\sigma\cdot B_0 = \gamma\hbar(\hat{I}_x\sigma_{xx} + \hat{I}_y\sigma_{yy} + \hat{I}_z\sigma_{zz})B_0 \tag{2.12}$$

Only the last (the symmetric part) of the shielding tensor σ turns out to affect the NMR spectrum within the *secular approximation*. Neglecting the antisymmetric part of the chemical shielding tensor and transforming to its principal axis system yields σ_{iso}(isotropic value), the anisotropy Δ_{CS} and the asymmetry η_{CS} [Duer 04].

In rapidly tumbling liquid state, the isotropic average is observed. However, in solids, where fast isotropic motions are absent, the orientation dependence of the chemical shift anisotropy (CSA) generally lead to a significant broadening of resonance lines. The CSA depends on the orientation of the PAS with respect to the laboratory frame. Since no CSA measurements were done in this thesis it will not be discussed further.

The isotropic part of σ_{iso} is independent on the orientation of the sample with respect to the magnetic field. It leads to a site specific correction of the Larmor frequency for each nucleus in a molecule, which is called the chemical shift δ and commonly given in *ppm* of the Larmor frequency of the observed nucleus relative to the Larmor frequency of a suitable reference compound :

$$\delta[ppm] = \frac{\nu - \nu_{ref}}{\nu_{ref}} \cdot 10^6 \tag{2.13}$$

The great advantage of the *ppm*-scale is its independence of the strength of the external magnetic field B_0, which greatly simplified the comparison between spectra measured at different spectrometers.

2.1.5 Dipole-Dipole Interaction

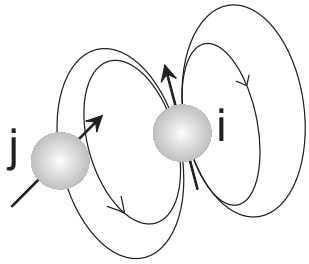

Figure 2.5: *The dipole-dipole interaction.*

The presence of neighboring magnetic nuclei alters the local field and therefore the energy of a nucleus. The dipole-dipole coupling is an anisotropic direct spin-spin interaction through space without involving the electron clouds. It is present between all types of spins with $I > 0$. Since each nuclear spin is magnetic, it generates a magnetic field, looping around in the surrounding space, according to the direction of the spin magnetic moment. Then a second nuclear spin interacts with this magnetic field. The interaction between the spins is mutual. The first nuclear spin also experiences the field generated by the second nuclear spin. The dipole-dipole coupling may be either intramolecular or intermolecular. In the *secular* approximation the Hamiltonian for a homonuclear spin-pair $\mathbf{I}, \mathbf{J}$ reads as

$$\hat{H}^{IJ}_{D,homo} = -\frac{\mu_0 \hbar \gamma^2}{4\pi r^3} \cdot (3\cos^2\theta - 1)(3\hat{I}_z\hat{J}_z - \hat{I}\cdot\hat{J}) \tag{2.14}$$

The dipole-dipole coupling depends on both, the distance between the two spins involved as well as the angle between the internuclear vector and the B_0 field.

Since the Larmor frequencies of a heteronuclear spin pair differ significantly, the polarization exchange tends to zero and the dipolar Hamiltonian can be reduced to

$$\hat{H}^{IJ}_{D,hetero} = -\frac{\mu_0 \hbar \gamma_j \gamma_i}{2\pi r^3} \cdot (3\cos^2\theta - 1)(\hat{I}_z\hat{J}_z) \tag{2.15}$$

The γ is a characteristic value of the isotope, which is about four times larger for ^{1}H than for ^{13}C . Thus, the homonuclear ^{1}H -^{1}H diolar coupling constant is about four times larger than the heteronuclear ^{1}H -^{13}C dipolar coupling constant.

In general, motion reduces dipolar couplings. This is well known from liquids, where all dipole-dipole couplings are averaged due to an isotropic random motion of the molecules, which covers all possible angles θ. This corresponds to an interaction of the space part of the dipolar Hamiltonian over a full sphere which is zero.

But in anisotropic solids, the strong dependency on the distance of the dipolar coupling constant gives valuable information on proximities between nuclei.

2.1.6 *J*-coupling

A coupling between nuclei which does not average to zero in liquids is the indirect spin-spin coupling or *J* coupling through the involvement of electrons. Indeed, important information on connectivity within a molecule is carried by the symmetrical multiplet splittings due to *J* coupling of nearby nonequivalent nuclear spins, thus providing a direct spectral manifestation of the chemical bonds. *J* coupling represents the second great link between NMR and chemistry next to chemical shifts. The corresponding Hamiltonian of the *J* coupling interaction between spins I_i and I_j on the same molecule is

$$\hat{H}_{jk}^{J,full} = 2\pi \hat{I}_j \cdot J_{jk} \cdot \hat{I}_k \tag{2.16}$$

where J_{jk} is the *J*-coupling tensor, a 3×3 real matrix. The factor of 2π appears because the *J*-coupling is conveniently quoted in units of Hz. In anisotropic liquids and solids, the anisotropic part of the *J* coupling survives, however, it is usually much smaller than the direct dipole-dipole coupling, and is often ignored [Levitt 01].

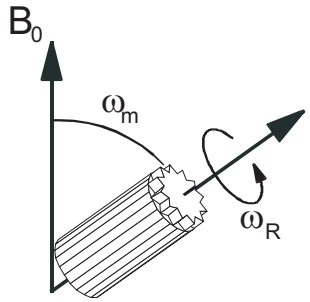

Figure 2.6: *Magic Angle Spinning: MAS*

2.2 Magic Angle spinning

In solid state NMR, generally most of the samples are powder state. Samples are consist of many crystallites with random orientations. The nuclear spin interactions which affect solid-state NMR spectra such as chemical shielding, dipole-dipole coupling and quadrupole coupling, are all dependent on the crystallite orientation. As a result of this, the NMR spectrum of a powder sample contains broad lines, or powder patterns, as all the different molecular orientations present in the sample give rise to different spectral frequencies. Hence, it is necessary in solid-state NMR to apply techniques to achieve high resolution in spectra. In solution NMR spectra, effects of chemical shift anisotropy, dipolar coupling, quadrupolar coupling are rarely observed. This is because the rapid isotropic tumbling of the molecules in a solution averages the molecular orientation dependence of the transition frequencies to zero. In the late 1950s, Andrew and Lowe introduced a technique where the sample is rapidly spun about an axis inclined at an angle of 54.7° with respect to the magnetic field B_0, so that the orientation dependence is averaged out: $(3\cos^2\theta - 1) = 0$ [Andrew 58, Lowe 59]. In the case of dipole-dipole coupling this process is called dipolar decoupling. However, complete averaging of an anisotropic interaction to zero is only achieved when the sample is spun with a frequency much greater than the characteristic interaction frequency. This is mechanically quite demanding. For this reason considerable effort has been taken to achieve the highest possible MAS frequency. Currently commercially available MAS hardware is capable of spinning at 70kHz utilizing 1.3mm outer diameter rotor. According to Maricq and Waugh, linebroadening effects can be divided into homogeneous and inhomogeneous ones. Inhomogeneous line broadening is caused by the orientational dependence of anisotropic interactions, and is simply a superposition of resonance lines originating from different orientations of the molecules, where the broadening is refocused over a rotor period. This is the case for CSA, first

order quadrupolar couplings and dipole-dipole coupling of isolated spin pairs. Homogeneous line broadening arises from dipole-dipole coupling between multiple spins. It occurs in particular for protons, as they have high natural abundance and a high gyromagnetic ratio. Due to the spin-spin couplings the energy levels of single transitions are no longer degenerate, but split into a multitude of levels that prevents the complete refocusing of the signal after one rotor period. Since the homonuclear dipole-dipole coupling among protons can reach up to 100kHz in solids, resolution in proton spectra usually suffers from homogeneous line broadening even under fast MAS.

At this point it should be mentioned that there exist various multiple-pulse experiments to reduce the linewidth in solid-state spectra. This approach was already introduced 30 years ago by Waugh, Huber and Haeberlen [Waugh 68, Haeberlen 68]. By applying a multiple-pulse sequence (WHH-4), the dipole-dipole interactions are decoupled through the spin part of the dipolar Hamiltonian. There have also been several approaches combining multiple-pulse experiments with MAS. A well known example is the Combined Rotation And Multiple-Pulse Spectroscopy(CRAMPS) experiment [Gerstein 85], applying slow MAS(2-3 kHz). However, in recent years, other methods have been presented that are applicable at faster MAS frequencies, such as frequency-switched and phase-modulated Lee Goldburg, DUMBO and symmetry-based methods. More details about those pulse sequences can be found in references [Vinogradov 99, Vinogradov 00, Brown 01].

2.3 Multiple Quantum Coherence

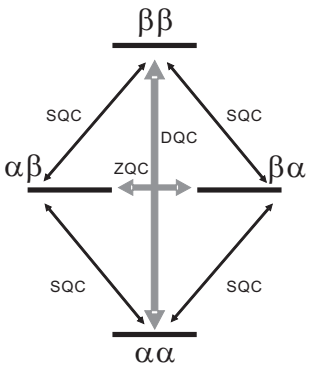

Figure 2.7: *Schematic energy level diagram for a coupled two-spin system, DQC=double-quantum coherence and ZQC=zero-quantum coherence.*

A coherence in NMR describes the relationship between states of different transi-

tions in a system. Coherences can be classified by a coherence order, p, which is an integer taking values 0,$\pm$1, $\pm$2, $\pm$3, ... and is defined by the difference in the magnetic quantum numbers between the two states associated with the transition, ΔM. For a single nucleus (I=1/2) only two energy levels are present and thus only one transition is possible which changes the spin-quantum number by $\Delta M = \pm 1$ and is therefore called a single-quantum coherence(SQC). For a coupled two spin system, four energy levels result. Transitions changing the spin-quantum number by $\Delta M = \pm 1$ again correspond to SQCs, while $\Delta M = \pm 2$ and $\Delta M = 0$, correspond to double quantum (DQC) and zero-quantum (ZQC), respectively. If more than two nuclei are coupled, also higher order coherences can be excited. Any coherence with the order of $\Delta p > 1$ can in principle be termed multiple-quantum coherence (MQC). Since multiple quantum coherences cannot be detected directly, 2D NMR spectroscopy is required to observe the evolution of multiple-quantum coherences in the indirect dimension t_1. Selective excitation of certain multiple quantum coherences has been achieved by using appropriate phase cycling [Marion 83, Marion 89].

Since the first multiple-quantum NMR experiments in the solid-state, many further methods have been developed. Of particular interest are those involving the homonuclear and heteronuclear dipolar coupling, allowing quantification of the dipolar coupling constant and thus internuclear distance determination [Weitekamp 82, Munowitz 87]. In the presence of many coupled spins, double-quantum dipolar Hamiltonian created high multiple-quantum coherences, which are limited only by the size of the spin system [Hughes 04]. One can therefore use this method for spin counting and for determining cluster sizes and the dimensions of coupling networks in solids. The experiment which is used in this work to solve proton-proton proximity is also based on the observation of double-quantum coherences.

Chapter 3

NMR Experiments and Pulse sequences

In this Chapter, the solid-state NMR experiments which are applied throughout this work will be discussed. The discussion begins with the basic single-pulse excitation experiment and the fundamentals of NMR signal detection. This will be followed by the basic concepts of heteronuclear dipole-dipole decouplings techniques and cross-polarization which represent tools that are essential for the observation of nuclei with low natural abundance in solid state NMR. Then the echo techniques which can solve the so-called "dead-time" problem in the solid state will be introduced. Finally after short explanation about basic two-dimensional NMR experiments, the more specific recoupling techniques involving the re-coupling of homo/hetero nuclear dipolar couplings under fast MAS such as ^{1}H -^{1}H DQ 2D and ^{1}H -^{13}C REPT-HSQC experiments will be explained.

With the aid of these multiple-pulse recoupling pulse sequences, it is possible to solve structural as well as dynamical problems in the solid state using non-labeled samples. ^{1}H -^{1}H double quantum (DQ) spectra elucidate ^{1}H -^{1}H proximities up to about 3.5 Å, and two-dimensional ^{1}H -^{13}C spectra benefit from the higher chemical shift resolution of ^{13}C nuclei.

3.1 Single-pulse excitation and signal detection

The most basic experiment in FT-NMR consists of a single 90° pulse (Fig. 3.1). Starting from thermal equilibrium, after applying a 90°_{x} pulse the net magnetization is flipped from the *z* axis to the *y*-axis and precesses in the *xy*-plane with its resonance frequency. This induces an weak oscillating voltage in the RF-coil, which is amplified

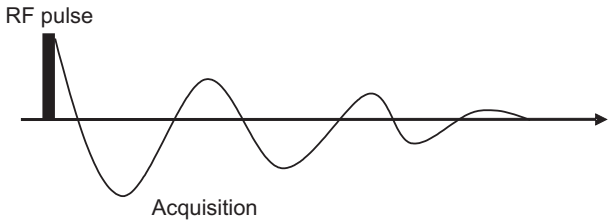

Figure 3.1: *The single pulse experiment*

and later converted into a digital signal (ADC) that can be handled by a computer. As ADCs are usually not fast enough and one is anyhow only interested in the response in the rotating frame, the signal is mixed with a reference frequency (LARMOR frequency) before digitization. To obtain the sign of the rotation it is necessary to also record the phase of the induced signal. In modern NMR spectrometers this is done by mixing the signal with two reference signals having the same frequency but a phase shift of 90 ° (so called quadrature detection). The data points are then collected in complex form.

3.2 ^{1}H decoupling in solid state NMR

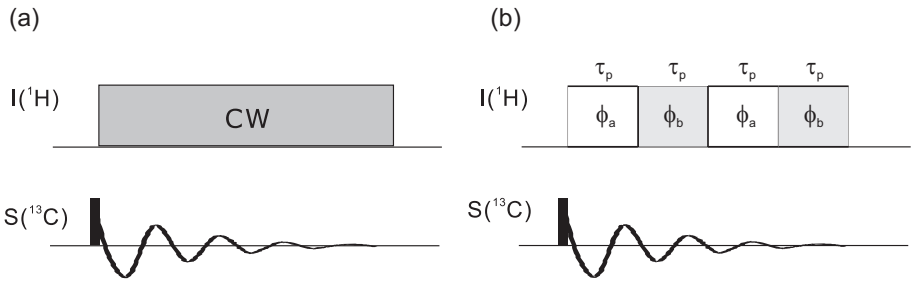

Figure 3.2: *Heteronuclear decoupling sequences. (a) For CW-decoupling the RF-field is simply switched on for the whole decoupling period. (b) For TPPM decoupling scheme the constant RF-field is replaced by a composite pulse train.*

In a NMR experiment one can usually only observe one kind of nucleus at a time, such as ^{1}H , ^{13}C or ^{15}N. Historically, ^{1}H NMR was the first to be exploited widely, and ^{1}H is still the most recorded nucleus. As a result, all nuclei which are not protons are grouped together and called heteronuclei. When dealing with heteronuclei *S* in low natural abundance, homonuclear coupling can safely be neglected. However, even at fast MAS up to 30KHz the heteronuclear dipolar coupling between the *S* nuclei

and high abundance nuclei I (usually ^{1}H) still causes significant line broadening. To overcome this problem various decoupling scheme have been devised and improved [Ernst 03, Khitrin 03]. The most simple method for decoupling is continuous wave (CW) decoupling, where a continuous rf-pulse of fixed phase is applied for the duration of the acquisition of the free induction decay (FID). In order to obtain sufficient decoupling efficiency, a high rf-power is needed, which is not desirable in technical point of view. Therefore improved high-power multiple-pulse decoupling schemes are considered the most efficient methods for solids under fast MAS. The most widely adopted scheme is the two-pulse phase-modulated (TPPM) decoupling sequence and provides significant improvement in both linewidth and intensity under a wide range of experimental conditions [Bennett 95] . It achieves s strongly reduced linewidth as compared to CW, the reasons for which are explained in [Carravetta 00, Gan 97]. TPPM decoupling consists of two pulses each corresponding to a flip angle of about 170°. The phase difference between the two pulse is on the order of 10-50°. Experimentally, the decoupling efficiency depends on the precise setting of these two parameters, which have to be optimized empirically. Several variants of the TPPM decoupling sequence were proposed but none of them offers significant improvement in rigid solids over a large range of experimental parameters. An alternative decoupling scheme is the XiX (X inverse-X) sequence [Detken 02]. XiX decoupling consists of a windowless rf irradiation with a repeat of two pulses of equal width phase-shifted by 180°. For crystalline samples it usually performs a little better, otherwise it is comparable to TPPM, but more sensitive to an imperfect experimental setup.

3.3 Cross Polarization (CP)

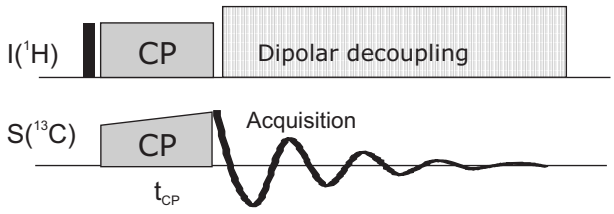

Figure 3.3: *The pulse sequence of cross polarization experiment.*

Observing dilute spins such as ^{13}C and ^{15}N presents a number of problems including

- The low abundance of the nuclei means that the signal-to-ratio is inevitably poor
- The relaxation times of low abundance nuclei tend to be very long. This is because strong homonuclear dipolar interactions which can stimulate relaxation transitions are largely absent. The long relaxation times mean that long gaps must be left between scans and the spectra may take a very long time to collect [Duer 04].

In the cross polarization (CP) method both problems can be solved by deriving the ^{13}C polarization from the more abundant high -γ nuclei such as ^{1}H spins [Pines 72, Pines 73]. The polarization transfer is mediated by the the dipole-dipole interaction. Usually the flip-flop term is suppressed for heteronuclear dipole-dipole interactions. In CP experiment it is reintroduced for a certain time (called contact time), by application of r.f. pulses on I and S spins at the same time. The amplitude of the two contact pulses in the cross-polarization experiment have to be carefully set so as to achieve the Hartmann-Hahn matching condition

$$\gamma_H B_1(^1H) = \gamma_S B_1(S) \tag{3.1}$$

In this simplistic approach, this sets the energy gaps between the respective rotating frame spin states of ^{1}H and S spins to be equal. This condition implies that in their respective rotating frames of reference the protons and carbons precess at equal rates and that the effective energies are comparable, thus allowing a rapid transfer of magnetization.

Under MAS condition, this matching condition changes to

$$\gamma_H B_1(^1H) = \gamma_X B_1(S) \pm n\omega_R \tag{3.2}$$

(ω_R being the spinning frequency) with maximum signal for $n = \pm 1$.

Magic angle spinning, which averages the dipolar coupling to zero, can severely disrupt cross-polarization transfer if the spinning rate approaches the dipolar coupling constants governing the cross-polarization transfer. So under MAS condition this problem can be overcome by using a ramped-amplitude cross-polarization sequence (ramped-CP) [Metz 94]. In ramped-CP the amplitude of the lock pulse on either channel is linearly increased over the contact time. This produces flat matching profiles over a wide range of matching conditions.

For ^{1}H - ^{13}C CP experiments the carbon signal ideally can be enhanced up to a factor of four. Moreover, the repetition time of the experiment is then determined by the proton T_1 and no longer governed by the long carbon T_1. It should be noted that

the efficiency of the polarization transfer depends on the local environment of the S spins, and the spectra cannot give exact quantitative information.

3.4 Echo experiment

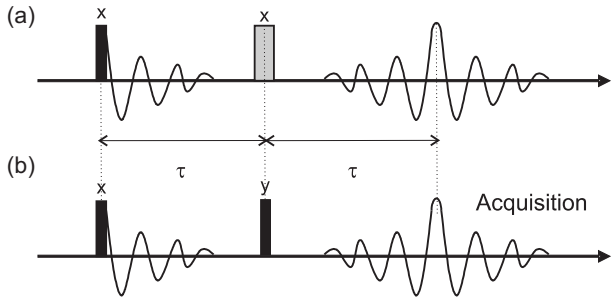

Figure 3.4: *(a) Hahn spin echo and (b) solid echo pulse sequences.*

In the solid state rapidly decaying FIDs due to the strong quadrupolar couplings, dipole-dipole couplings and chemical shift anisotropy can be problematic. In such cases the signal cannot be adequately detected because of the coil not having enough time to fully recover from the initial RF pulse. This means a significant part of a short FIDs cannot be recorded, leading to severe phase distortions and loss of signal. An elegant way to overcome this so called "dead-time" problem is to apply echo pulse sequence instead of single-pulse sequences, where to form an echo of the original signal and detect that. This is achieved by allowing the spins to evolve for a given amount of time τ after the initial 90° excitation pulse, and then applying a suitable echo pulse. The FIDs is then only acquired after the same time τ after the echo pulse. The echo pulse sequences are shown in Fig. 3.4. Depending on the type of interactions, which should be refocused, the effective flip angle of the echo pulse needs to be different. For interactions linear in I_z (chemical shift, resonance offset and heteronuclear dipole-dipole coupling) a 180° pulse is applied to generate the echo. This type of echo is generally known as Hahn spin echo [Hahn 50]. The bilinear interactions of the same spin species, e.g. homonuclear dipolar coupling and quadrupolar coupling are refocused by a 90° echo pulse , which is phase shifted by 90° from the initial pulse. This sequence referred to as the solid echo [Powles 63, Davis 76]. In deuteron NMR molecular reorientation during the solid echo sequence cause frequency changes and lead to characteristic line shapes from which detailed information concerning molecular motion, molecular orientation, and morphology can be provided [Spiess 81, Macho 01].

In particular in this work, the solid echo pulse sequence is used for study of molecular dynamics.

3.5 Two-Dimensional experiments in general

In this section, first the general principle of two-dimensional NMR experiments will be described. A two dimensional NMR data set is generated by introducing a second time variable t_1 in the experiment before the detection period (with time t_2). A set of FIDs is recorded with incremented t_1 and after Fourier transformation in both dimensions, the two-dimensional NMR spectrum is obtained. The principles underlying the generation of a two-dimensional NMR were first presented in a lecture in 1971 by Jeener [Jeener 71], although it was a number of years later that the approach found wider application. During the 1980s the world of NMR, and consequently the chemist's approach to structure determination, was revolutionized by the development of numerous two-dimensional techniques, and nowadays many higher-dimensionality methods also exist [Claridge 99]. No matter what the nature of the interaction to be mapped, all two dimensional sequences have the same basic format and can be subdivided into four well defined units termed the preparation, evolution, mixing and detection periods.

Figure 3.5: *The four stages of a 2D NMR experiment.*

The preparation and mixing periods typically comprise a pulse or a cluster of pulses and/or fixed time periods, the exact details of which vary depending on the nature of the experiment. The detection periods is entirely analogous to the detection period of any one-dimensional experiment. The evolution period t_1 which is inserted into the pulse sequence between evolution and mixing period provides the key to the generation of the second dimension. During the evolution the coherence of interest is excited by one or more pulses. The resulting magnetization then evolved during t_1. It is followed by the mixing procedure and finally the acquisition time, defined as t_2. Hence, the free induction decay (FID) detected during the acquisition is a function of both times, i.e. $S(t_1, t_2)$. t_1 is incremented, therefore the pulse sequence is repeated for increasing values of t_1 and for each step an FID is recorded. A double Fourier transform (FT) then converts the data to 2D spectrum which is a function of two frequency variables, $S(\omega_1,\omega_2)$.

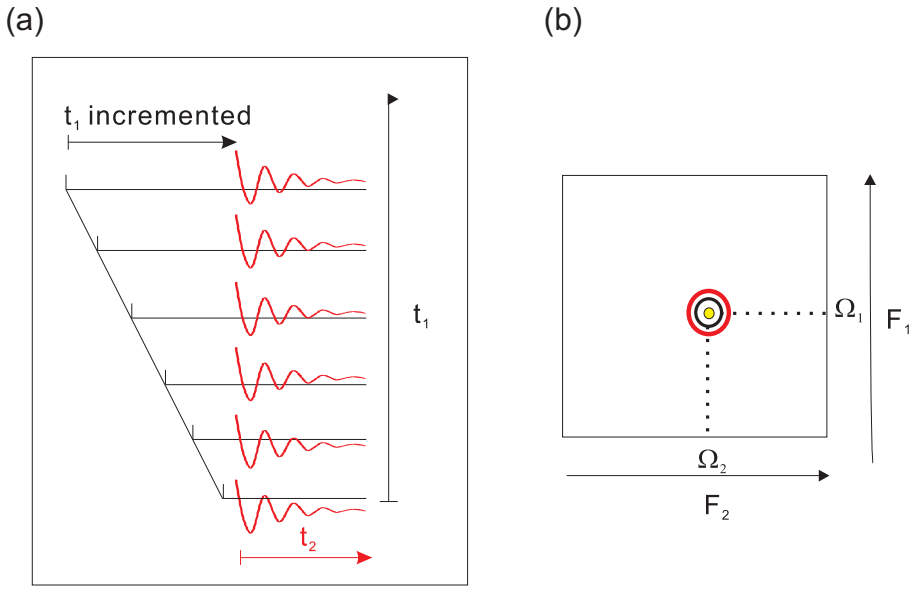

Figure 3.6: *The idea of Jeener. (a) Stepwise increasing of the evolution time* t_1*. (b) Double Fourier Transform in both dimensions.*

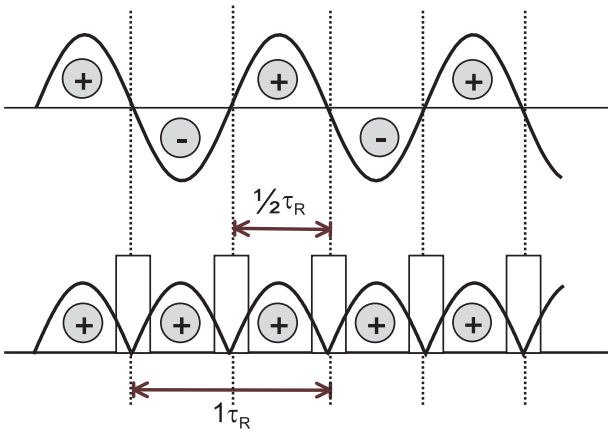

Figure 3.7: *Recoupling under fast MAS. The spin-space of the dipolar Hamiltonian is manipulated by applying π pulses after half a rotor period. In this way the effective dipole-dipole coupling is re-introduced.*

3.6 The concept of recoupling under MAS

As mentioned in the previous Chapter about MAS (Chapter 2.2), by fast magic angle spinning the line-broadening problem in solid state NMR can be overcome very effectively. However, it should be noted that the anisotropic interactions which are removed just before by MAS contain valuable information about molecular structure and dynamics, which normally the solution state NMR cannot give. They include all orientation dependent phenomena, and especially for the dipolar coupling, distance information can be derived. Hence, removing the dipolar coupling with magic-angle spinning to achieve proper line narrowing and reintroducing it selectively while simultaneously keeping the spectral resolution are desirable. This can be done by employing so-called recoupling techniques [Gullion 89a, Carravetta 00], which can recover anisotropic interactions during certain parts of NMR experiments by manipulating the spin-part of the dipolar Hamiltonian. Recoupling takes advantage of the fact that MAS, as a rotation in real space, affects only the space part of an interaction Hamiltonian. Conversely, the RF pulses affect only the spin part of an interaction Hamiltonian. As shown in Fig. 3.7 rotor-synchronized radio-frequency pulse-sequences are applied which invert the sign of the wave function every other half rotor period. Effectively, this induces a counter-rotation in space part and compensates for the effect of MAS and, thus, selectively re-introduce dipole-dipole couplings during specific periods of NMR experiments. A great variety of pulse sequences are currently available for recoupling of various NMR interactions

[Gullion 97, Lee 95, deAzevedo 99, Dusold 00, Schnell 01, Saalwächter 02]. In this work only the Back-to-Back pulse sequence [Feike 96, Schnell 01] which is applied in this work very frequently for proton-proton homonuclear recoupling will be described. The most simple and basic technique, REDOR, to illustrate the hetero nuclear recoupling principle will also be presented briefly in the following sections.

3.7 2D ^{1}H Double-Quantum Techniques:Back-to-Back pulse sequence

In this work to observe proton-proton proximities the Back-to-Back pulse sequences based on the double quantum coherence was used frequently. Two-dimensional double-quantum (DQ) MAS spectroscopy is based on homonuclear dipole-dipole couplings and provides information about through-space ^{1}H -^{1}H proximities [Brown 07]. A ^{1}H 2D DQ MAS spectrum is recorded in a rotor-synchronized fashion in t_1, where t_1 is incremented in steps of full rotor periods, $t_1=N\tau_R$. The creation of double-quantum coherences (DQC) between two protons relies on the existence of a sufficiently strong dipole-dipole coupling between them. Since the intensity of the DQC depends on the strength of dipole-dipole coupling, which in turn depends on the internuclear distance r_{ij}, it is clear that spatial proximities of protons can be directly inferred from the DQ signals. Figure 3.8 schematically shows such a DQ spectrum. The double-quantum dimension elucidates the ^{1}H -^{1}H proximities in the sample. DQCs between like (AA) spins give rise to a so-called *auto*-peak, a single peak on the "DQ" diagonal of the spectrum at (ν_A, (ν_A + ν_A)), referring to the position in the (SQ, DQ) dimension, respectively. For DQCs between unlike (AB) spins two so-called cross peaks are observed at (ν_A, (ν_A + ν_B)) and (ν_B, (ν_A + ν_B)). The resonance frequency of a given DQC is simply the sum of the two SQ frequencies of the two spins involved.

The Back-to-Back (BaBa) pulse sequence is used in 2D MAS experiments, because it is very robust and suitable for fast MAS (25-70kHz), which derives its name from the presence of Back-to-Back pulses. The sequence consists of segments of duration half a rotor period, where an evolution period is bracketed by two 90° pulses, with the phases of the pulses in adjacent segments being shifted by 90°. This shifting of the phases achieves a negation of the spin-part of the DQ Hamiltonian, which exactly compensates the negation of the spatial part caused by MAS. During the excitation time, DQCs are created, which evolve during the evolution time t_1 under the influence of the dipolar interactions in the sample. Since DQCs cannot be detected directly as mentioned above, they need to be converted to SQCs during the

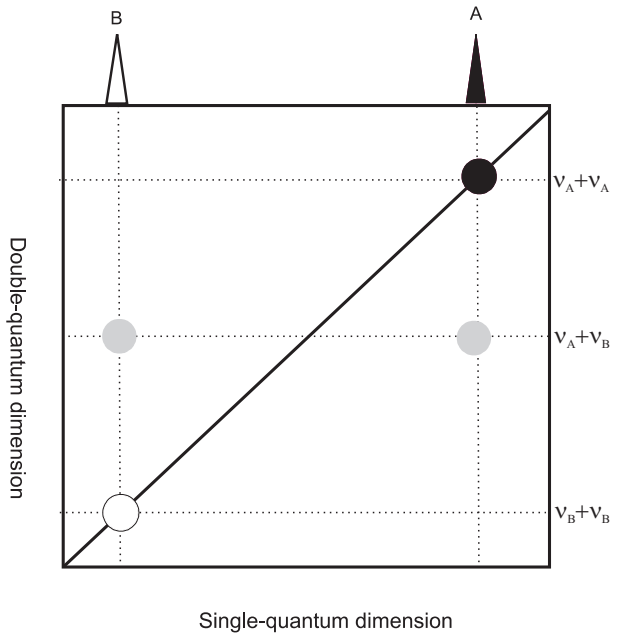

Figure 3.8: *Schematic representation of a DQ spectrum. A and B protons with different resonance frequencies,ν_A and ν_B, respectively. The cross-peaks refer to an A-B proximity and the auto-peaks to A-A and B-B proximities.*

reconversion time. Usually the excitation time equals the reconversion time, and both are integer multiples of the rotor period. The easiest way to excited DQC are two $\frac{\pi}{2}$ pulses phase shifted by 180° (x and $-x$ in Fig. 3.9). But for the excitation of DQC under fast MAS, the interference with the sample rotation must be taken into account. Consider the 90°-τ-90° pulse sequence element employed in solution-state NMR for the excitation of MQ coherence [Brown 07]. Under MAS, the excitation (and reconversion) time is limited to $\tau_R/2$, since the rotor modulation causes the action of the pulse sequence in the second half of the rotor period to be the time reversal of that which occurred in the first half of the rotor period. Therefore, two additional $\frac{\pi}{2}$ pulses with 90° shifted phase are applied during the second half of a rotor-period (y and $-y$ in Fig. 3.9), effectively inverting the sign of the wave-function and, in this way, recoupling the DQCs. This recoupling technique can be viewed as a "counter-rotation" in spin space compensating for the effect of MAS. The reconversion corresponds to an inversion in time, hence the average Hamiltonian describing the reconversion has the opposite sign than the Hamiltonian of the excitation ($\hat{\mathcal{H}}_{rec} = -\hat{\mathcal{H}}_{exc}$). Finally, a suitable phase cycle must be applied to ensure the selection of the coherence transfer pathway depicted in Fig 3.9 and in this way guaranteeing that solely DQCs contribute to the observed signal.

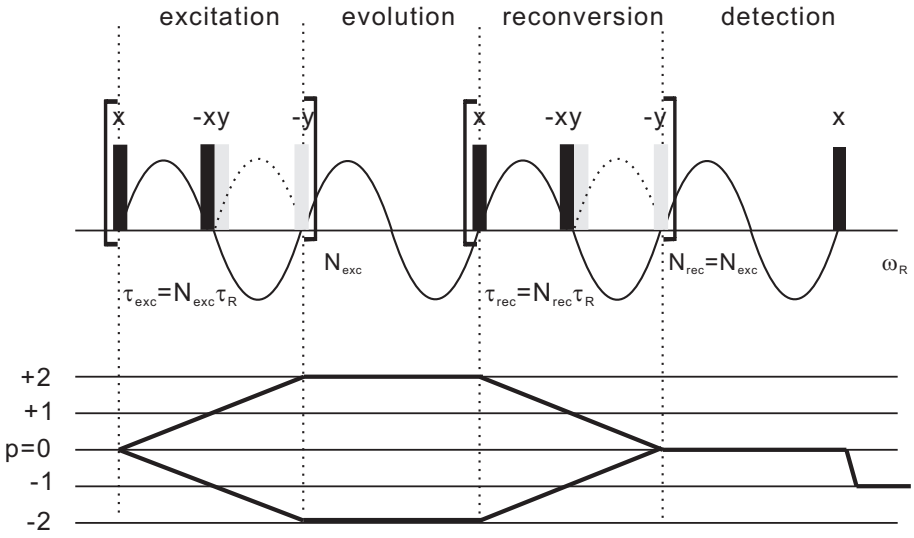

Figure 3.9: *Back-to-Back recoupling pulse sequence with coherence transfer pathway below. The sinusoidal curve visualizes the rotor modulations, with the dashed line indicating the effect of the pulse sequence.*

In the limit of short recoupling times and for an isolated spin-pair, it can be shown that the signal intensity, $I^{DQ}{}_{ij}$ is directly proportional to the effective dipolar coupling constant $D_{(ij)}$ squared. The intensity of a DQ signal is hence given by:

$$I_{ij}^{(DQ)} \propto (D_{(ij)})^2 \cdot \tau_{exc}^2 + \ldots \tag{3.3}$$

$$\propto \frac{\tau_{exc}^2}{r_{ij}^6} + \ldots \tag{3.4}$$

The dependence on the internuclear distance to the sixth power explains why usually only proton-proton distance of < 3.5 Å can be detected. A more quantitative measurement of homonuclear couplings and internuclear distances is provided by DQ spinning sidebands patterns, which arise in the indirect dimension of the 2D experiments as a result of rotor-encoding the dipolar interaction. While the experiment mentioned above is carried out in a rotor-synchronized fashion ($\Delta t_1 = \tau_R$), t_1 now is incremented in fractions of a rotor period ($\Delta t_1 < \tau_R$), which increases the spectral width and, in this way, gives rise to MAS spinning sideband patterns. The details of the rotor-encoded spinning sideband pattern experiment can be found in [Fischbach 03, Schnell 01, Saalwächter 01b, Brown 07].

3.8 REDOR type based 2D REPT-HSQC pulse sequence

In this work to resolve hetero nuclear proximities (^{1}H -^{13}C , ^{1}H -^{2}H , ^{1}H -^{31}P), REDOR(Rotational Echo, Double Resonance)[Gullion 89b, Gullion 89a] based rept-HSQC [Saalwächter 01a, Saalwächter 01b] experiments are performed frequently.

Compared to homonuclear ^{1}H methods, the heteronuclear approach benefits from the higher chemical shift resolution of most *S*-nuclei. All experiments rely on the homonuclear decoupling efficiency of very fast MAS and are based on REDOR-type π pulse trains in order to achieve heteronclear dipolar recoupling. Before turning to the details of REPT-HSQC experiment, REDOR-type π pulse trains will be described first. The REDOR recoupling is based on 180° pulses spaced by half a rotor period, which invert the sign of the Hamiltonian and thus recouple the heteronuclear dipole-dipole interaction that would otherwise be averaged by MAS. From initial proton transverse magnetization on the *I* spins, and applying the pulses on the *S* spins, the evolution of the *IS* spin system during one REDOR segment is:

$$\hat{I}_x \xrightarrow{\Phi 2\hat{I}_z\hat{S}_z} \hat{I}_x\cos\Phi + 2\hat{I}_y\hat{S}_z\sin\Phi \tag{3.5}$$

$$\xrightarrow{\pi\hat{S}_x} \hat{I}_x\cos\Phi - 2\hat{I}_y\hat{S}_z\sin\Phi \tag{3.6}$$

$$\xrightarrow{\Phi' 2\hat{I}_z\hat{S}_z} \hat{I}_x(\cos\Phi\cos\Phi' + \sin\Phi\sin\Phi') - 2\hat{I}_y\hat{S}_z\left(\sin\Phi\cos\Phi' - \cos\Phi\sin\Phi'\right)$$

$$\overset{\Phi=-\Phi'}{=} \hat{I}_x\cos 2\Phi - 2\hat{I}_y\hat{S}_z\sin 2\Phi \tag{3.7}$$

$$\xrightarrow{\pi\hat{S}_y} \hat{I}_x\cos 2\Phi + 2\hat{I}_y\hat{S}_z\sin 2\Phi \tag{3.8}$$

$$\tag{3.9}$$

For clarity, the shorthand notations $\Phi = -\Phi_{Dis}|_0^{\frac{\tau_R}{2}}$ and $\Phi' = -\Phi_{Dis}|_{\frac{\tau_R}{2}}^{\tau_R}$ are used. Comparing Eq. (3.5) with Eq. (3.9) shows that the evolution over one rotor period of the recoupling π pulse train can conveniently be described by an average Hamiltonian,

$$\hat{\bar{H}}_{is} = \bar{\Phi} 2\hat{I}_z\hat{S}_z\frac{1}{\tau_R}, \text{ where} \tag{3.10}$$

$$\bar{\Phi} = 2\Phi = -2\Phi_{Dis}|_0^{\frac{\tau_R}{2}} = \frac{D_{is}}{\omega_R}2\sqrt{2}\sin 2\beta\sin\gamma \tag{3.11}$$

Consequently, the evolution over a pulse train of *N* rotor periods length is given

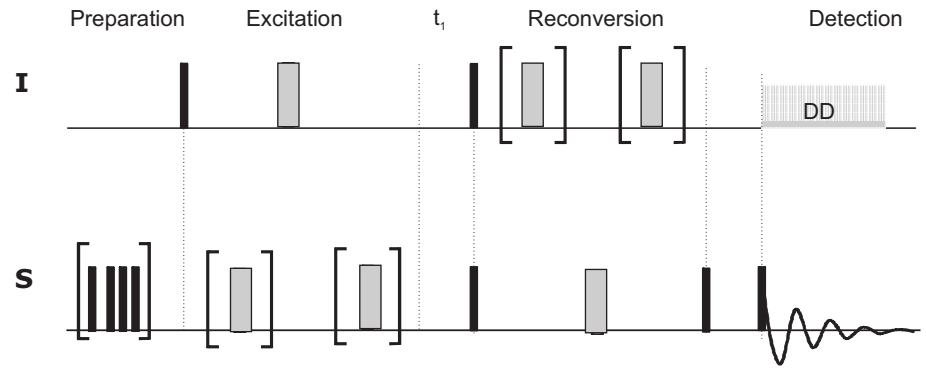

Figure 3.10: *Pulse sequence of the REPT-HSQC experiment.*

by

$$\hat{I}_x \xrightarrow{\bar{\hat{H}}_{IS} N\tau_R} \hat{I}_x \cos(N\bar{\Phi}) + 2\hat{I}_y\hat{S}_z \sin(N\bar{\Phi}) \tag{3.12}$$

Since the 180° pulses only lead to an inversion of the sign, they can as well be applied on the *I* channel without changing the average Hamiltonian. A whole variety of experiments were designed using the REDOR scheme that differ by the nucleus from which the recoupling process is started, the detected nucleus (either conversional *S* or inverse ^{1}H -detection), and the coherence state probed in the indirect dimension [Fischbach 03, Saalwächter 01b]. In the following REPT-HSQC will be described.

The REcoupled Polarization Transfer-Heteronuclear Single Quantum Correlation (REPT-HSQC) experiment is a two dimensional experiment correlating the chemical shifts of two different nuclei, usually ^{1}H and ^{13}C , through dipole-dipole coupling. In this work the correlation between ^{1}H -^{2}H , ^{1}H -^{31}P were probed by 2D REPT-HSQC pulse sequences, but the basic scheme of the experiment is very similar. The experiment is carried out under fast MAS, so normally homonuclear dipolar coupling can be ignored and only ^{13}C -^{1}H couplings need to be considered. REDOR recoupling is applied to selectively recouple heteronuclear dipole-dipole coupling by creating a single quantum coherence (SQC), which evolves during t_1. It is similar to the HSQC experiments known from solution-state NMR, apart from the fact that the latter relies on J-coupling rather than dipole-dipole coupling. In Figure 3.10 the pulse sequence of a REPT-HSQC experiment is shown.

The REPT-HSQC experiment, can be thought of as the heteronuclear equivalent to the BaBa experiment. As a 2D experiment, if t_1 is incremented in full rotor periods, a heteronuclear correlation (HETCOR) spectrum correlates *S* nuclei chemical

shift in the direct dimension with *I* chemical shift in the indirect dimension. In order to understand the interactions probed during t_1, the dependence of the *S* spin detected signal with respect to t_1 for this experiment needs to be considered. During the t_1 period the antiphase coherence $\hat{I}_x\hat{S}_z$, created by the excitation π pulse-train, evolves under the influence of chemical shift and dipolar couplings. At the end of t_1, two 90° pulses are applied on both channels to transfer the magnetization to the *S* spin by interchanging transverse and longitudinal spin states between *I* and *S* spins. After the second recoupling period, where pulses now are applied on the *S* channel using again the central pulse on the *I* spin to refocus the CS evolution, the signal is acquired on the *S* channel. The intensity of the correlation peaks being determined by the strength of the underlying dipolar coupling and the number of recoupling cycles $n_{exc/rec}$. Due to the mediating interaction being the through-space dipolar interaction, the correlation seen is not limited to directly bound ^{1}H -S spin pairs only, as would be the case if J-coupling mechanism was used. This leads to the possibility of probing strong dipolar interactions with short recoupling times, and weaker interactions with longer recoupling times. Typically at short recoupling times of $\tau_{exc} = 1 \cdot \tau_R$, only directly bound spin pairs are observed, the resulting spectra being useful for spectral assignment purposes, however, at extended recoupling times correlation between long range non-bound heteronuclear spin-pairs may be observed. This can provide valuable information regarding the supramolecular structure.

Chapter 4

Barbituric acid derivatives

4.1 Introduction

Artificial chromophoric receptors for biologically active molecules have attracted considerable attention from the viewpoint of molecular recognition [Demeunynck 03, Silva 97, Sando 04, Okamoto 05, Thompson 05]. In particular, interactions mediated by hydrogen-bonding play an important role in both chemical and biological systems [Paulini 05]. Barbiturates are important members of the pyrimidine family, and show very selective affinities at binding adenine or its derivatives thereby yielding strongly hydrogen-bonded complexes [Kyogoku 68, Voet 72]. However, the observed biological activity of barbiturates is mainly attributed to tautomerism, acid-base equilibria, and to the nature of their substituents [Zuccarello 03]. Recently, it has been shown that related Merocyanine dyes containing the barbituric acid moiety as an electron withdrawing group create new self-assembled structures [Bohanon 95, Bohanon 99], or are effective sensitizers with interesting photophysical properties [Würthner 03, Würthner 04]. More importantly, such dyes exhibit hydrogen-bonding patterns with an ADA sequence (A = hydrogen bond acceptor site, D = hydrogen bond donor site) suitable for selective binding to bases offering a complementary DAD pattern.

In this contribution, the solid state structures of a new enolizable chromophor **1-n-butyl-5-(4-nitrophenyl)-barbituric acid (NiBu)** that features adjustable hydrogen-bonding properties and its corresponding assemblies with three different bases are investigated by advanced solid state NMR experiments which are described in the previous chapter. The corresponding bases are **Proton Sponge (PS)**, adenine-mimetic bases **2,6-diaminopyridine (DAP)**, and **2,6-diacetamidopyridine (DAC)** in the order of basicity. The prototropic tautomerism of **NiBu** facilitates an adjustment to comple-

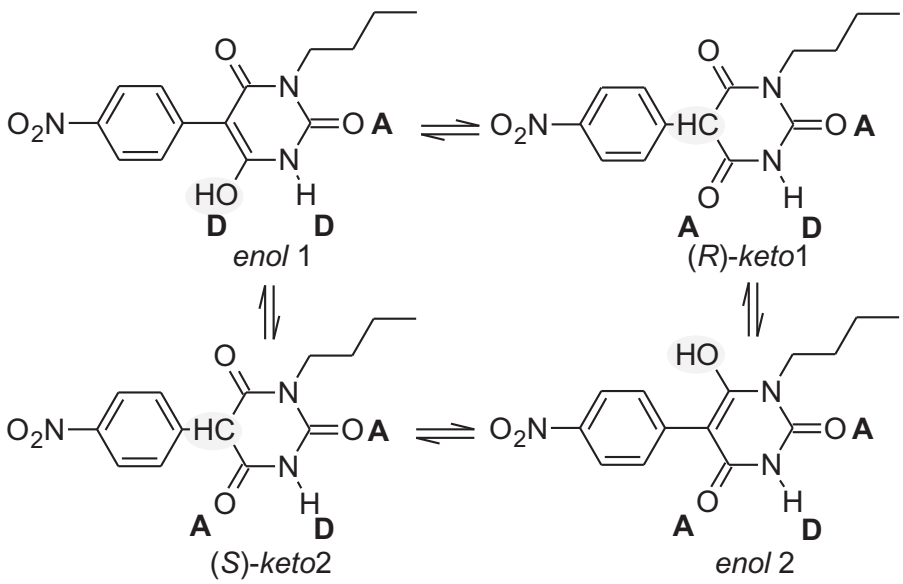

Figure 4.1: *Keto-Enol tautomerism of NiBu. Two different enol forms with either vicinal or opposed OH and NH protons are possible*

mentary bases containing a DDA or ADA sequences.(Fig. 4.1)

The switching between the two principle tautomeric forms of **NiBu** (keto1/keto2 or enol1/enol2, cf. Fig. 4.1) is associated with dramatic changes in the extent of π-conjugation: the enol-substituent contributes to a push-pull system due to the para-conjugation with the nitro group, while the keto-substituent belongs to a common nitro-substituted aromatic system. Thus, externally induced formation of the *enol*1 or *enol*2 form should cause a significant bathochromic shift in the UV/Vis spectrum. In contrast to the established Merocyanine dyes, the enolizable barbituric acid serves as a +M-substituent, which is of importance for the construction of chromophoric probes relating to this type of compounds that are still not established for probing molecular recognition. However, the possible occurrence of both tautomeric forms as well as molecular adducts complicates a clear assignment of observed UV/Vis absorption spectra to a well-defined molecular structure. Therefore, to identify whether mere salt formation occurs or rather genuine supramolecular complexes are built, solid-state NMR experiments are required. Moreover, since in most cases except for pure **NiBu** single-crystals suitable for X-ray analysis could not be obtained, the information derived from solid-state NMR experiments which in recent years has shown to be a versatile and powerful tool for the characterization of materials [Brown 01, Eckert 05, Benedicte 06, Benedicte 05, Lesage 01] are more cru-

cial. Generally in solid state NMR, acquiring mere ^{1}H-NMR spectra may not be successful since the proton resolution is not always sufficient even under fast magic angle spinning ($\approx$ 30kHz). But in case of hydrogen-bonded chemical systems like barbituric acid derivatives, information about hydrogen-bonding in the solids can be obtained by ^{1}H magic-angle spinning (MAS) NMR and 2D ^{1}H-^{1}H dipolar double-quantum (DQ) techniques [Pawsey 03, Densmore 05, Alam 07], because protons involved in hydrogen-bonded structures typically appear mainly between 8 and 20ppm being well-separated from other protons. Also the sensitivity of the ^{1}H chemical shift to hydrogen bonding [Wasserfallen 05, Brown 00] makes ^{1}H solid state NMR ideally suited to follow changes of the hydrogen bond arrangements.

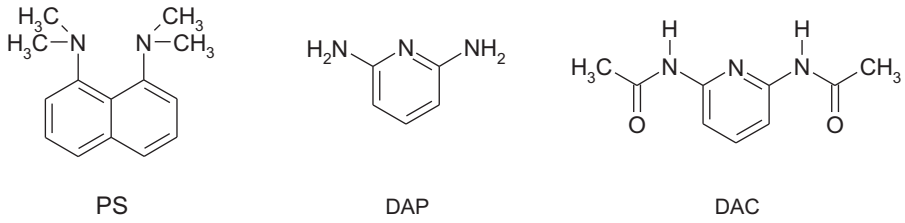

Figure 4.2: *The structures of corresponding bases*

In this chapter, the structure of **NiBu** will be discussed first. In the following further studies about the structures of **NiBu** complexes with different type of bases mentioned above will be presented. In Figure 4.2 the structure of each base are shown. While investigating the **NiBu** system, two reference compounds are used to support the given interpretation of the respective solid state NMR results. Those are **1-n-butyl-5-phenyl-barbituric acid (Bu)** and **1,3-dimethyl-5-(4-nitrophenyl)-barbituric acid (NiDMe)** which have slightly modified structures from **NiBu**.

4.2 1-*n*-butyl-5-phenyl barbituric acid(Bu)

Before exploring the solid state structure of the new enolizable chromophor **1-n-butyl-5-(4-nitrophenyl)-barbituric acid (NiBu)**, the starting material **n-butyl-phenyl-barbituric acid (Bu)** is considered first.

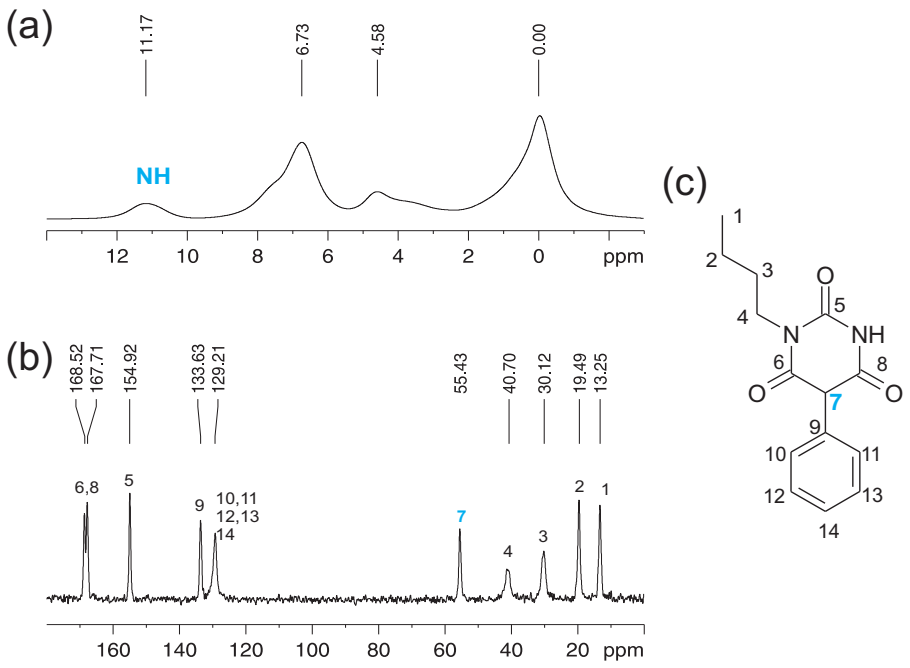

Figure 4.3: *(a) ^{1}H-MAS and (b) ^{13}C-CP MAS of Bu. (c) the solid state structure of Bu.*

The ^{1}H MAS NMR spectrum of **Bu** (Fig. 4.3(a)) exhibits only one hydrogen bonded proton at 11.17ppm, which highly implies that **Bu** is present in keto form in the solid state. Indeed, a methine carbon resonance at 55.4ppm in the corresponding ^{13}C -CPMAS spectrum (Fig. 4.3(b)) clearly confirms the keto form.

To further study the hydrogen bonding network within **Bu**, ^{1}H DQ MAS NMR spectra which are particularly suited to identify specific proton-proton contacts were acquired. By simple inspection of the observed peaks or often more importantly, which are absent, much insight is obtained into proton-proton proximities. The reliability of such a semi-quantitative approach has been clearly demonstrated for cases where an X-ray single crystal structure is available to corroborate the proton-proton proximities extracted from ^{1}H DQ MAS spectra. The ^{1}H DQ MAS spectrum of **Bu** is shown in Fig. 4.4. Recalling Chapter 3.7 (2D ^{1}H Double-Quantum Techniques:Back-to-Back pulse sequence), in the DQ dimension, resonances are present at the sum of the single-quantum (SQ) frequencies of the two involved protons. While DQCs

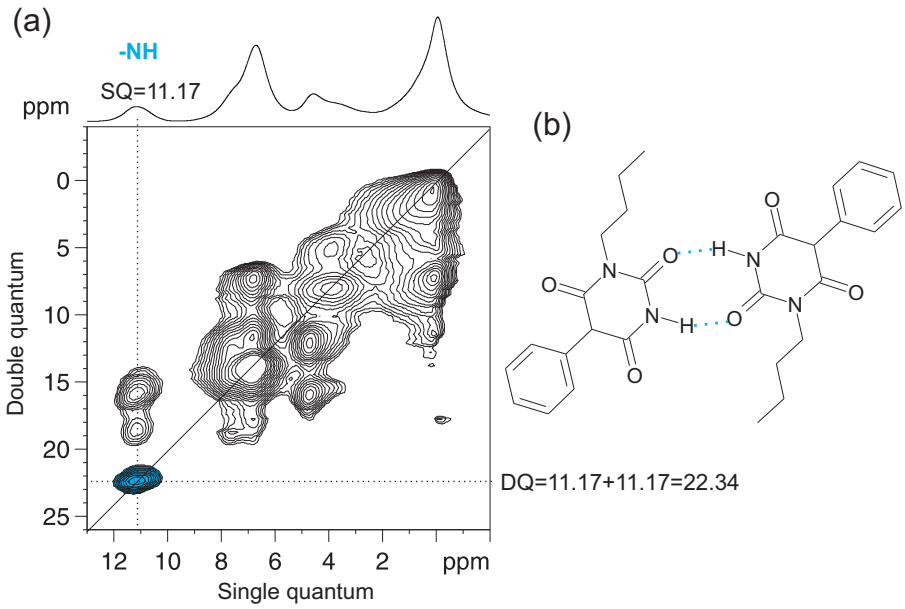

Figure 4.4: *(a)* ^{1}*H DQ MAS of Bu. The colored peak is an NH-NH auto-correlation peak. (b) Dimer structure of Bu.*

between protons with identical chemical shifts yield so-called *auto*-peaks along the diagonal, the DQCs between protons with different SQ chemical shift result in a pair of cross-peaks symmetrically arranged on either side of the diagonal. The intensity of each peak observed is proportional to both the number of proton pairs giving rise to DQCs, their distance ($\propto 1/r_{ij}{}^{6}$) as well as the efficiency of DQ excitation and re-conversion, with the latter depending strongly on the strength of the effective dipolar coupling.

The strong NH-NH auto correlation peak observed at 11.17+11.17=22.34 ppm in the double quantum dimension (F1) in ^{1}H DQ MAS spectrum clearly provides evidence for a dimeric hydrogen-bonded structure of **Bu** in Fig. 4.4(b).

4.3 1-*n*-butyl-5-(4-nitrophenyl)-barbituric acid(NiBu)

Based on the result derived from **Bu**, the solid state structure of **NiBu** is investigated. First the result of monomer structure of **NiBu** will be presented. This will be followed by the discussion of dimeric structure of **NiBu**.

4.3.1 Monomer Structure of NiBu

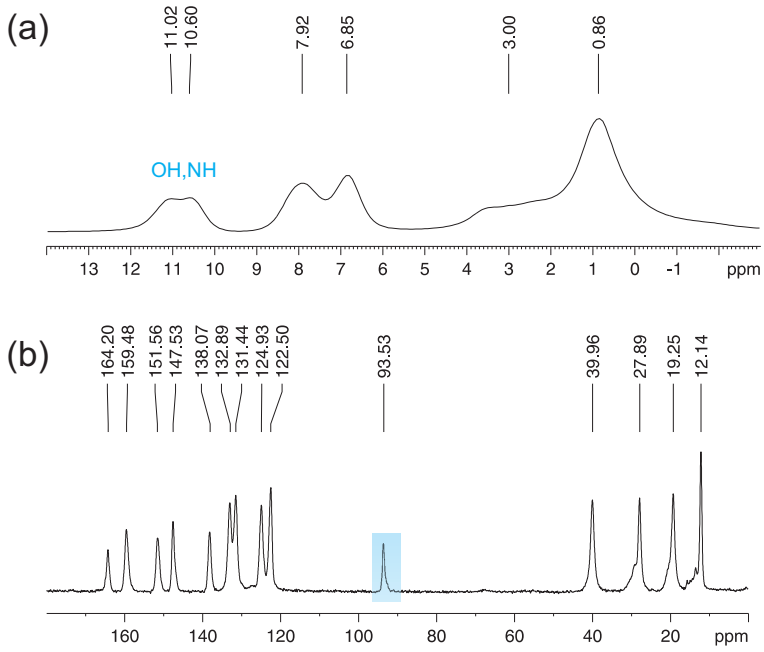

Figure 4.5: *(a)*^{1}*H-MAS and (b)* ^{13}*C-CPMAS of NiBu*

An inspection of the ^{1}H MAS NMR spectrum of **NiBu** reveals two high-frequency shifted protons at 11.02ppm and 10.60 ppm reflecting that these protons are indeed involved in hydrogen-bonding. Moreover, the lack of a methine carbon around 55ppm (characteristic feature of the keto form) and the appearance of a new peak at 93.53ppm (which is assigned to carbon-7 in Fig. 4.7) unambiguously confirms an enol type structure for **NiBu**. Since in solution a rapid equilibration between both the keto and enol forms of **NiBu** occurs, it is important to distinguish the two possible enol structures in the solid-state (Fig. 4.1). However, *enol*1 and *enol*2 cannot be distinguished via ^{13}C chemical shift assignment.

In the case of *enol*1, the vicinal NH and OH protons form a spin pair that could be probed by ^{1}H DQ MAS NMR spectroscopy whereas in the *enol*2 structure the ex-

changeable protons are opposite to each other. The presence of a strong (NH-OH)-DQ contact peak observed in the ^{1}H DQ MAS NMR spectrum of **NiBu** at the 1tR (one rotor period) (in Fig. 4.6) highly implies that it is originating from *intra*-molecular interactions, which strongly endorses an *enol*1-type structure of **NiBu**. At 1tR recoupling time, distances within 3.5 Å can commonly be detected.

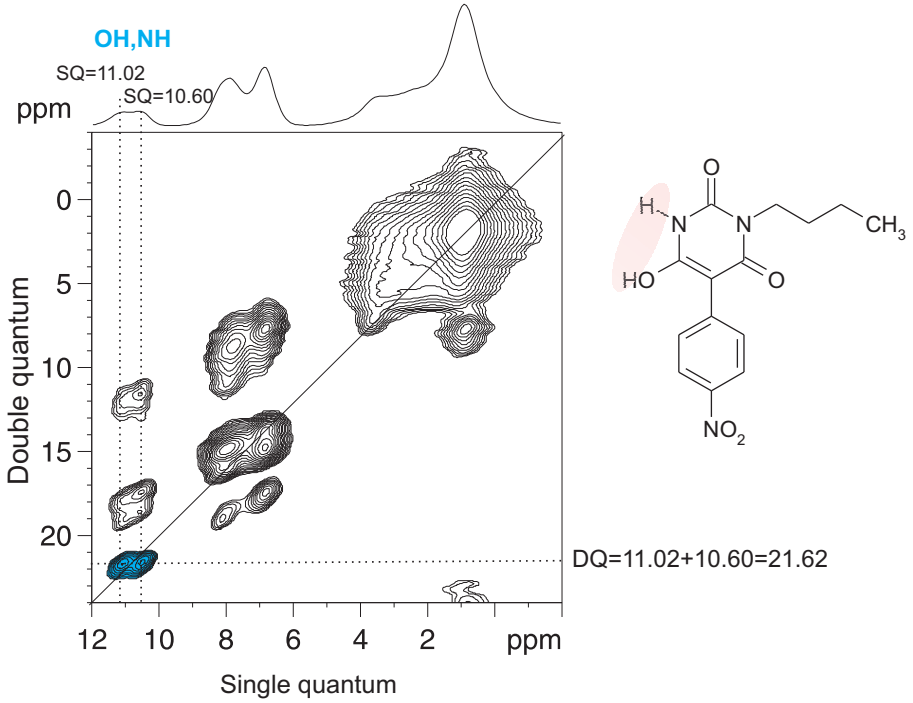

Figure 4.6: ^{1}*H DQ MAS spectrum of NiBu on 850MHz NMR. The colored peak is a strong DQ contact between NH–OH protons.*

Just for the comparison, the ^{1}H DQ MAS spectra recored in different field (500MHz *vs*. 850MHz) are shown in Figure 4.7. Generally, sensitivity and resolution of the observed NMR signal is strongly enhanced by high magnetic fields. This is nicely demonstrated by the comparison of ^{1}H DQ MAS spectra of **NiBu** measured on 500 MHz and 850 MHz machines. Clearly, the two different protons (NH and OH) are **not** resolved at 500 MHz, which might lead to misunderstanding of the properties of material. In contrast, the state-of-the art 850 MHz NMR allows for an unambiguous assignment of the two different chemical shifts of -OH and -NH protons thereby yielding a strong correlation peak in the ^{1}H DQ MAS spectrum that reveals valuable structural details (*enol*1).

More quantitative insight into distances may be obtained from ^{1}H DQ MAS spinning sideband pattern obtained for the NH resonance of **NiBu** with recoupling time

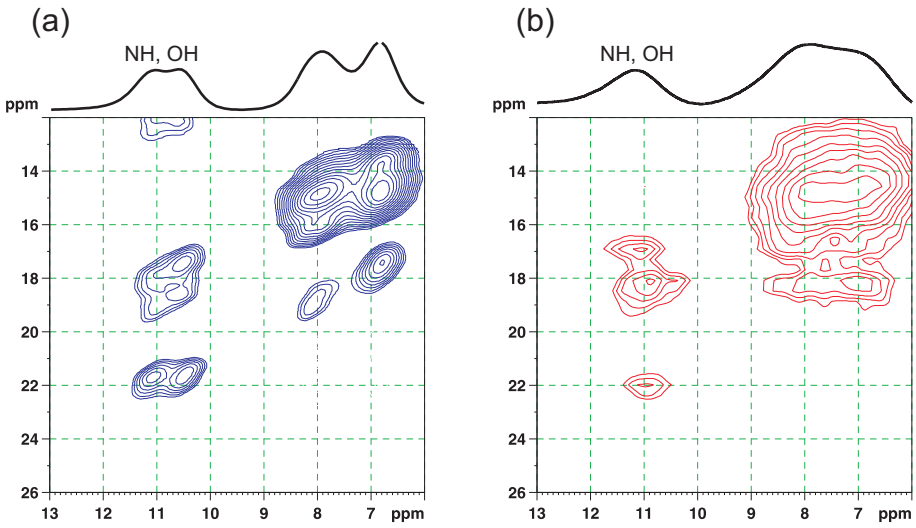

Figure 4.7: *Comparison of ^1H DQ MAS spectra of NiBu on (a)850MHz and (b)500MHz NMR.*

τ_{rcpl} equal to $1tR$ period at a spinning speed of 30 kHz. An inspection of the spectra in Fig. 4.9 reveals the existence of spinning sidebands due to all three different DQCs - note that the DQ peak for the NH-OH pair is at the first-to-right position. The best fit for the ^{1}H DQ side bands pattern of the NH-OH DQ peak gives a dipole-dipole coupling of D≈6.3 kHz, which corresponds to an distance between NH and OH protons r_{NH-OH}=0.27*nm*, a rather typical value of for vicinal protons.

No. of Carbon	Chemical shift(ppm)
1	12.14
2	19.25
3	27.89
4	39.96
5	152.56
6	164.20
7	93.53
8	159.48
9	138.07
10,11	131.44, 132.89
12,13	122.50, 124.93
14	147.53

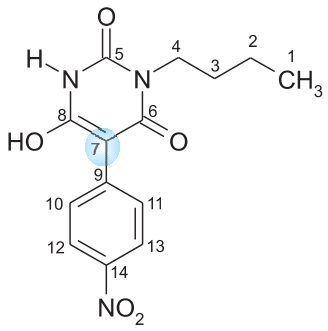

Figure 4.8: ^{13}C *chemical shift assignments of NiBu*

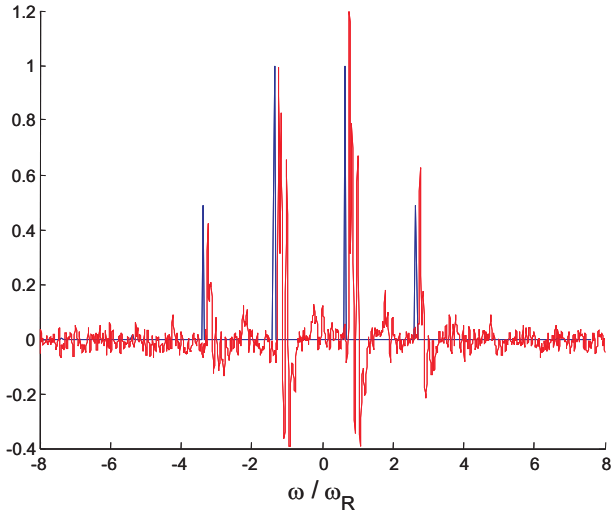

Figure 4.9: *Sideband pattern of NiBu recorded under MAS at 30kHz (red line : experimental, blue line : calculated).*

4.3.2 Dimer structure of NiBu

Once proved *enol*1 type structure, further investigation about hydrogen bonding network of **NiBu** is performed. Insighted by the result from **Bu** dimer, it is assumed that **NiBu** adopts a rather similar dimeric structure, where the NH-NH hydrogen bonding is still maintained for **NiBu**. Additional hydrogen bonding may be present because **NiBu** is enol form having one more hydrogen bonding site. However, due to severe signal overlap of the OH and NH proton resonances in ^{1}H DQ spectrum (Fig.4.6) shown above, possible aggregation of **NiBu** cannot be addressed directly.

The development of heteronuclear correlation techniques for fast MAS NMR opened the possibility to acquire ^{1}H-^{13}C heteronuclear correlation spectra, which greatly benefit from the enhanced resolution in the ^{13}C spectra, and therefore, allow for the determination of solid state packing effects present in the sample. In ^{1}H-^{13}C REPT-HSQC spectrum of **NiBu**, especially interesting region, 140-170ppm in ^{13}C-dimension, is zoomed (Fig. 4.10). All three quaternary carbons show cross peaks with hydrogen bonded protons in the F1 dimension. The relatively strong two peaks of carbon 8 and 5 are presumably intra-molecular contacts, (i.e -OH with carbon 8, -NH with carbon 5, 8). The relatively weak signal at carbon 6 is attributed to long-range correlation. The latter, however may originate from either intra- and inter- molecular interactions, rendering it difficult to derive unambiguous details of the hydrogen bonding network based on ^{1}H -^{13}C REPT-HSQC spectrum.

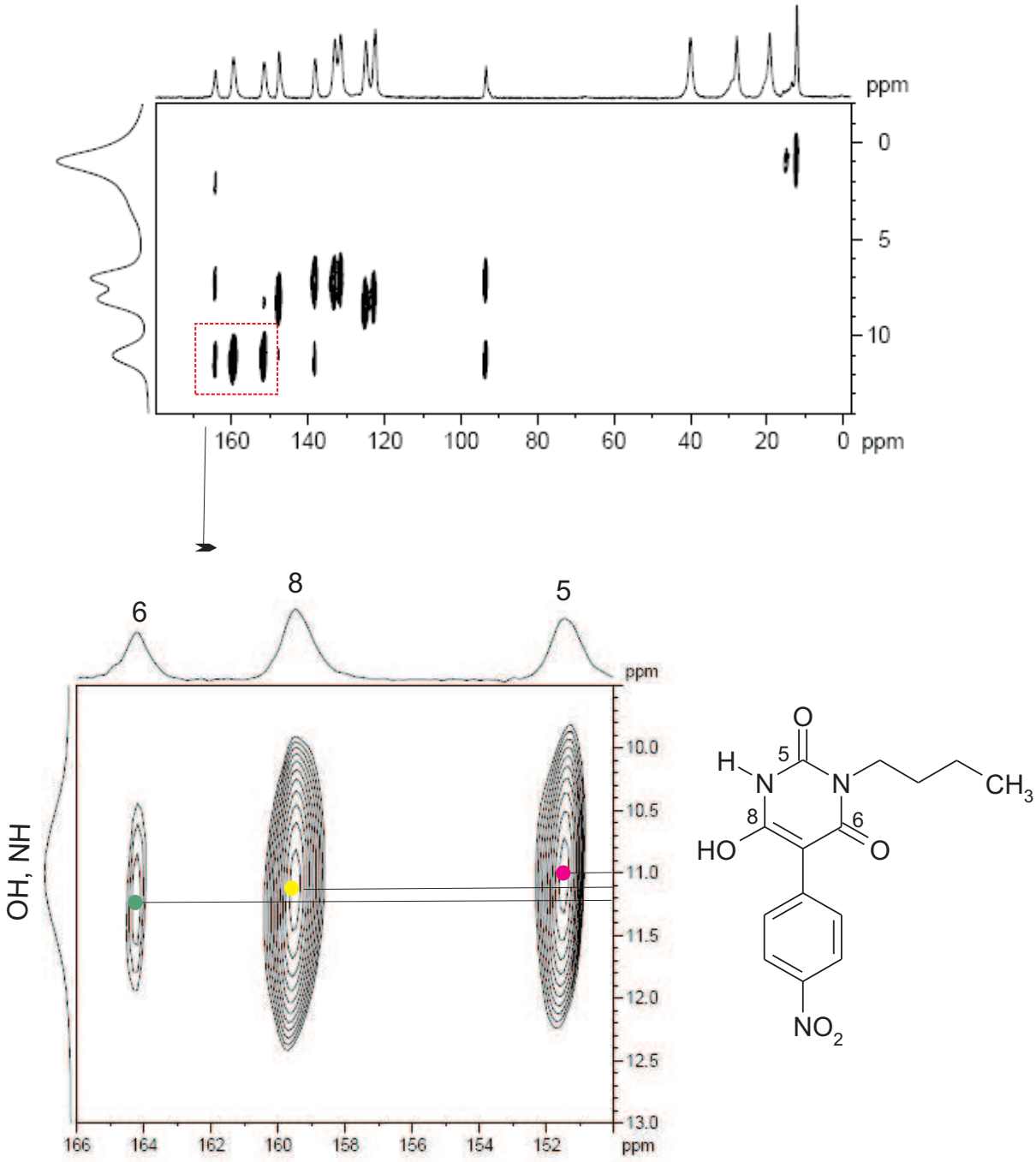

Figure 4.10: *Two-dimensional* ^{1}H *-*^{13}C *REPT-HSQC spectrum of NiBu obtained under MAS at 30kHz and* $\tau_{rcpl}=4\tau_R$.

4.3.3 Deuterated NiBu

As mentioned above, it is assumed that due to the severe signal overlap of the OH and NH protons resonances, the possible aggregation of **NiBu** cannot be addressed directly. Hence, part deuteration of two exchangeable protons thereby reducing line broadening due to ^{1}H -^{1}H homonuclear dipolar coupling is performed. Indeed, the use of deuteration to increase the ^{1}H resolution is becoming increasingly important in solid-state NMR studies of peptides and proteins [Zhou 06, Paulson 03, Morcombe 05]. For **NiBu**, deuteration is attempted from D_2O at first. The corresponding ^{1}H-MAS spectrum is expected to exhibit narrower lines for the exchangeable protons due to reduced homodipolar broadening. Instead, the ^{1}H-MAS spectrum shows two resonances well-separated at 13.0 ppm and 11.2 ppm.(Fig. 4.11(b))

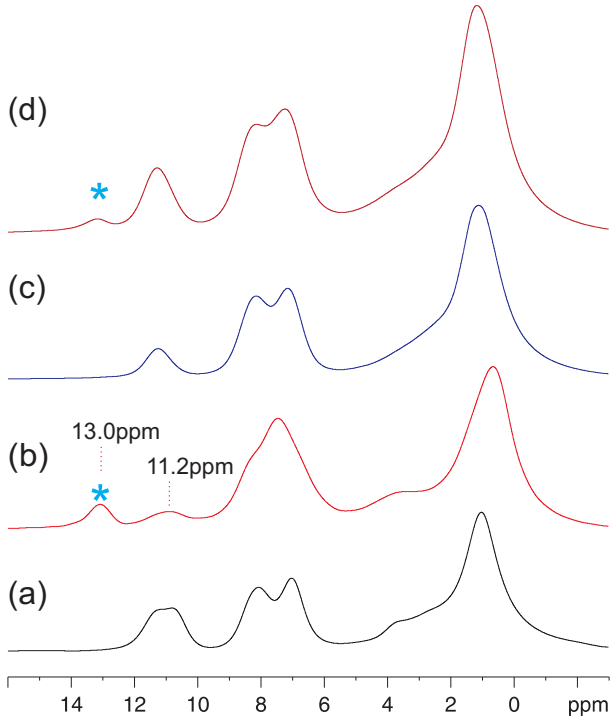

Figure 4.11: *Comparisons of ^{1}H -MAS spectra of (a) pure NiBu (b) deut-NiBu from D_2O (c) deut-NiBu from MeOD (d) air-exposed NiBu*

At first sight this observation may be attributed to an isotopic effect but rather indicates a mere change of the hydrogen-bonding network, with the peak at 13.0ppm tentatively assigned to the -OH protons. The same peak is observed for air-exposed **NiBu** even though the intensity is weaker.(On purpose **NiBu** is exposed to air for several weeks.) (Fig. 4.11(d)) From this, the observation of the well-separated resonances

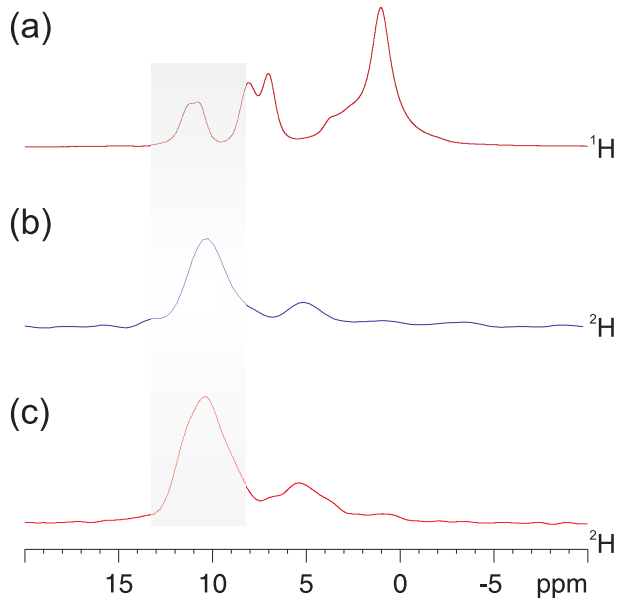

Figure 4.12: *(a) ^1H -MAS spectrum of pure NiBu (b) ^2H -MAS spectrum of deut-NiBu from D_2O (c) ^2H -MAS spectrum of deut-NiBu from MeOD*

peaks at 13.0 ppm and 11.2 ppm for deuterated **NiBu** from D_2O is clearly due to the water molecule effect on hydrogen bonding network. To check whether it is truly water effect, the deuteration is performed in different solvent, MeOD. Interestingly for part-deuterated **NiBu** from MeOD the new peak at 13.0ppm is not observed (Fig. 4.11(c)). From Figure 4.11, summarizing all the observation above, it is evident that while deuteration water molecule is involved the hydrogen network system and this water molecule cannot be removed easily. In Figure 4.12 the comparisons among ^{2}H spectra of deuterated-**NiBu** from different solvents and ^{1}H-MAS spectrum of **NiBu** are shown. However, the resolution of ^{2}H peak is not sufficient to distinguish ND and OD resonance peaks.

Summarizing all the result above, it is obvious that the water molecule has influences on hydrogen bonding network system of **NiBu** during the deuteration, however up to now not so detailed information can be obtained. It should be noted that in selecting deuterating solvent, the keto-enol tautomerizm should be considered for the **NiBu** system. The ^{13}C -CPMAS of deuterated **NiBu** from D_2O clearly proves enol form although there are line-broadenings in the aromatic carbon region for deuterated **NiBu** (Fig. 4.13(a)). Further investigation about this aspect is needed. However in the present study it is not discussed any more.

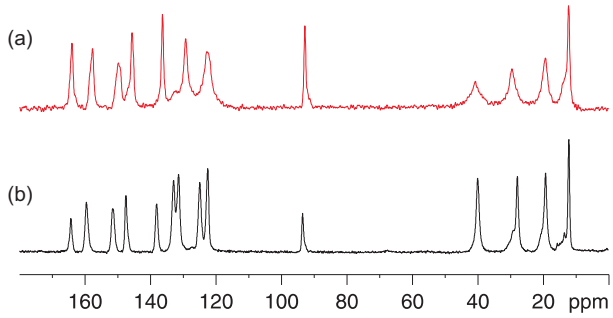

Figure 4.13: *Comparison of ^{13}C -CPMAS spectra of (a) deut-NiBu from D_2O (a) pure NiBu.*

4.3.4 2D NMR of deuterated NiBu and X-ray structure

Assigning the peak at 13.0 ppm for deuterated-**NiBu** from D_2O as -OH proton and 11.2 ppm as -NH proton, ^1H 2D DQ MAS and ^1H -^{13}C REPT-HSQC experiments were performed. First the observation of possible auto correlation contacts of NH-NH protons in ^1H DQ MAS spectrum suggests the dimeric structure of deuterated-**NiBu** as shown in Fig. 4.14(a). Moreover, from the ^1H -^{13}C REPT-HSQC spectrum, possible hydrogen bonding network structure might be derived.

In the ^1H -^{13}C REPT-HSQC spectrum given in Fig. 4.14(b), the interesting region 140-170ppm in ^{13}C -dimension (F_2) is highlighted. Here, the NH and OH protons show three correlation peaks : NH proton shows cross peak with carbon-5 and carbon-8, OH proton shows cross peak with carbon-6 and carbon-8.

Most importantly, the OH proton shows a cross peak only with carbon-6 and not with carbon-5, which highly suggests that it is related with *inter* molecular interactions. Based on symmetry considerations, carbon-5 and carbon-6 are located at similar distances from the -OH proton. Therefore, it is assumed that the cross peak between carbon-6 and -OH proton is not intra-molecular interaction, but rather it reflects hydrogen bonding between dimers of **NiBu** as shown in Fig. 4.14(c).

Additional structural information has been obtained by single-crystal X-ray analysis (recrystallization from diethyl ether), where the available NMR data greatly simplified the structure refinement. It was found that **NiBu** recrystallizes with two independent molecules in the asymmetric unit, which differ in the conformation of the *n*-butyl side groups. In one of the two molecules, the *n*-butyl group is disordered, i.e. it occupies two distinct orientations populated by about 50 percent. Two independent molecules of **NiBu** are linked together by symmetric and strong hydrogen bonds between the C=O and NH groups of the barbituric acid moieties. Each molecule

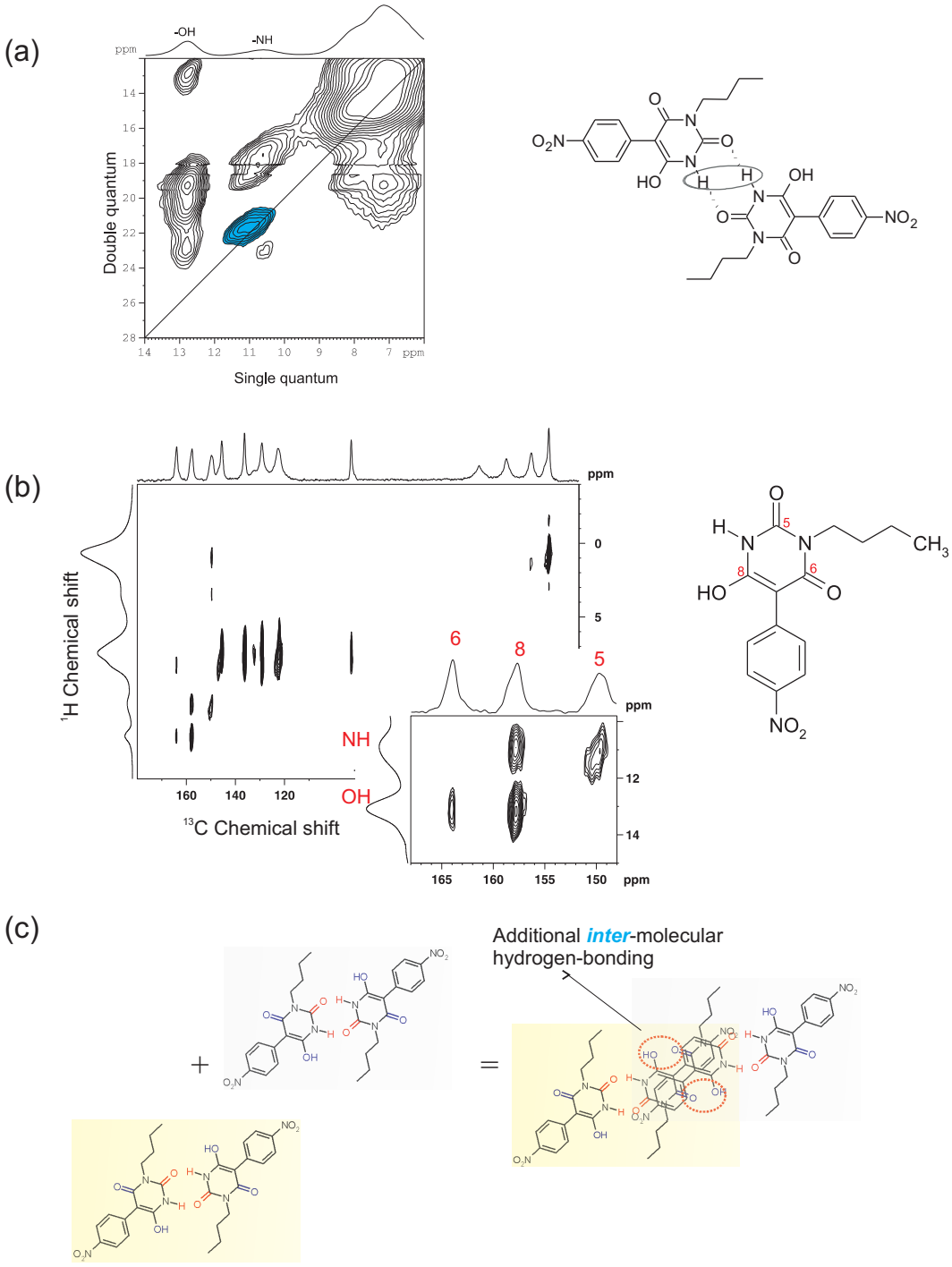

Figure 4.14: *(a)* ^{1}H *DQ MAS NMR spectrum of and partly deuterated NiBu from* D_2O *and corresponding dimeric structure.(indicating possible auto-correlation peak among the NH protons.) (b)* ^{1}H *-*^{13}C *REPT-HSQC spectrum of partly deuterated NiBu from* D_2O*. The presence of various intermolecular* ^{1}H *-*^{13}C *contact peaks between both C=O and OH groups confirm the stacked arrangement of the dimeric units in partly deuterated NiBu from* D_2O*. (c) suggested hydrogen bonding network system of partly deuterated NiBu from* D_2O*.*

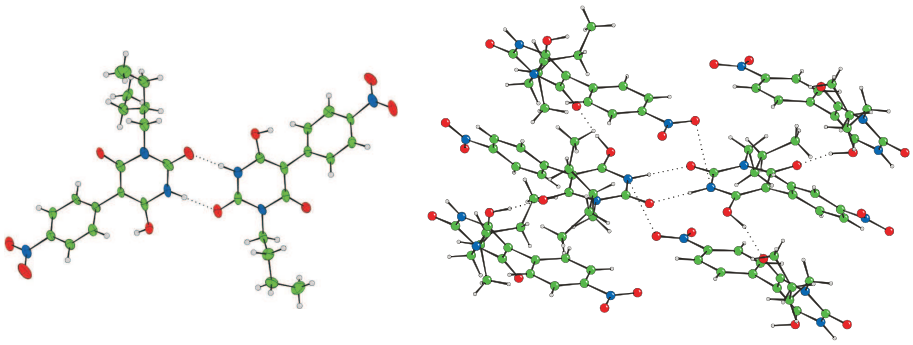

Figure 4.15: *The molecular structure of dimeric NiBu and its packing. Each dimer is surrounded by symmetry-produced neighboring molecules along the main axis. The dotted lines emphasize the hydrogen bonds that stabilize the structure, e.g. : N-H—O=C (d=1.97(0) Å, D=2.798(0) Å, θ=165.(9)° ; d=1.95(9) Å, D=2.842(2)Å θ=169.(0)°) ; C=O—HO (d=1.67(7)Å, D=2.56(0) Å, θ=164.(2) °) ; NO_2—NH (D=3.05(2)Å.). The N—O and O—O distances (D) are obtained from single-crystal X-ray data, while the hydrogen atoms were refined with respect to known geometries using SHELXS86 software yielding hydrogen bond lengths). Done by Volker Enkelmann.*

is involved in additional hydrogen bonds between C=O and OH groups stabilizing the stacked arrangement of the dimeric units (Fig. 4.15). Searching the Cambridge Structural Database (CSD)[Allen 02] for barbiturates reveals that the majority of compounds form centrosymmetric dimers that are stabilized by hydrogen bonds. However, the disorder of the alkyl chains of **NiBu** prevents centrosymmetry. Notably, the occurrence of this disorder depends of the recrystallization (e.g. on the polarity of the solvent used). After slow recrystallization from diethyl ether, **NiBu** showed substantially less disordered alkyl chains, while recrystallization from acetone yielded a perfectly centro-symmetric structure with ordered alkyl chains (data not shown).

Recalling the dimeric structure of deuterated **NiBu** from D_2O suggested by ^{1}H -^{13}C REPT-HSQC experiment, the dimeric structure from X-ray result is consistent. However, up to now the water molecule effect is not clearly explainable as mentioned in the previous section, which needs further study about that.

4.4 NiBu + 2,6-diacetamidopyridine(DAC) complex

On the basis of the information obtained about the pure **NiBu** structure, the solid state structure of several complexes with **NiBu** will be described. First **NiBu** is treated with an equimolar amount of **2,6-diacetamidopyridine (DAC)** offering a complementary hydrogen-bonding pattern.

The ^{1}H-MAS and ^{13}C-CPMAS spectra of **DAC** are shown in Fig. 4.16.

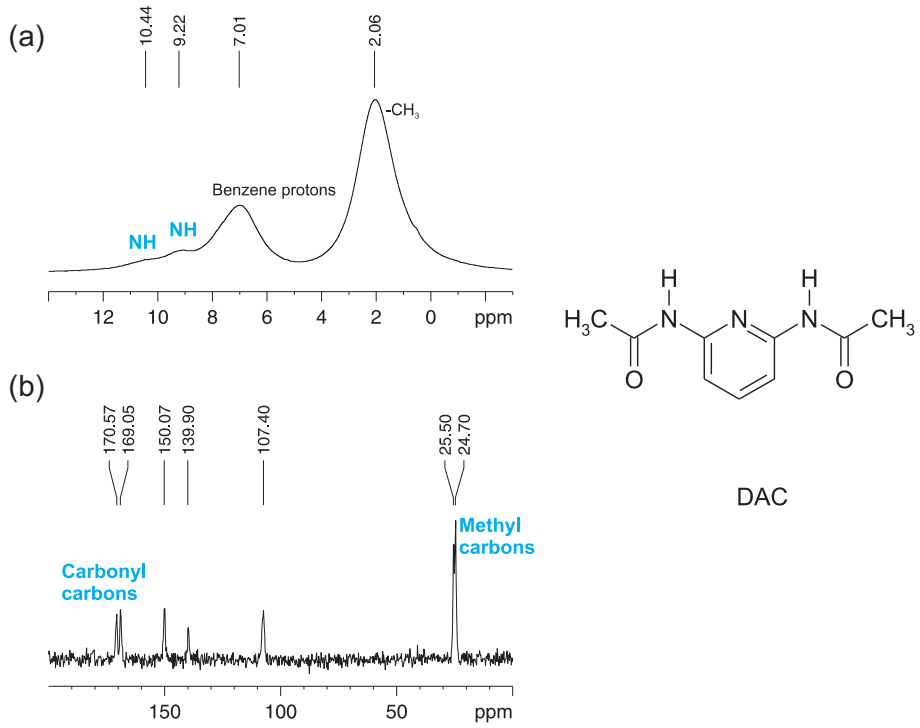

Figure 4.16: *(a)^{1}H -MAS and (b) ^{13}C -CPMAS spectra of DAC*

The two -NH protons of **DAC** appear at 9.22ppm and 10.44ppm separately. Moreover, both of the carbonyl carbon and methyl carbon of **DAC** show two different resonances, which is possibly due to solid state packing effects.

The corresponding solid-state UV/Vis spectrum of **NiBu+DAC** exhibits two absorption band at 414nm and 334nm, respectively (Fig. 4.17(a)). Since the latter indicates self-aggregated **NiBu**, it is noted that the complexation is incomplete. In other words, a substantial fraction of self-aggregated **NiBu** indicates that the hydrogen-bonded dimer of *enol*1-type is fairly stable. The position and intensity of the UV/Vis absorption maximum at 414nm, strongly supports a complexed enol-type structure of **NiBu**. The hydrogen bond between one of the NH proton of **DAC** and the enol oxygen

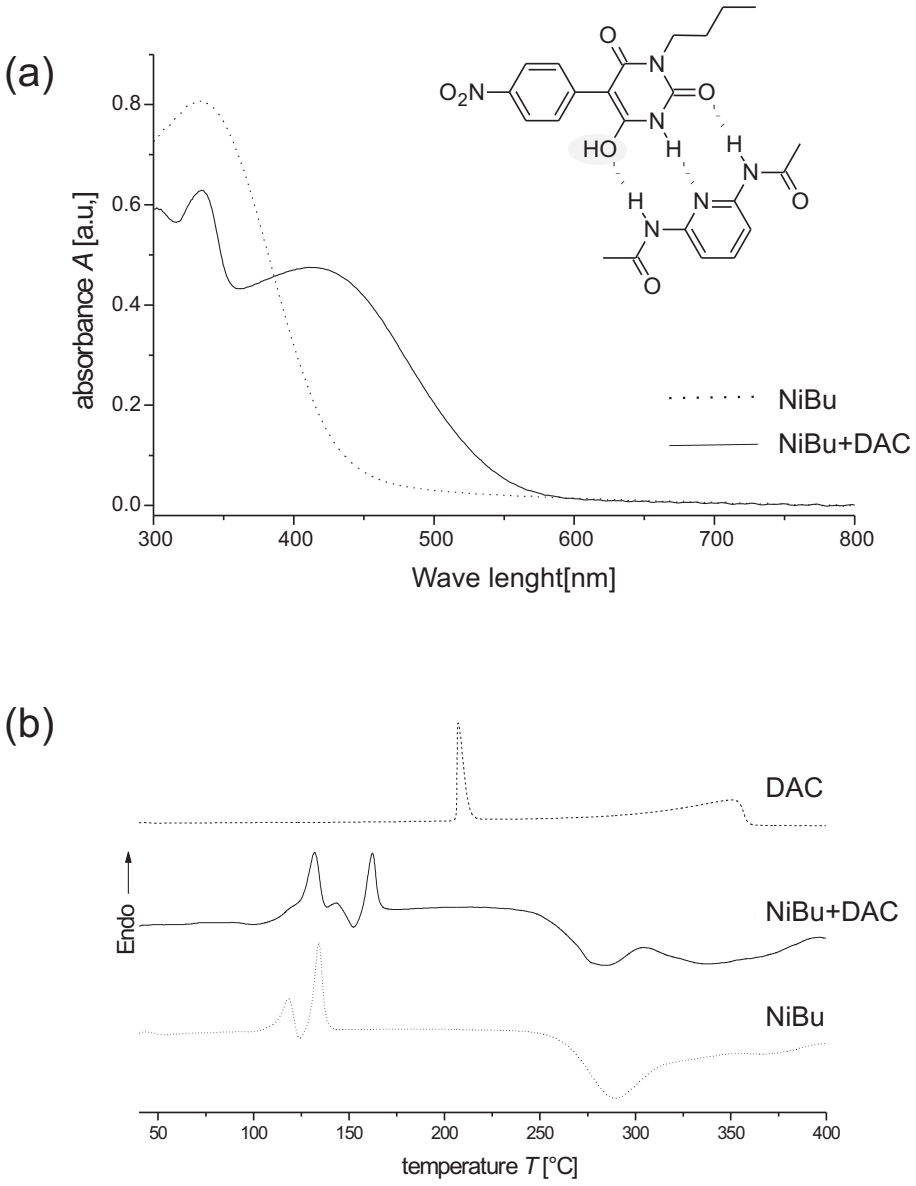

Figure 4.17: *The solid-state UV/Vis spectra (a) and DSC thermograms (b) of the complex NiBu+DAC in comparison with the starting compounds. In the UV/Vis spectrum, the self-aggregated enol1-type structure absorbs at 334 nm, whereas the complexed enol shows an absorption maximum at 414 nm. The DSC trace exhibits two endothermic transitions of unbound NiBu at approximately 110°C and at 121°C , respectively. The weaker transition at 132°C is attributed to the melting process of the complex that is affected by the presence of unbound DAC. Done by Ina Bolz.*

decreases the +M-effect of the barbiturate, which is indicated by a hypsochromic shift ($\Delta\lambda$=6 nm) of the UV/Vis absorption band of **NiBu** in contrast to dynamic solution-state UV/Vis studies.
In good agreement with the UV/Vis spectrum, the DSC trace of the compound **NiBu+DAC** shows three endothermic peaks as well as a broad exothermic peak (Fig. 4.17(b)). Both, the small shoulder at about 110°C and the first endothermic peak at 121°C are attributed to self-aggregated **NiBu**, while the second endothermic transition at 132°C may result from an eutectic behavior of the complex **NiBu+DAC**. In contrast, the third transition at 154°C reflects unbound **DAC** that is affected by the presence of the complex. Finally, the broad exothermic peak at 254°C indicates the decomposition of **NiBu**. Based on the UV/Vis and DSC result the possible complex structure is suggested. It is assumed that the instability of **NiBu+DAC** system is due to the repulsion of the OH proton of NiBu from the NH proton of **DAC** changing the local electron density on the enol oxygen.

With **DAC**, the ^{1}H MAS NMR spectrum of this complex exhibits three exchangeable proton sites at 16.3 ppm, 12.3 ppm, and 10.3 ppm, respectively. Considering the signal intensities, it appears that the resonance at 10.3 ppm contains two protons. Since the two NH protons in pure **DAC** resonate at 9.2 ppm and 10.4 ppm, it is assumed that the NH proton of **NiBu** and one of the NH protons of **DAC** overlap at about 10.3 ppm. Notably, in the complex **NiBu+DAC**, the OH proton resonance of **NiBu** is substantially 5 ppm downfield shifted compared to pure **NiBu**, reflecting that this proton is involved in hydrogen-bonding. However, the complex shows a dynamic structural fluctuation in the solid-state, as evidenced in the time-dependent ^{1}H MAS spectra, where two additional exchangeable protons sites appear over a time period of 10 days (Fig. 4.18). So due to the instability of **NiBu+DAC** system, solid state NMR experiment cannot support the idea suggested by UV/Vis and DSC works. Moreover if **NiBu+DAC** system is composed of several possible aggregation which showing similar chemical shift values it is very difficult to distinguish each of them. The homonuclear dipolar ^{1}H DQ MAS NMR spectrum of **NiBu+DAC** (freshly prepared complex) shows several cross-correlation peak in hydrogen bonding region (Fig. 4.19). Based on the observation of highly shifted -OH proton chemical shift, it can be simply hypothesized that the -OH proton might be trapped by **DAC** base and make hydrogen bonding one of the NH protons of **DAC**.

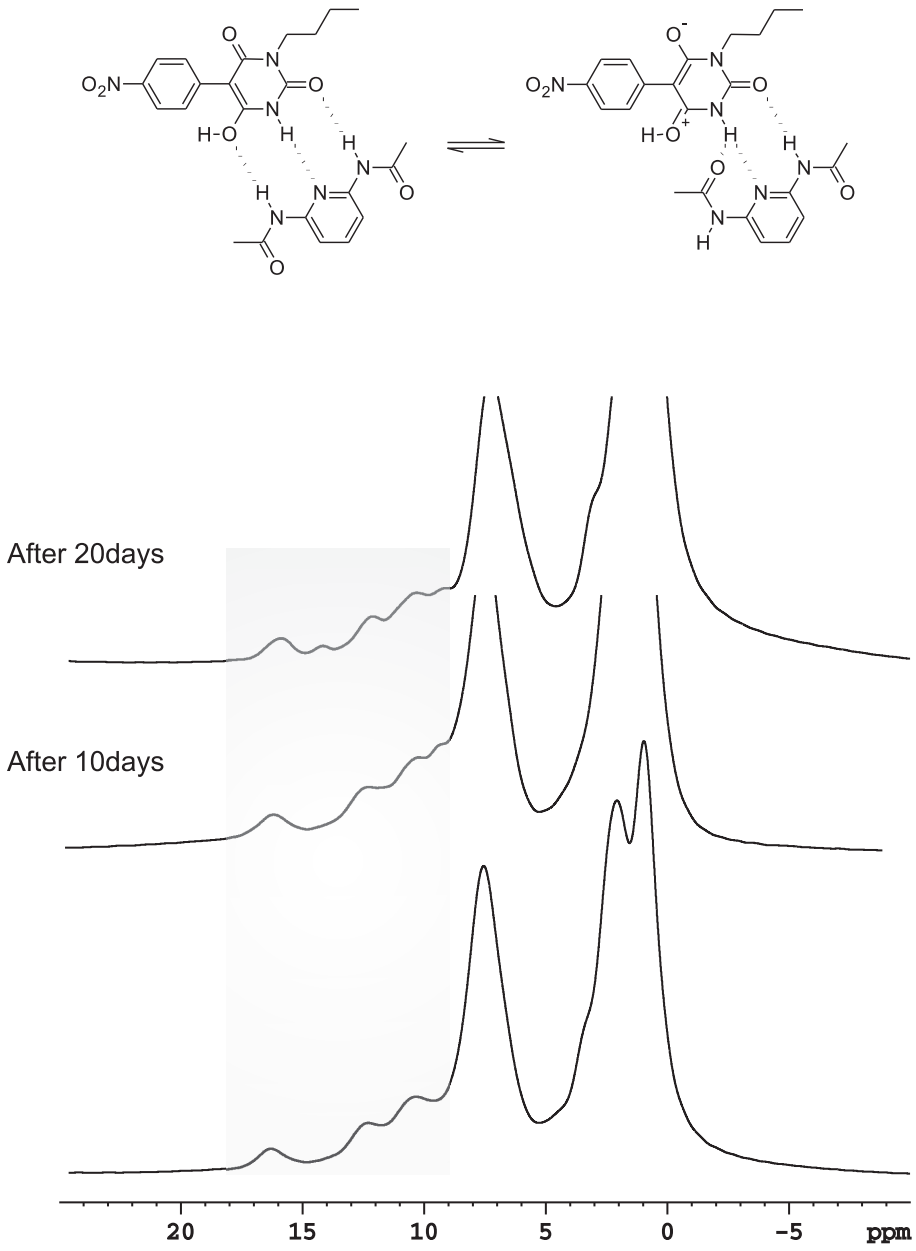

Figure 4.18: *Time-dependent ^1H MAS NMR spectra of the complex NiBu+DAC. After 10 days and 20 days, two additional exchangeable protons are observed at 9.3 ppm and 14.2 ppm. It is assumed that the repulsion between the OH proton of NiBu and the NH proton of DAC changes the electron density on the enol oxygen resulting in an oxonium structure.*

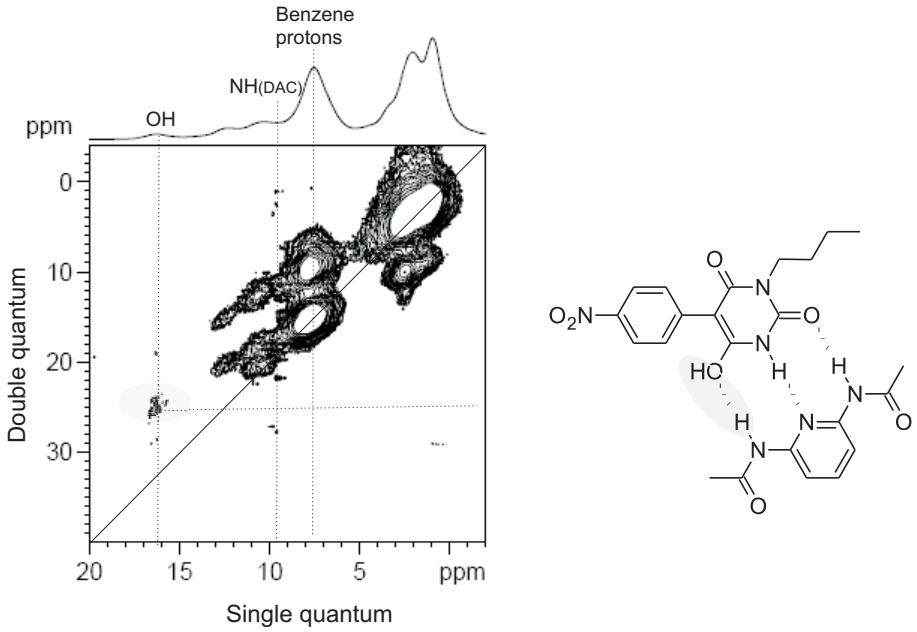

Figure 4.19: ^{1}H *DQ MAS of NiBu+DAC*

4.5 NiBu + 2,6-diaminopyridine(DAP) complex

In the following, **NiBu** is reacted with **2,6-diaminopyridine (DAP)** at a 1:1 ratio. **DAP** also offers a complementary hydrogen-bonding pattern but it is a considerably stronger base than **DAC** due to the much larger electron donating effect of the NH_2 group in comparison to the amide function of **DAC** [Kaljurand 05, Yu 99] . The solid state ^{1}H MAS and ^{13}C CPMAS spectra of pure **DAP** are shown in Fig. 4.20.

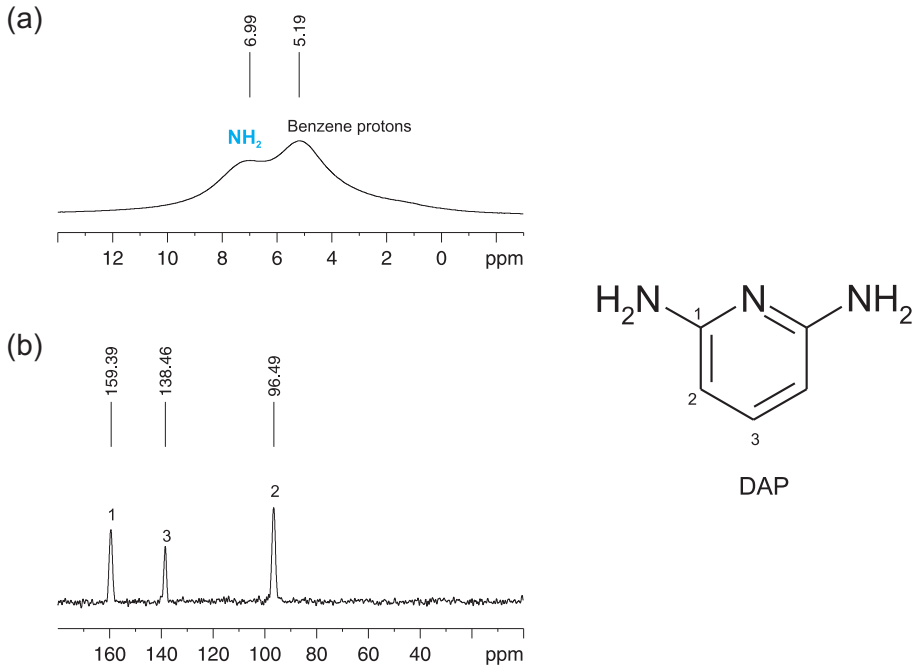

Figure 4.20: *(a) ^{1}H-MAS and (b) ^{13}C -CPMAS spectra of DAP*

Since **DAP** is a stronger base than **DAC** (The pK_a values of used bases in this study are shown in Table 4.1) it is anticipated that the **DAP** will trap the -OH proton(-OH is more acidic than -NH) of **NiBu**, while forming a hydrogen-bonded complex of **NiBu+DAP**.

However, the corresponding solid state NMR results reveal a rather different situation: the ^{1}H MAS NMR spectrum of **NiBu+DAP** displays exchangeable protons at 11-12ppm, but the resolution is not sufficient to detect how many protons exist in that region. However, ^{1}H 2D DQ spectrum displays two exchangeable protons at 11.8 ppm and 12.4 ppm, respectively (Fig. 4.21). Based on the presence of a strong autocorrelation peak at 11.8+11.8=23.6ppm in double quantum dimension (F_1) in ^{1}H DQ MAS spectrum of **NiBu+DAP**, the resonance at 11.8 ppm was assigned to the NH proton of the barbiturate. In addition, the lack of an unambiguous (NH-OH) cross

	pK_a values in CH_3CN	pK_a values in H_2O
NiBu+DAC	-	3.86[a]
NiBu+DAP	14.77	6.00
NiBu+PS	18.62	12.10

Table 4.1: *Comparison of the pK_a values of the conjugated acids of the used bases DAC, DAP, and PS. (a) calculated using Advanced Chemistry Development (ACD/Labs) Software V8.14 for Solaris. Done by Ina Bolz.*

peak most likely results from salt formation due to proton transfer reaction yielding a **DAP**-trapped proton which is observed at 12.4 ppm in single-quantum dimension (Fig. 4.21). This trapped proton also reveals itself by the presence of a weak cross peak with the NH_2 protons of **DAP**. However, in liquid-state ^{1}H NMR titration experiments [Bolz 06], a **DAP**-trapped proton is observed at 11 ppm. Therefore, it can be concluded that packing effects in the solid-state may strengthen hydrogen bonds. Furthermore, the (NH-NH) auto-correlation peak reveals the persistence of a dimeric structure of the enolate anion.

The suggested complex structure of **NiBu+DAP** system becomes more evident supported by model compound **Bu**. The structure of **Bu** is already shown in section 4.1. The ^{1}H DQ MAS spectrum of **Bu+DAP** is similar to that of **NiBu+DAP**. Moreover, in the ^{1}H DQ MAS spectrum of **Bu+DAP** nicely resolved auto correlation peak (NH-NH) is observed (Fig. 4.22). In the view point of solid state NMR work, **Bu+DAP** shows better resolution than **NiBu+DAP** and it can be anticipated that the complex structures are nearly same. The -NO_2 group does not have big influence on arranging the complex structure. It should be emphasized that in all cases where **NiBu** is reacted with the adenine-mimetic bases **DAC** and **DAP**, respectively, only partial complexation or salt formation is observed as shown by both UV/Vis spectroscopy as well as DSC analyses. Rather, a substantial fraction of self-aggregated **NiBu** is retained indicating that the hydrogen-bonded dimer of *enol*1-type NiBu is fairly stable. However, in the solid state NMR, the observation of enol type NiBu is difficult for majorly resolution problem and sensitivity problem.

It is evident that the cross peaks between the H^+ and the aromatic protons and the aliphatic protons are missing at the aliphatic SQ frequency. This phenomenon is commonly observed for cross peaks to alkyl chain protons.

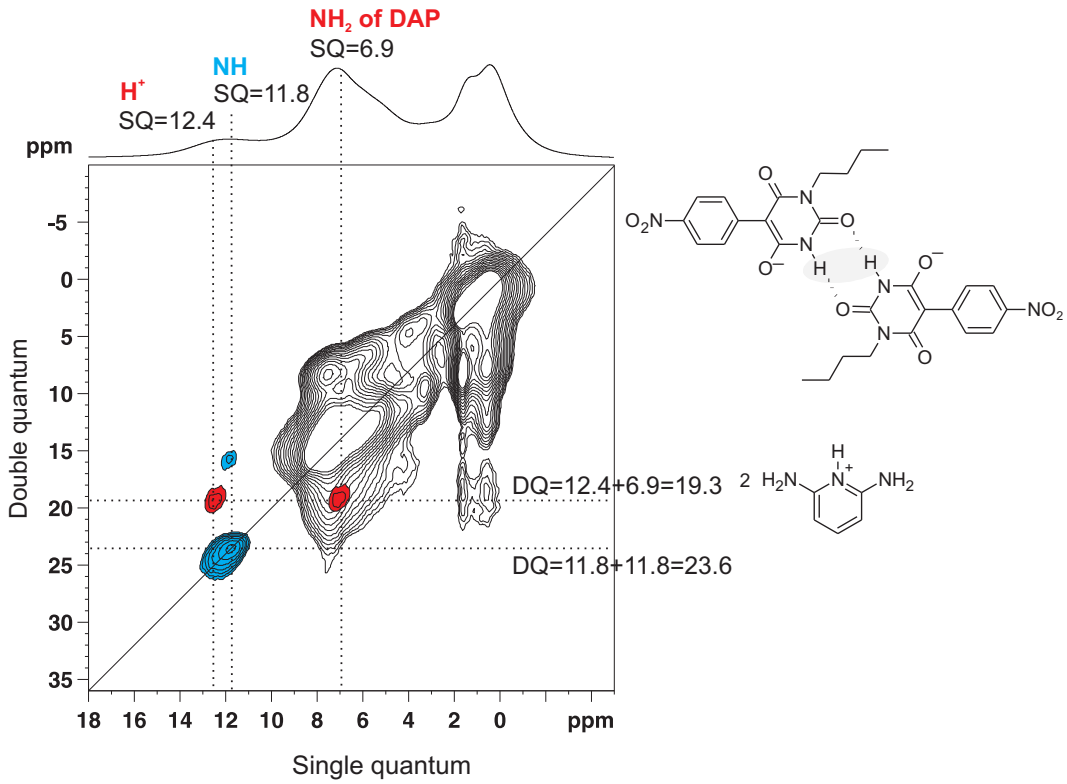

Figure 4.21: ^{1}H *DQ MAS spectrum of NiBu+DAP.*

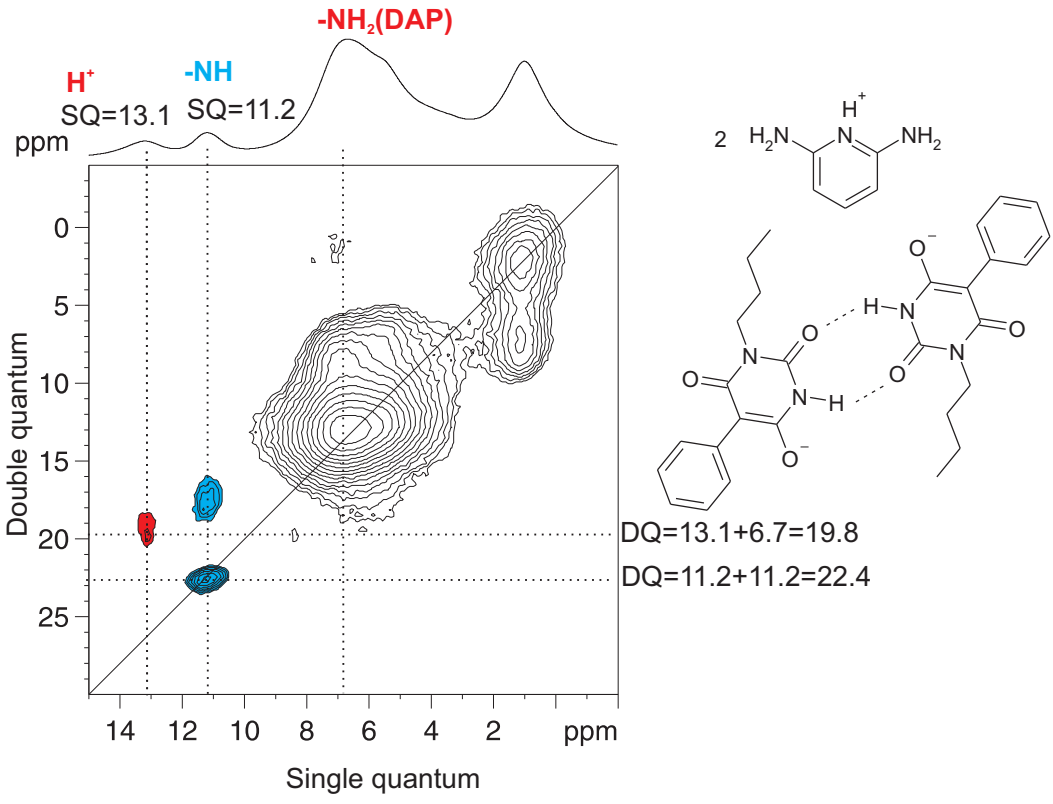

Figure 4.22: ^{1}H *DQ MAS spectrum of Bu+DAP.*

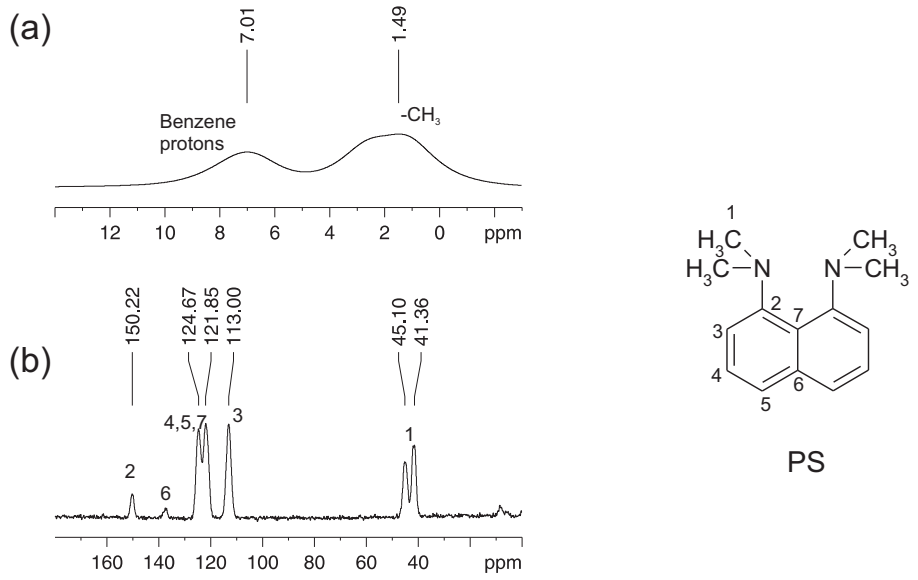

Figure 4.23: *^{1}H-MAS and ^{13}C -CPMAS of PS*

4.6 NiBu + Proton Sponge(PS) complex

Complex formation can be enforced upon addition of the so-called **Proton Sponge(PS: 1,8-bis(dimethylamino)-naphthalene)**. Proton sponge shows both high thermodynamic basicity and slow intermolecular proton transfer kinetics [Llamas-Saiz 94, Alder 89, Staab 88], and thus, facilitate complete deprotonation of **NiBu**. The structure of **PS** and it's ^{1}H and ^{13}C-CPMAS spectra are shown in Fig. 4.23.

Indeed, the ^{1}H-MAS NMR spectrum of **NiBu+PS** exhibits a high-frequency shifted resonance at 18.0 ppm that is not observed for both pure **PS** or **NiBu** and which is much more highly shifted than **DAP** case.

It reflects a chelated proton resulting from the acid-base reaction of **PS** and the acidic OH proton of **NiBu** while the NH proton peak at 10.5 ppm is maintained. This assignment is backed-up by *ab initio* DFT chemical shift calculations, where the chemical shifts of both the chelated proton and the NH proton of the enolate anion are computed at 19.0 ppm and 9.9 ppm, respectively. The homonuclear dipolar ^{1}H DQ MAS NMR spectrum of **NiBu+PS** is shown in Fig. 4.24. The strong (NH-NH) auto-correlation peak proves the dimeric structure of the enolate anion of **NiBu** in the same way as for **NiBu+DAP**. Further support for this complex structure stems from the ^{1}H -^{13}C REPT-HSQC spectrum, where the chelated proton shows cross peaks with several carbons of **PS** but no interaction with **NiBu**. (Fig. 4.25). Taken together, this

demonstrates that the dimeric unit in **NiBu** is not affected by the presence of the proton sponge and the -H^+ proton is strongly associated with **PS**. Indeed, this behavior is quite expected since **PS** does not possess a molecular recognition sequence suitable for selective binding to an ADA sequence offered by the enolate anion.

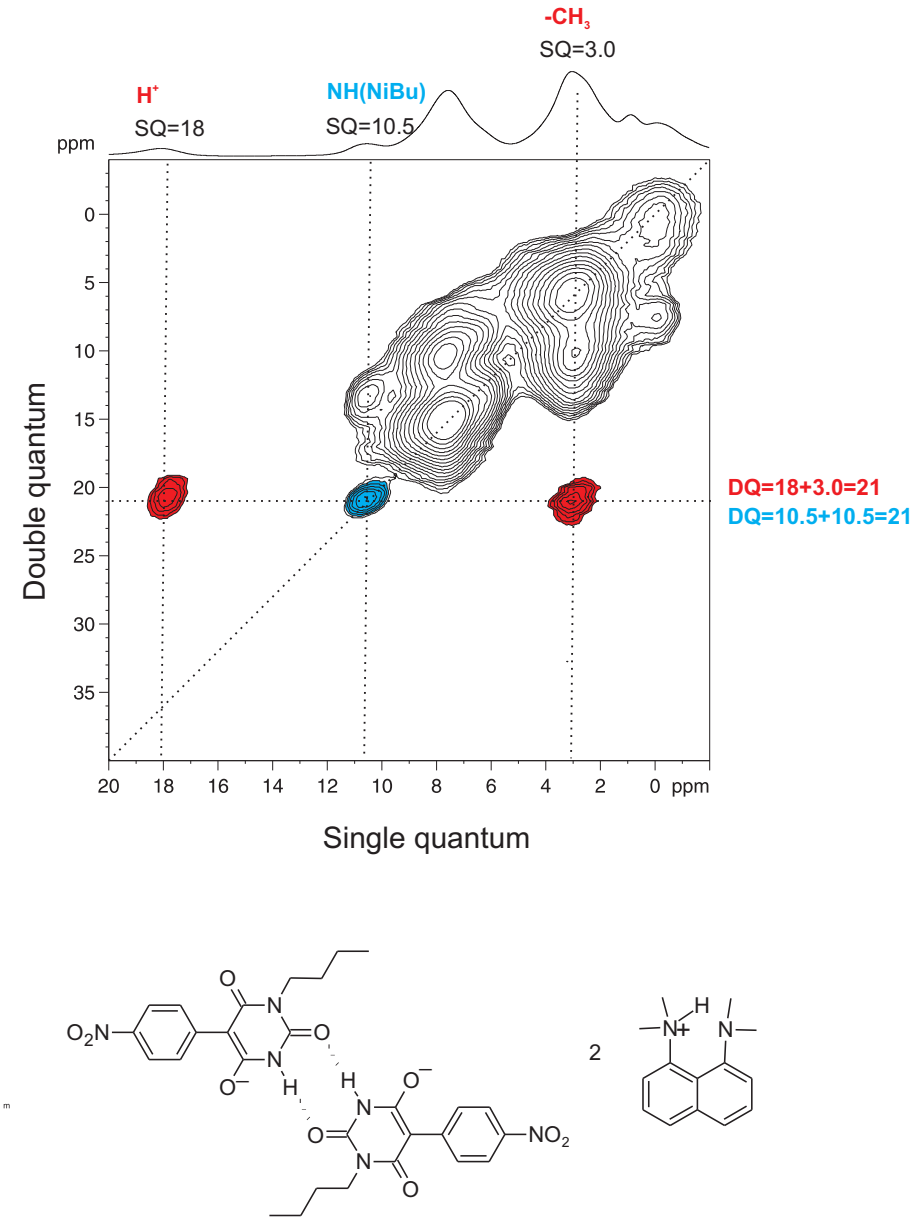

Figure 4.24: ^{1}H *DQ MAS spectrum of NiBu+PS and Dimer structure*

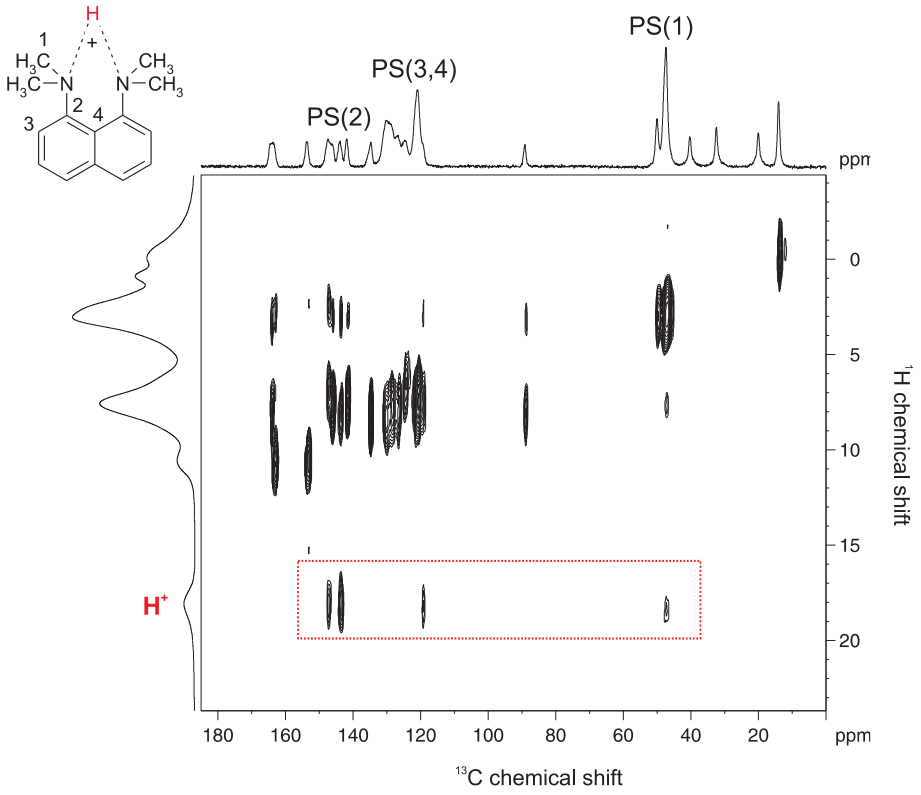

Figure 4.25: *Two-dimensional ^1H -^{13}C REPT-HSQC spectrum of NiBu+PS obtained under MAS at 30kHz and $\tau_{rcpl}=4\tau_R$.*

4.7 NiBu+PS+DAC complex

Adding the adenine-mimetic base **2,6-diacetamidopyridine (DAC)** to the system **NiBu+PS**, we offer a complementary hydrogen-bonding pattern to the enolate anion of **NiBu**, which should allow for complex formation as suggested from liquid-state ^{1}H NMR titration data [Bolz 06]. Three different exchangeable proton sites are resolved at 19.0 ppm (chelated proton), 11.6 and 10.0 ppm in the solid-state ^{1}H MAS NMR spectrum of the mixture **NiBu+PS+DAC**.

The resonance at 10.0 ppm contains two NH protons, the NH proton of the enolate anion of **NiBu** and one of the NH protons of **DAC**. Again, the formation of the enolate anion of **NiBu** in the presence of **PS** is evidenced by a strong DQ cross-peak between the chelated proton at 19.0 ppm and the methyl protons of **PS** at 2.6 ppm in the corresponding ^{1}H DQ MAS NMR spectrum (Fig. 4.26).

Most importantly, the cross-peak between -NH proton of **DAC** and -NH of **NiBu** was observed, which highly implies that the former dimer of the enolate anions like in **NiBu+PS** is broken and, rather, suggests the formation of an enolate **NiBu+DAC** complex fulfilling the complementary hydrogen-bonding pattern.

This assumption is supported by an *ab initio* chemical shift calculation using an optimized geometry of the enolate **NiBu+DAC** complex (Fig. 4.27). The computation yielded chemical shifts of 12.1 ppm (NH proton of **DAC**), 12.9 ppm (NH' proton of **DAC**), and 12.2 ppm (NH of **NiBu**) indicating moderate hydrogen-bonding strengths. Summarizing all the observation (liquid state ^{1}H NMR titration [Bolz 06], solid state ^{1}H DQ MAS experiment, DFT calculation), the new complex structure is suggested like in Fig. 4.26(b).

With the aid of ^{1}H -^{13}C REPT-HSQC experiment (Fig. 4.28), clear ^{1}H and ^{13}C chemical shift assignments were possible. The strong signal for the peaks at 168-172 ppm in F_2 dimension (^{13}C dimension) can be assigned due to the strong intramolecular interaction between -NH protons and carbonyl carbons of **DAC**, which confirms the two different -NH proton sites. However, based on the suggested complex structure of **NiBu+PS+DAC**, the peak at 172ppm in F_2 dimension might contain the intermolecular contact between -NH proton of **NiBu** and carbonyl carbon 1 of **DAC** (Fig. 4.28). The carbon 6 and 8 of **NiBu** and carbon 3 of **DAC**, carbon 5 of **NiBu** show cross peaks ranging broad region in ^{1}H dimension (Fig. 4.28).

The resulting cross peak between -NH protons of **DAC** and -NH of enolate is more clearly seen in the ^{1}H DQ MAS spectrum of **Bu+PS+DAC**. To derive solid state NMR result more clearly, **Bu** system is again employed for comparison with **NiBu**. Before investigating **Bu+PS+DAC** system, **Bu+PS** is measured first to confirm that **Bu** is

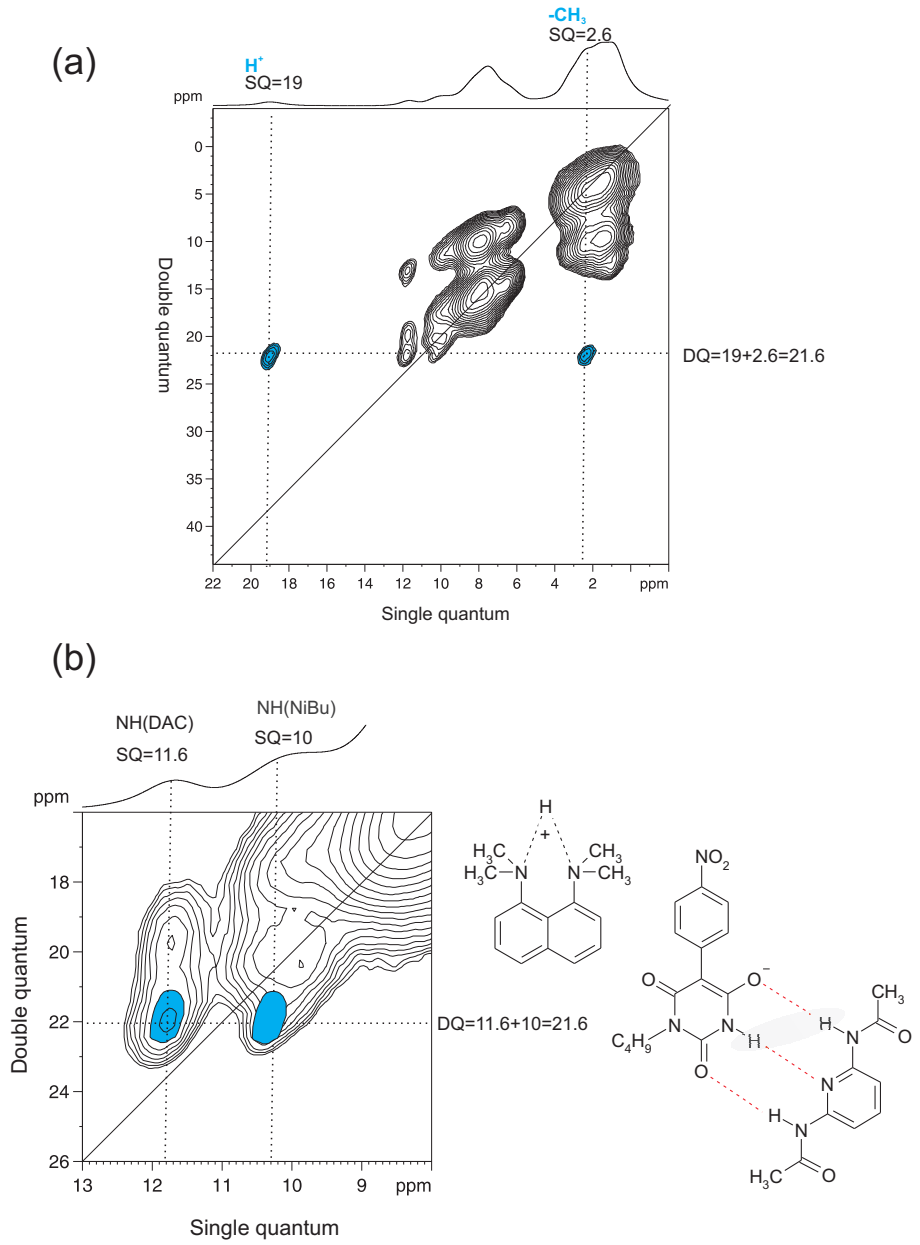

Figure 4.26: *(a)* ^{1}H *DQ MAS spectrum of NiBu+Ps+DAC and (b) expanded spectrum and complex structure*

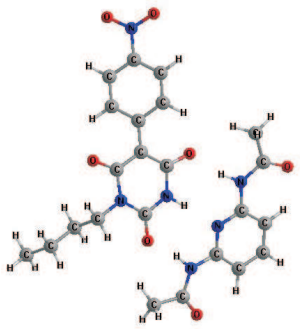

Figure 4.27: *The optimized structure of enolate NiBu+DAC complex using the ADF program and BLYP/TZ2P level of theory. The computed distances are: N-H—O=C (d=1.83(8) Å, D=2.86(4) Å; d=1.86(2) Å, D=2.88(6) Å; N-H—N (d=2.02(6) Å, D=3.05(6) Å) Done by G.Brunklaus*

present in enolate form only with **PS**. Regardless of -NO_2 functional group, again in solid state NMR result, **Bu** is enolate form and shows same result with **NiBu+PS**. The ^{1}H spectrum of **Bu+PS+DAC** looks very similar to that of **NiBu+PS+DAC**. It shows two exchangeable protons at 10.4ppm and 11.5ppm.(except the PS trapped hydrogen at 18ppm). However, the relative intensity of these two peaks is 2:1 ratio.(In case of **NiBu+PS+DAC**, it is 1:2 ratio). So in **Bu** case the peak at 11.5 ppm is assigned to NH(**NiBu**) and NH(**DAC**). The peak at 10.5ppm is assigned to the other -NH of **DAC**. In Fig. 4.29 the comparison of the ^{1}H spectra of **NiBu** and **Bu** system is shown. In ^{1}H 2D DQ spectrum of **Bu+PS+DAC** (Fig. 4.30), clearly the NH-NH auto correlation peak disappeared, which implies the breaking of enolate dimer structure of **Bu**. Instead, the cross peak between -NH(**Bu**) and -NH of (**DAC**) is observed more clearly than **NiBu+Ps+DAC** system. However, with better resolution spectrum (than **NiBu+PS+DAC**) it is clear only one -NH proton of **DAC** shows cross peak. Possible explanation for that may be that the -NH proton of **DAC** which makes hydrogen bonding with negatively charged oxygen atom of **NiBu** enolate show cross peak in ^{1}H 2D DQ spectrum. Further work will be performed in this respect.

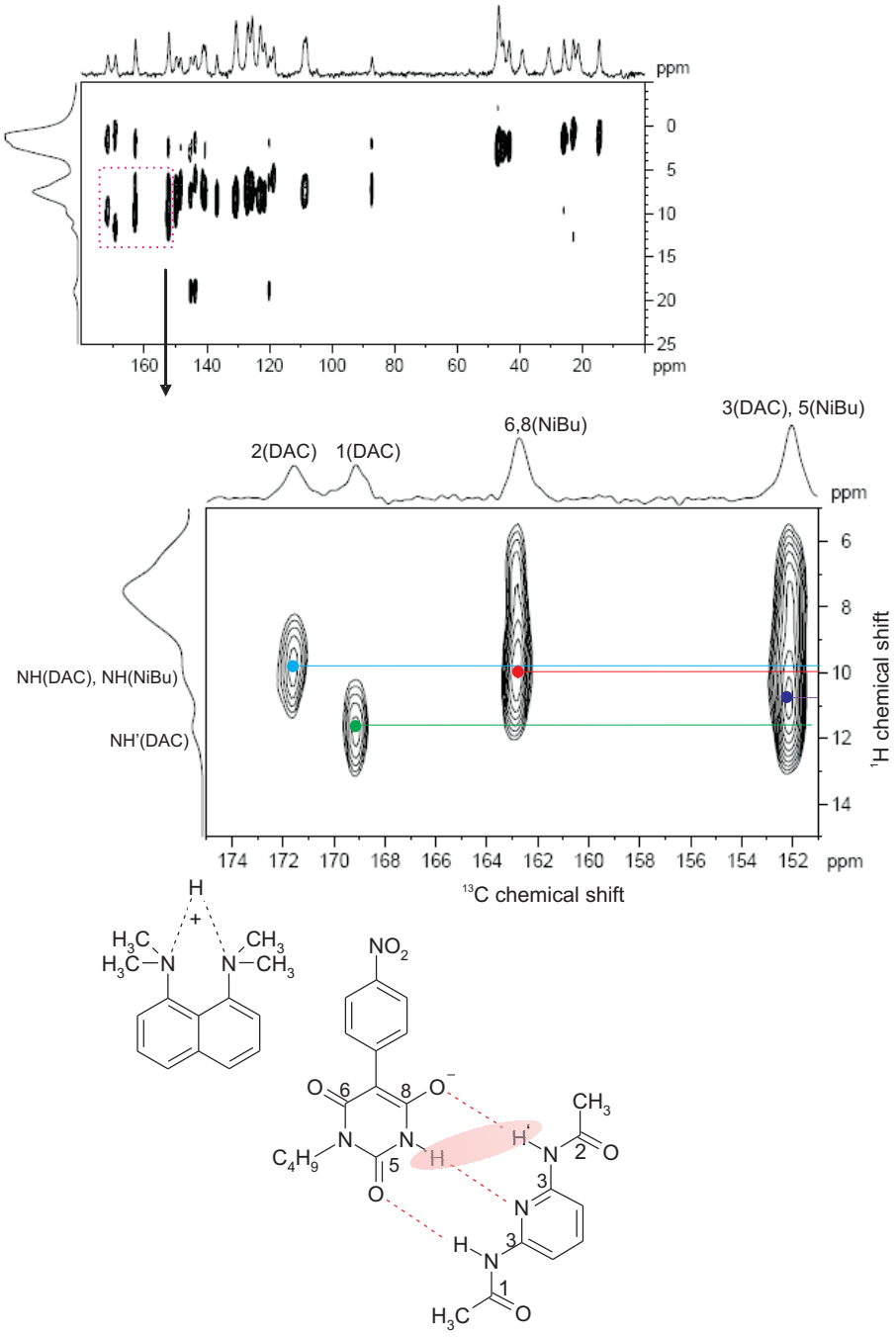

Figure 4.28: *Two-dimensional* ^{1}H *-*^{13}C *REPT-HSQC spectrum of NiBu+PS+DAC obtained under MAS at 30kHz and* $\tau_{rcpl}=4\tau_R$.

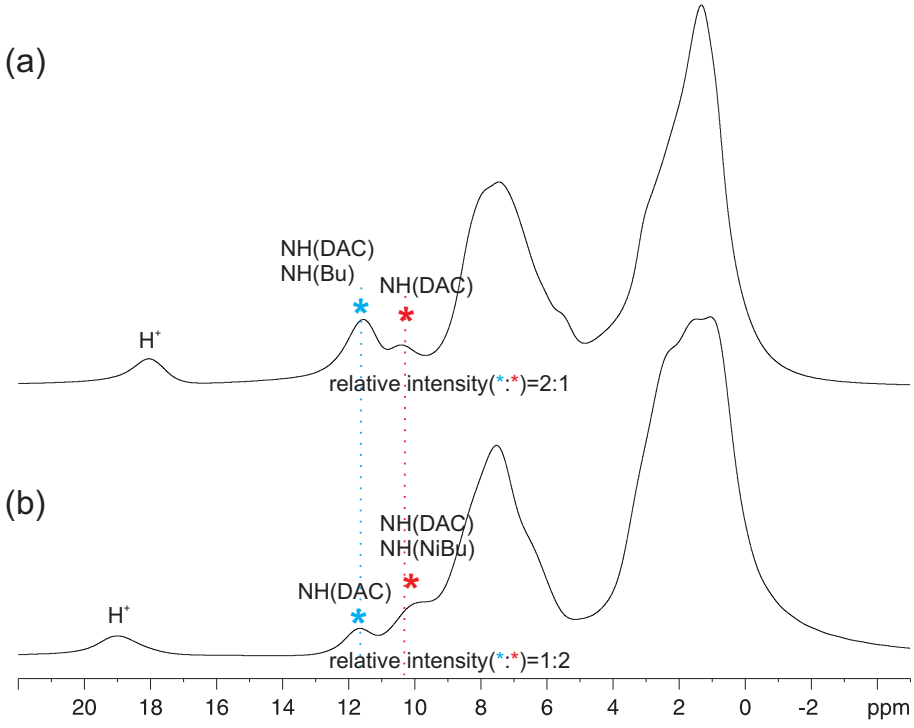

Figure 4.29: *The comparison of* ^1H *-MAS of (a)Bu+PS+DAC and (b)NiBu+PS+DAC*

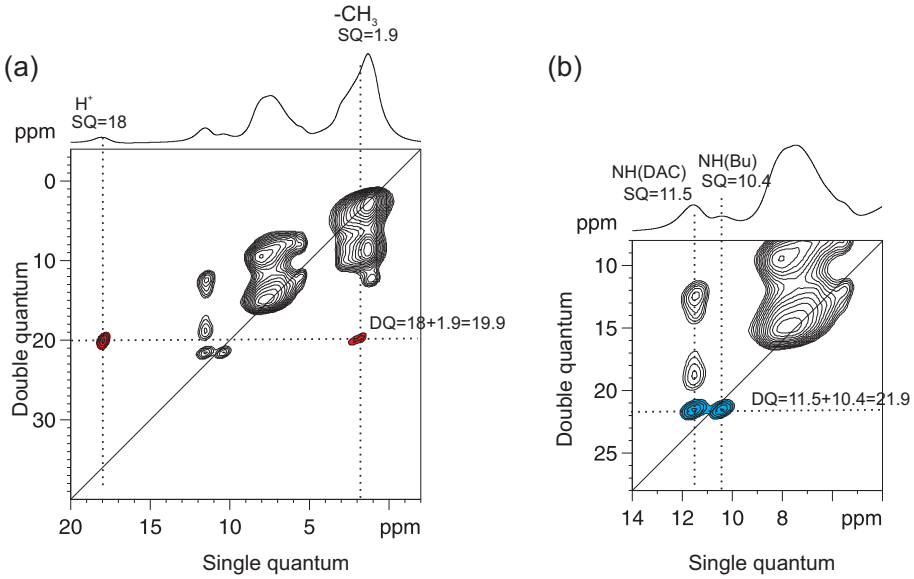

Figure 4.30: *(a)* ^1H *DQ MAS spectrum of Bu+PS+DAC (b) expanded spectrum*

4.8 1,3-dimethyl-5-(4-nitrophenyl)-barbituric acid(NiDMe) complexes

In addition to **Bu**, **"1,3-dimethyl-5-(4-nitrophenyl)-barbituric acid" (NiDMe)** served as a simplified reference compound, since **NiDMe** has only one exchangeable proton. The -NH protons are modified to -NCH_3, with no proton donating group in pure **NiDMe**, and thus, it can help to better understand the solid state NMR data of **NiBu**. It has also chromophoric properties due to the attached -NO_2 functional group that elongates the conjugated π-system. The same bases for **NiBu** system are used as counter base part (**Ps**> **DAP**> **DAC** : in the order of basicity). The **NiDMe** mixtures not only corroborate the results obtained for **NiBu**, but also demonstrate systematic changes of NMR spectra depending on strength of the corresponding base.

4.8.1 ^{1}H and ^{13}C spectra of NiDMe family

Indeed, depending on the basicity of each base, the complexes show different NMR spectra. All ^{1}H and ^{13}C spectra of **NiDMe** family are shown in Fig. 4.31. Particular attention is given to the region between 10-15ppm for ^{1}H spectra (corresponding to hydrogen-bonded protons) and 50-60 ppm for ^{13}C spectra (methine carbon region), respectively. The presence of a methine carbon resonance at 55ppm and the lack of an -OH proton of pure **NiDMe** clearly confirms that it exists in keto form. However, upon reaction with the relatively strong base **PS**, **NiDMe** is changed into enolate form, which is accompanied by both a new carbon peak at 90 ppm and the appearance of a proton peak at 18 ppm attributed to the "trapped" proton. Even in the presence of moderately strong bases like **DAP**, **NiDMe** is still present in enolate form with the trapped proton (-H^{+}) peak at 12.5 ppm, being significantly less downfield shifted when compared with **PS**, which in turn suggests weaker hydrogen bonding to the base. In contrast to **PS** and **DAP**, **NiDMe** still exists in keto form upon mixing with the rather weak base **DAC**, reflected by only slightly shifted resonances in the corresponding proton spectrum. No salt formation is observed.

4.8.2 ^{1}H DQ MAS spectra of NiDMe family

In the previous section, it has been shown that one dimensional ^{1}H - MAS and ^{13}C CPMAS spectra can provide information whether or not salt formation occurred. To gain further insight into possible complex structures, ^{1}H DQ MAS spectra were acquired (Fig. 4.32). Indeed, the DQ-spectrum of **NiDMe+PS** is highly reminiscent of

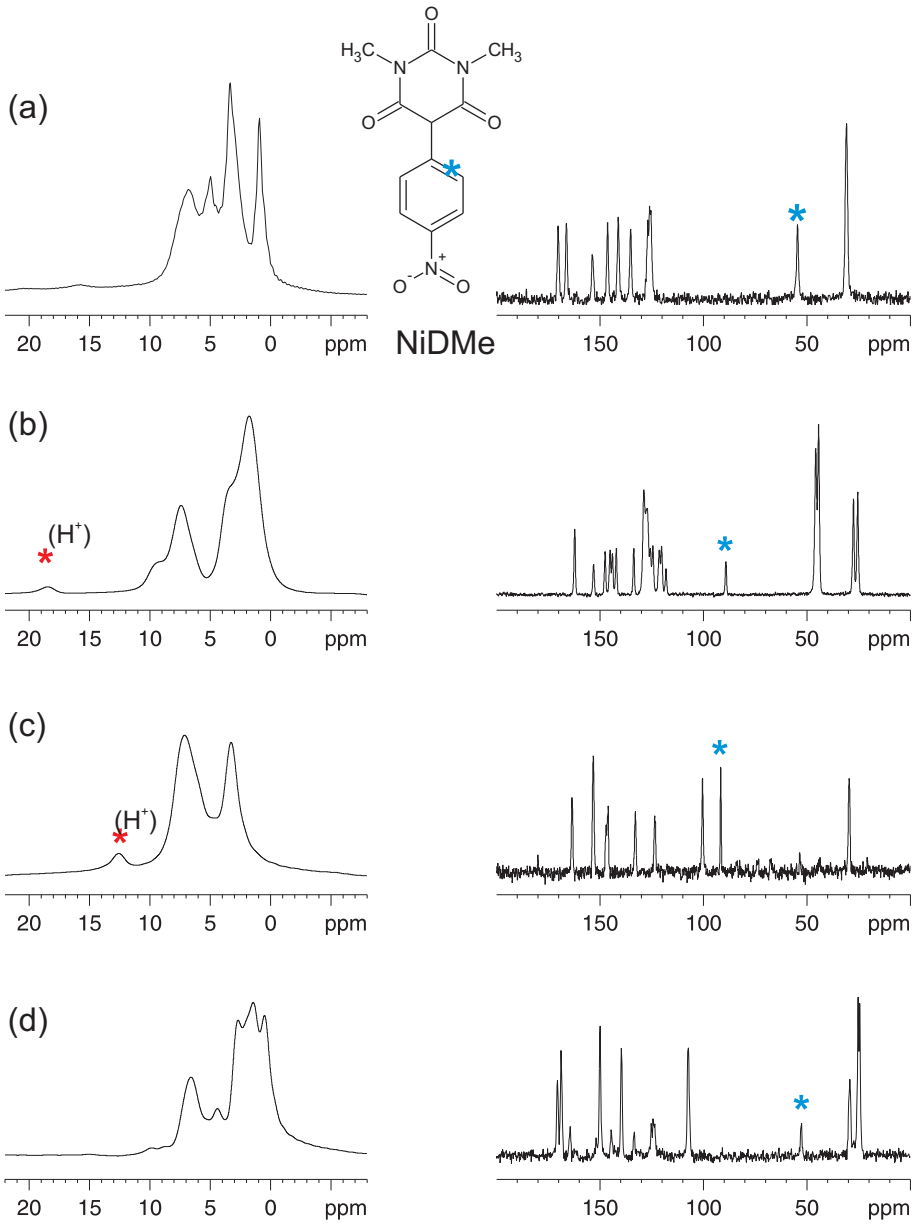

Figure 4.31: *Comparisons of ^{1}H and ^{13}C spectra of NiDMe family (left : ^{1}H spectra right : ^{13}C spectra) (a) pure NiDMe (b) NiDMe+PS (c) NiDMe+DAP (d) NiDMe+DAC*

NiBu+PS. The trapped proton(H^+) reveals DQ contacts only to the -CH_3 protons of proton sponge, and, hence, appears rather isolated from the **NiDMe** moiety (here, the proton peaks at 1.8 ppm are assigned to -CH_3 of **PS**.) The position of the center of this peak corresponds to a SQ frequency slightly shifted from the maximum in the SQ projection, which is, however, not surprising since the three methyl group protons are likely to give rise to proton resonances with slightly different chemical shifts.

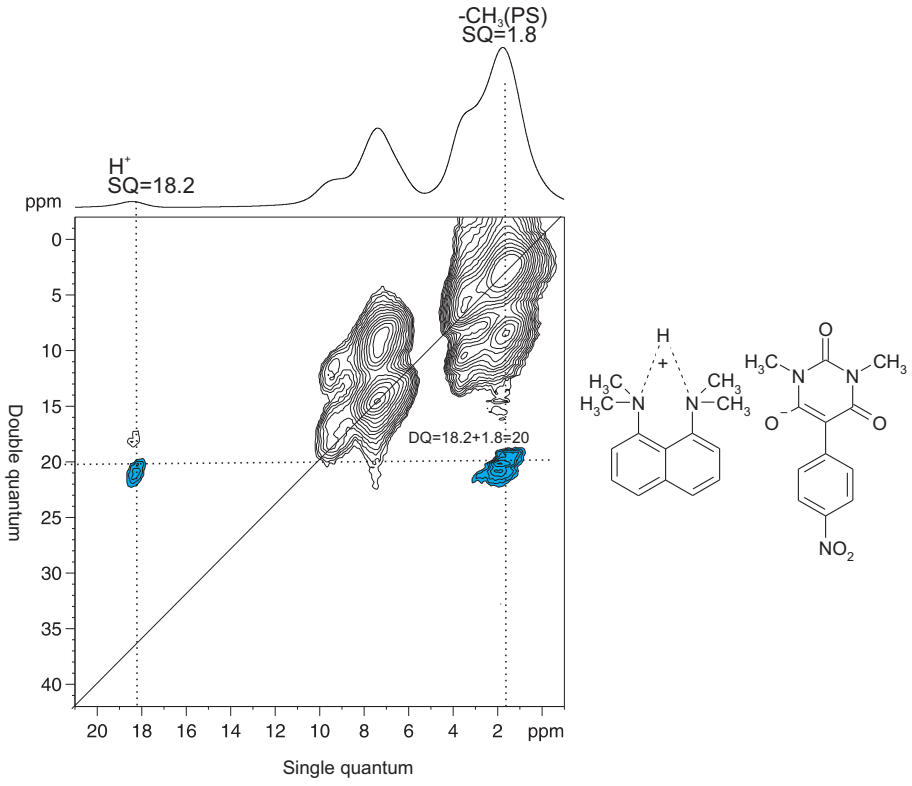

Figure 4.32: ^1H *DQ MAS of NiDMe+PS at* $\tau_{rcpl}=2\tau_R$

However, for **NiDMe+DAP**, it appears that the trapped (H^+) proton shows two cross-peaks in the DQ spectrum using an excitation of two rotor period: a cross peak with -NH_2 protons of **DAP**, which is highly expected from the previous data, as well as a cross peak with the -CH_3 protons of **NiDMe** (Fig. 4.33). The latter may be explained by solid state packing effects that possibly allow for close proximity of the trapped (H^+) proton and the -CH_3 protons. Such solid state packing effect most likely are removed in solution state, as indeed evidenced by a NOESY-type experiment in solution (MeOD), with **NiDMe** in enolate form similar to the solid state.

As expected, the NOESY spectrum in Fig. 4.34, the trapped (H^+) peak shows cross peaks only with the -NH_2 group of **DAP**.

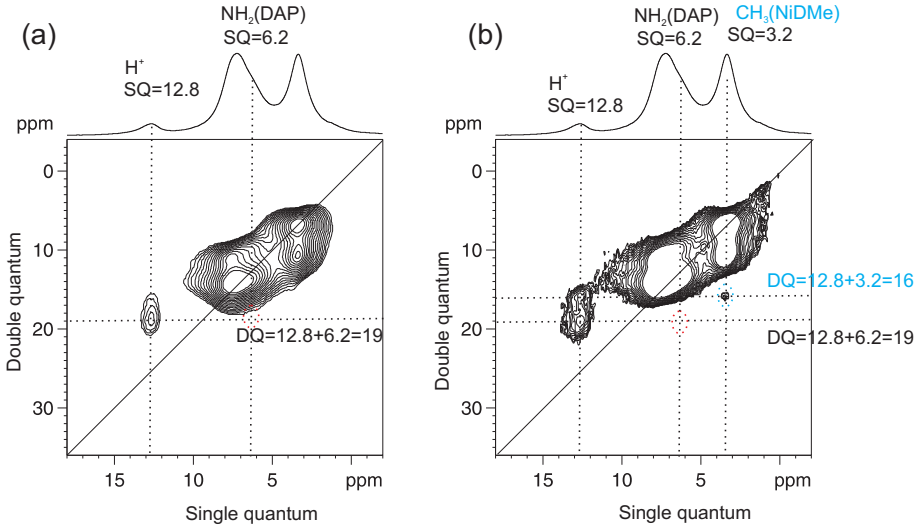

Figure 4.33: ^{1}*H DQ MAS spectra of NiDMe+DAP at (a)* $\tau_{rcpl}=1\tau_R$ *and (b)* $\tau_{rcpl}=2\tau_R$

In both mixtures, **NiDMe+DAP** and **NiDMe+PS**, mere salt formation occurred but the strongly bonded (H^+) proton of **NiDMe+PS** system seems relatively isolated from **NiDMe**, while for **NiDMe+DAP**, stronger interactions are observed.

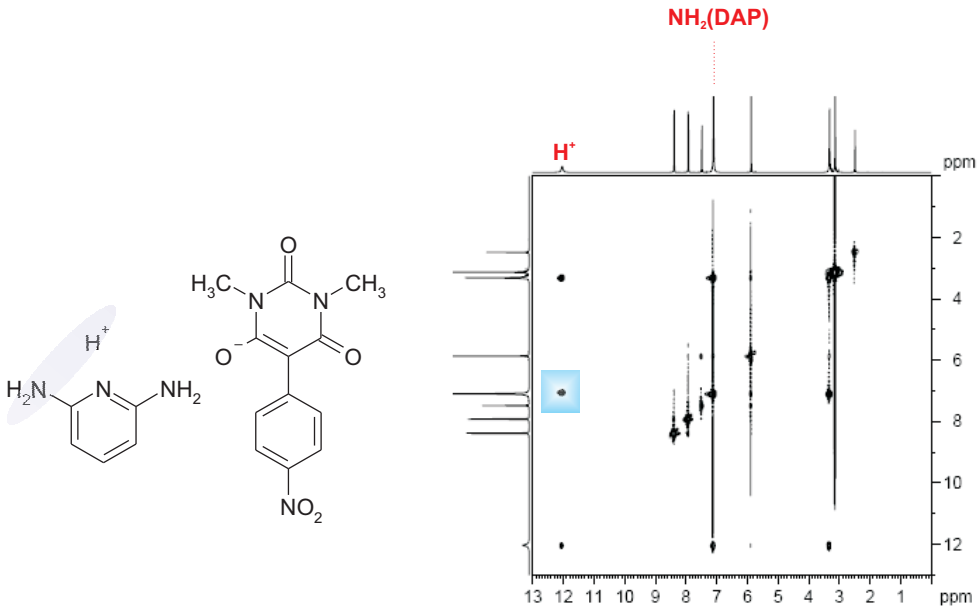

Figure 4.34: *Liquid state ^1H and 2D-NOESY of NDMe+DAP in MeOD (the peak in colored region is the cross peak between H^+ and NH_2 protons.)*

4.9 Conclusions

In this Chapter the solid state structures of barbituric acid derivatives and their corresponding assemblies with three different bases are investigated by advanced solid state NMR experiments. In particular ^{1}H DQ MAS has been extensively applied to provide insights into the role of hydrogen bonding in determining the adopted supramolecular structure.

1-*n*-butyl-5-phenyl barbituric acid (Bu) was found to be present in keto form in solid state, which was proved by the inspection of ^{1}H MAS and ^{13}C CPMAS spectra. Based on the observation of a strong NH-NH auto correlation peak in the ^{1}H DQ MAS spectrum, a dimeric hydrogen bonded structure of **Bu** could be revealed.

In contrast the novel enolizable solid chromophor **1-*n*-butyl-5-(4-nitrophenyl)-barbituric acid (NiBu)** preferably adopts an **enol1** form with vicinal NH and OH protons. However, due to severe signal overlap of the OH and NH proton resonances, the possible aggregation of **NiBu** could not be addressed directly. In the presence of strong bases like the so-called proton sponge (**PS**), a simple acid-base reaction occurred where the OH proton of **NiBu** is stripped, where the corresponding enolate anion of the **NiBu** dimeric structure reflects the stability of this arrangement. It was found that the enolic dimer can be broken upon addition of the adenine-mimetic base **2,6-diacetamidopyridine (DAC)**, providing a complementary hydrogen-bonding pattern. However, if that pattern is offered to pristine **NiBu**, as in the case of **NiBu+DAC**, complex formation competed with self-aggregation of **NiBu** in the solid-state. A similar competition was observed upon addition of **2,6-diaminopyridine (DAP)** to **NiBu**. In the latter case, salt formation due to proton transfer was preferred to hydrogen-bonded complexation.

Solid **1,3-dimethyl-5-(4-nitrophenyl)-barbituric acid (NiDMe)** is also present in keto form but it turned into an enolated structure with **PS** as previously observed for **NiBu**. Even in the presence of **DAP**, **NiDMe** is still present in enolate form with the trapped proton resonance at 12.5ppm in the ^{1}H MAS spectrum. However, with the rather weak base **DAC**, no salt formation was observed. Based on the ^{1}H DQ MAS experiments, it was concluded that the H^{+} proton of **NiDMe+PS** is more isolated than **NiDMe+DAP** system.

Chapter 5

Probing Self-Assembly by DOSY NMR

5.1 Introduction

Molecules in solution are in constant motion and experience both rotational and translational motion. The process of translational motion in solution is commonly referred to as self-diffusion and is defined with a self-diffusion coefficient D (m^2s^{-1}). The value of D may be approximated by the Stoke-Einstein equation :

$$D = \frac{k_B T}{6\pi\eta R_H} \tag{5.1}$$

where k_B (JK^-1) is the Boltzman constant, T (K) the temperature, η is the solvent viscosity, and R_H (m) the hydrodynamic radius of the molecule. The relationship is strictly valid for a spherical particle with a radius R_H, but it may be used to estimate the size of molecules in solution [Waldeck 97, Crank 97, Cussler 84].

NMR experiments employing pulsed field gradients (PFGs) have been used for many years to measure the diffusion coefficients of species in solution [Torrey 56, Stilbs 87]. PFG NMR experiments directly measure the net displacement of nuclear spins during a defined delay, and such displacements can be related to the translational diffusion coefficients of the spins that give rise to the resonances in question [Dehner 05]. Because the diffusion behavior is related to properties of an individual molecule, such as size, shape and aggregation states, each component in a mixture can be pseudo-separated, based on its own diffusion coefficient on the diffusion dimension [Johnson 99]. As a noninvasive solution-state method to obtain both physical and chemical information, this experiment complements existing analytical methods

(e.g. light-scattering, chromatography) and provides a global view of particle sizes in the sample. Consider, for example, a broth containing vesicles, micelles, and protein fragments. Light-scattering experiments cannot resolve such mixtures, and chromatographic methods may disrupt fragile structures such as micelles and vesicles. The easy and cheap implementation can be another advantage of DOSY. It could be an important alternative to LC-NMR that is more expensive and time-consuming [Morris 92].

The most common experimental approach to measure such diffusion coefficients involves the use of a spin echo, and the resulting PFG-spin echo experiments have been widely applied. A series of spin echo spectra is measured with different pulsed field gradient strengths, and the signal decays are analyzed to extract a set of diffusion coefficients . Johnson and coworkers developed a formal method for using the PFG-spin echo NMR experiment for mixture analysis [Johnson 99, Morris 93, Morris 92]. The data processing approach, which they called Diffusion Ordered SpectroscopY (DOSY), results in a 2D-plot with a chemical shift in one dimension and a diffusion coefficient in the other. DOSY is an extremely useful data processing scheme because it enables one to correlate resonances with a specific moiety in solution, rather than a specific spin. For the standard DOSY experiment one envisions automated data collection with a programmed set of gradient areas, followed by data inversion by means of user selected transformations and the generation of two-dimensional spectra.

There are numerous reviews covering various aspects of DOSY NMR [Johnson 99, Cohen 05, Huo 03, Antalek 02] (e.g. diffusion probehead design, development of processing algorithms, pulse sequence design etc.) The following Sections just outline the underlying principles of a DOSY NMR experiment and more importantly two applications demonstrating its applications on supramolecular self-assemblies in solution.

5.2 The PFG spin-echo sequence

The basic scheme for the characterization of diffusion is the pulsed field gradient spin-echo sequence by Stejskal and Tanner in 1965 [Stejskal 65] (Fig. 5.1(a)). Without gradient pulses, this will refocus chemical shift evolution such that the detected signal is attenuated only by transverse relation during the 2τ period. When pulsed field gradient are employed, complete refocusing of the signal will only occur when the local field experienced by a spin is identical during the two gradient pulses.

By use of a first gradient, molecules can be spatially labelled depending on their position in the sample tube, and if they move during a certain time a second gradient is used to decode their new position. The detected signal would therefore be atten-

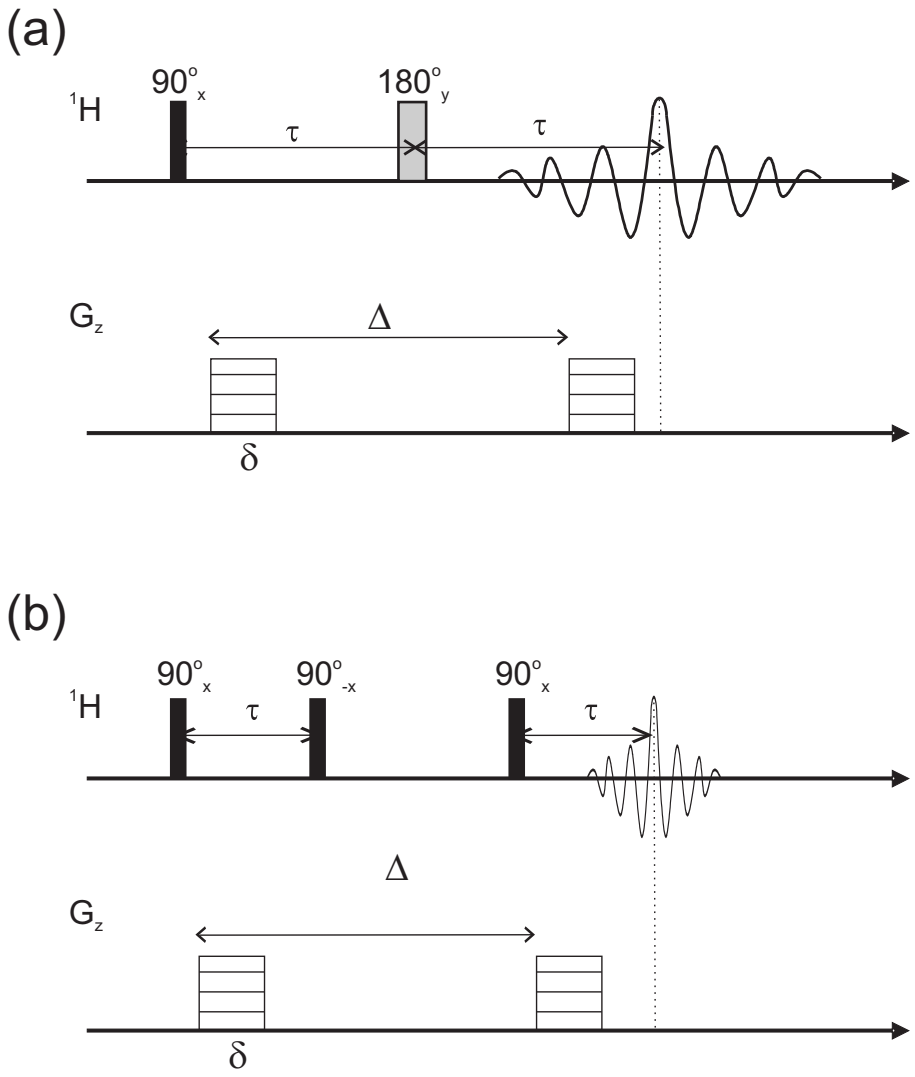

Figure 5.1: *Basic sequences for measuring molecular diffusion based on (a) the PFG spin-echo and (b) the PFG stimulated spin-echo. The diffusion during the period Δ is characterized by a series of measurements with increasing gradient strengths.*

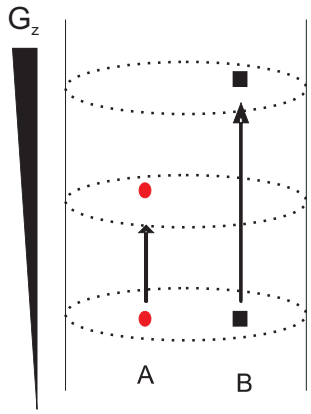

Figure 5.2: *A schematic representation of signal attenuation through molecular diffusion. The local field experienced by molecule A during the first gradient pulse does not precisely match that experienced during the second gradient pulse due to diffusion during the delay Δ(diffusion time). The signal of A does not fully refocus and its response is attenuated. Greater attenuation is observed for the faster moving molecule B due to the greater difference in local fields it experiences during the two gradient pulses.*

uated by an amount dictated by how far the molecule moved during the period Δ , and hence by its diffusion coefficient (Fig. 5.2). To obtain the diffusion rate, it is possible to progressively alter the delay Δ, the length of the gradient pulses δ or the strength of gradient pulses while monitoring the corresponding signal decay. However, changes made to the overall length of the echo sequence will introduce additional complications arising from increasing relaxation losses, so it is universal practice to increase gradient strengths whilst keeping all time periods invariant. Whilst T_2 relaxation losses still occur in this case, they are constant for all experiments and thus do not contribute to the progressive signal attenuation that is monitored. The observed signal intensity, I, for the basic PFG spin-echo experiment is given by

$$I = I_0 \exp\left(-\gamma^2\delta^2 D g^2(\Delta - \delta/3)\right) \tag{5.2}$$

where I_0 is the signal intensity at zero gradient strength, g is the gradient strength, D is the diffusion coefficient and the delay Δ and δ are diffusion time and gradient diffusion time, respectively. Plotting $\ln(I/I_0)$ vs g^2 for example, yields a linear plot whose slope is proportional to D and since the constants γ ,and δ and Δ are known, the diffusion coefficient may be calculated.

To generate a 2D spectrum with chemical shifts on the F_2 dimension and diffusion constants on the F_1 dimension, each column has to be fitted first. Out of the fitting

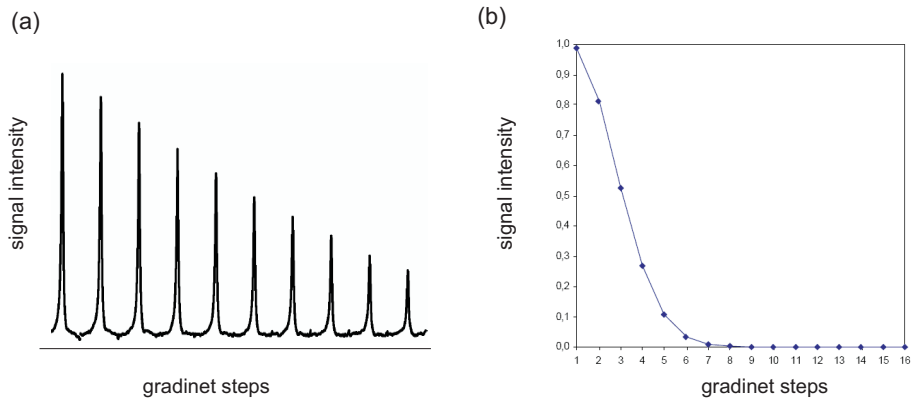

Figure 5.3: (a) the signal attenuation by varying gradient strength. (b) simulated diffusion decay curve.

results, 2D cross peaks are created where the centers of the cross peaks correspond to the calculated diffusion constant. The width of the peaks correlates with the fitting error. Only this way of presenting the diffusion data is called DOSY. All columns of the F_2 transformed spectrum are fitted independently using different algorithms. Columns containing only noise are left out and zeroed. Fitting a decaying curve is much more difficult than a straightforward Fourier transform and therefore needs much more parameters describing the fitting procedure. At this point it should be noted that at the heart of DOSY method are the analysis and display of data obtained with pulsed field gradient NMR techniques. There are several ways to process DOSY spectra and still it is an ongoing debate. It is based on diffusion differentiation while solving the following functional form

$$I(q,V) = \sum A_n(\nu) \exp\left(-D_n q^2(\Delta - \delta/3)\right) \tag{5.3}$$

where $q = \gamma g \delta$, and $A_n(\nu)$ is the amplitude at a frequency value of the nth pure component in solution having diffusion coefficient of D_n, and $A_n(\nu)$ can be thought of as the spectrum of pure component in the mixture that is attenuated in the PFG spin echo NMR experiment by an exponential function having a time constant controlled by D_n. Whereas Eq.5.2 describes the signal attenuation for a single resonance, Eq.5.2 was generalized to represent the sum of the spectra form all the pure components in the mixture. The technical details about powerful data inversion programs (e.g. SPLMOD, CONTIN, DECRA, MCR, CORE..) can be found in references [Johnson 99, Malinowski 91, Scarminio 93, Stilbs 96] but will not be discussed here.

In performing DOSY experiments in high resolution liquid state NMR, there are

two technical problems to be considered : one is short T_2 times and the other refers to eddy-currents. To overcome these two special problems, many pulse sequences were developed during the last 10 years. The PFG spin-echo sequence above is limited in practice by the aforementioned relaxation losses and is now little used for diffusion measurements. Because magnetization is transverse during the diffusion period, these losses are dictated by the transverse (T_2) relaxation time. T_2 can be short for slowly tumbling macromolecules, and this can lead to severe loss of signal. Since larger molecules require longer diffusion periods to move significant distances, the use of long Δ delays (diffusion time) can lead to unacceptable signal-to-noise degradation. To overcome signal loss, all recently introduced diffusion sequences are derived from the stimulated-echo sequence.

Sequences containing two and three 90° RF pulses were investigated by Hahn in his classic paper on spin echoes [Hahn 50]. He found that the three-pulse sequence with a steady (cw) gradient can generate up to five echoes [Tanner 70]. In the stimulated-echo sequence magnetization is longitudinal during the diffusion period, by virtue of the second 90° pulse, meaning the sequence is now limited by slower longitudinal T_1 relaxation rates instead. Following the diffusion period, the magnetization is returned to the transverse plane by the third 90° pulse for refocusing and detection (Fig. 5.1(b))

The second problem is given by eddy currents which are caused by fast switching (on and off) of the gradient pulse. Whenever the magnetic field changes, eddy currents simultaneously form within any closely located conductor [Jehenson 90]. These induced currents are opposing the change and in turn produce slowly decaying magnetic fields at the sample that lead to spectral distortions resulting from time dependent phase changes. Therefore, experiments must be designed to avoid or at least minimize the effects of eddy current. The best way to avoid eddy-currents is to prevent their formation in the first place. There are some easy but not completely effective solutions. For example, eddy currents in the probe can be reduced by special RF coil designs (active shielding of the gradient coils), and eddy currents in the inner bore of the magnet may be reduced by using widebore magnets.

The rate of change of the magnetic field when gradient pulse is switched on or off can be reduced by proper shaping the gradient pulse. Shapes that have been investigated include sine functions, sine square functions, and nearly rectangular functions with modified rise and fall times. Gradient pulse shaping is helpful and this capability is now available on many commercial NMR instruments. Many articles have been published that discuss ways to minimize this effect [Price 91, Merrill 93, Wider 94, Haitao 99].

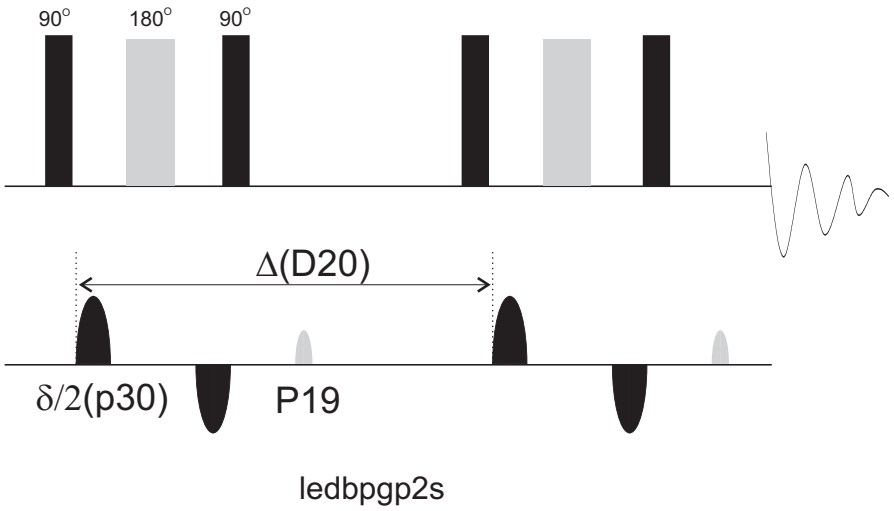

P30 : diffusion gradient time (little DELTA * 0.5 : ~1ms)
D20: diffusion time (big DELTA : 50~100ms)
D21: eddy-current delay (~5ms : LED)
P19 : addtional spoiling gradient (~1.1ms)
D16 : gradient recovery delay (50~100us for z-gradinet coil)

Figure 5.4: *The BPP-LED pulse sequence and experimental parameter values.*

At present, the BPP-LED sequence is the sequence of choice for many DOSY applications, since it uses maximum gradient strengths with small temperature rises, as one of the best ways to diminish the eddy current effects. By adding a fourth 90° pulse at the center of the stimulated echo, the magnetization is stored in the longitudinal direction while the eddy currents decay. Replacing the gradient pulse with two pulses of different polarity separated by 180° RF pulse, i.e. the composite bipolar gradient pulse (g-180°-(-g)) for the self compensation of the induced eddy currents. In this work all DOSY data were obtained on a Bruker AVANCE 700 NMR spectrometer equipped with dual z-gradient probehead using 55.2 Gcm^{-1} gradient strength. Stimulated-echo sequence incorporating bipolar gradient pulses and a longitudinal eddy current delay (BPP-LED) was used. The gradient strength was incremented in 32 steps from 2% up to 95% of the maximum gradient strength. The typical experimental parameters including diffusion time (Δ) and diffusion gradient pulse (δ) are shown in Fig. 5.4 with BPP-LED pulse sequence.

5.3 Probing calixarene urea self-assembled dendrimer by DOSY

Self-organisation on the molecular level is the driving force responsible for the selective formation of essential assemblies in living systems. This principle is also used to construct increasingly intricate artificial arrangements, and to synthesize novel compounds or materials. Various dimeric capsules, tetramers, hexamers, rosettes, numerous supramolecular polymers, and also dendrimers were obtained via self-assembly.

Calix[4]arenes, substituted on their wide rim by four urea residues, form dimeric capsules in aprotic, apolar solvents, which are held together by a seam of hydrogen bonds between the urea functions [Mogck 96b, Vysotsky 03]. This dimerization may be used to build up linear polymers [Castellano 98] from building blocks, in which two tetra urea units are covalently linked via their narrow rims. The exclusive formation of heterodimers in an equimolar solution of tetraaryl- and tetratosylureas can be used to introduce directionality along the chain or to obtain alternating polymers via self-assembly. It was recently reported (by Rudzevich et al [Rudzevich 05b]) that triurea derivatives derived from triphenylmethanes form hydrogen-bonded dimers analogously and their self sorting process can be used to self-assemble dendritic architectures, which are uniform in size and structure. While investigating corresponding systems, DOSY NMR was applied to provide a global view of hydrodynamic radius of each assemblies [Rudzevich 05b]. The rest part of this Section will be covered by the DOSY results.

In the DOSY experiment it was found that all the peaks of the ^{1}H spectrum of $\mathbf{3}_2\cdot\mathbf{4b}_6$ have the same diffusion coefficients within experimental errors. (Fig. 5.6) This proves the existence of a uniform dendritic assembly as well as the absence of both larger aggregates and smaller components. The corresponding diffusion coefficient of $\mathbf{3}_2\cdot\mathbf{4b}_6$ was $5.4\times10^{-11}m/s^2$ for all ^{1}H signals. Form the diffusion coefficient value of dendrimer, the effective hydrodynamic radius of $2.1\pm0.2nm$ was calculated using the the Einstein-Stokes equation which is given in Eq. 5.1.

DOSY experiments were also performed for the individual component **4b** and **3x** (a precursor of **3** bearing nitro groups instead of the urea functions of the calixarenes). Diffusion coefficients of 8.6×10^{-11} and $6.2\times10^{-11}m/s^2$ corresponding to hydrodynamic radii of 1.3 and $1.8nm$ were found. They reasonably agree with values expected for the homodimers $\mathbf{4b}_2$ and $\mathbf{3x}_2$ as models for the dimers at the outer sphere and in the core of the dendrimer. The uniform size of the dendritic assembly $\mathbf{3}_2\cdot\mathbf{4b}_6$ was also confirmed by dynamic light scattering, which led to a hydrodynamic radius of $2.4nm$. Considering the fact the relationship (Eq. 5.1) is strictly valid for a spherical particle

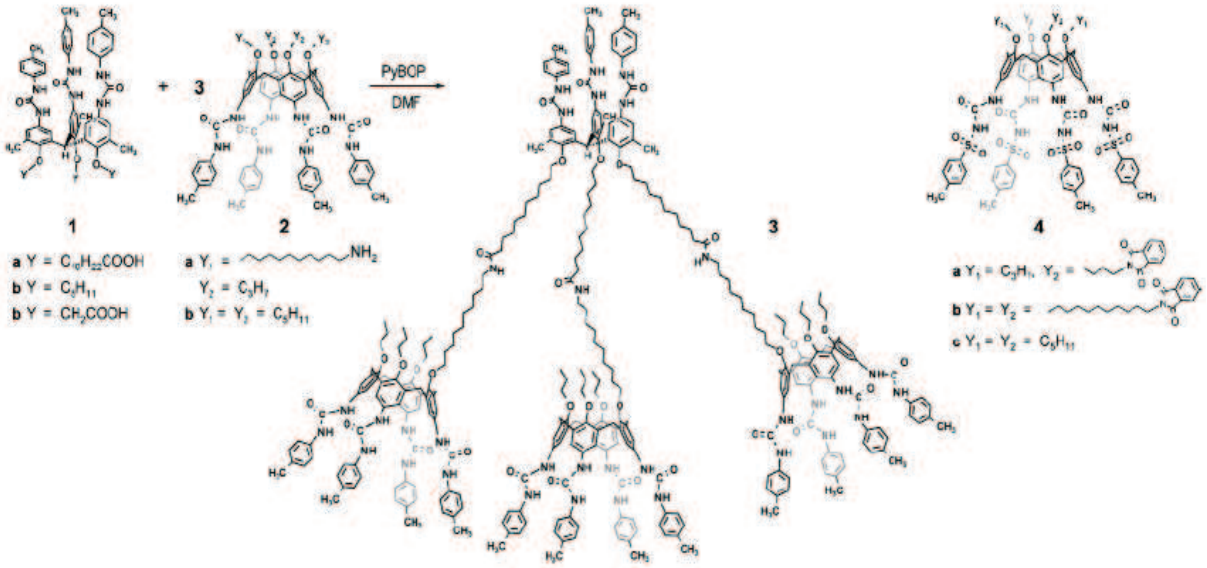

Figure 5.5: *Schematic building blocks of dendrimer*

(and that this radius describes only a sphere moving with the same speed), the values obtained by the two different methods are in good agreement [Rudzevich 05b].

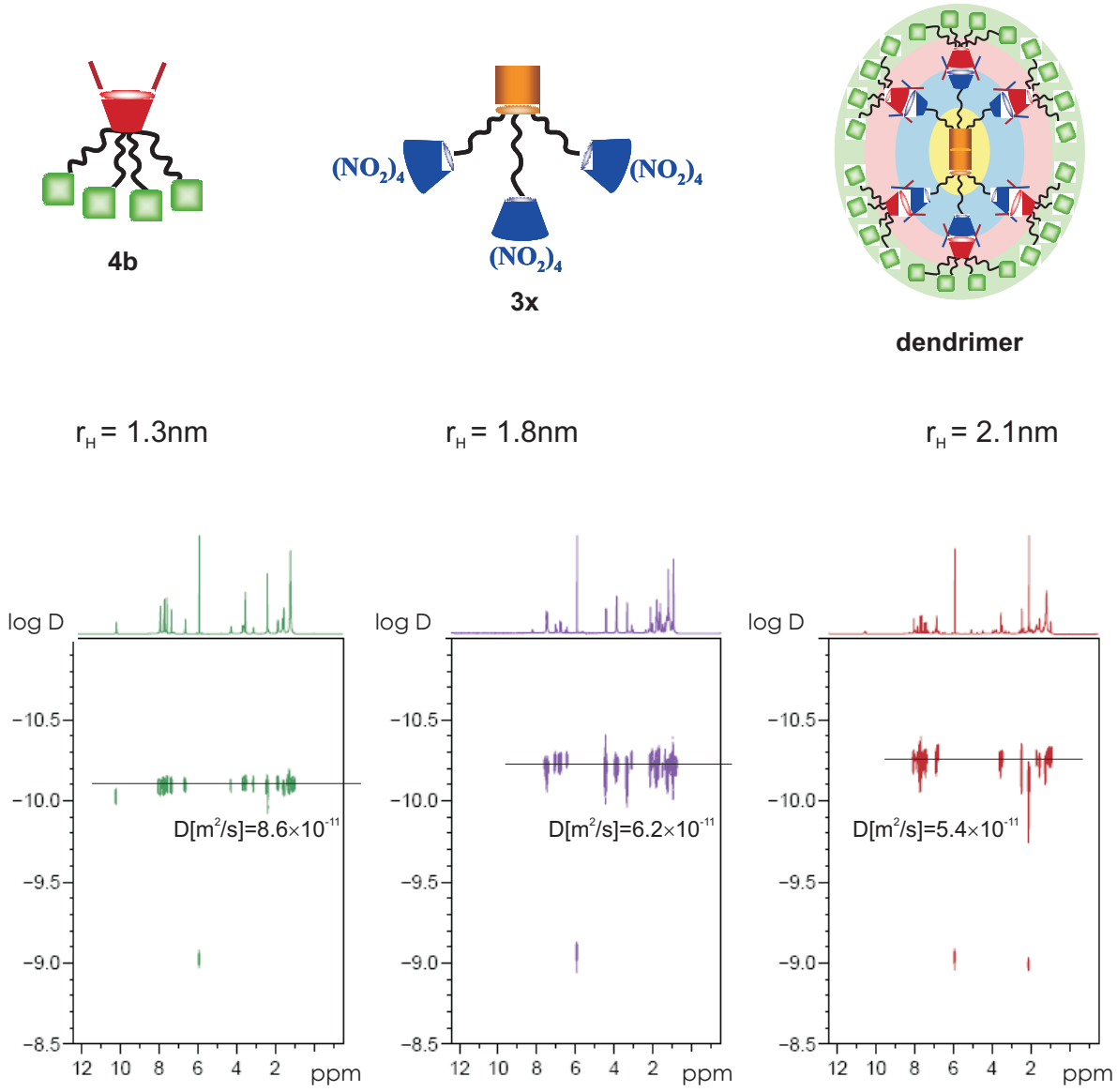

Figure 5.6: *2D-DOSY NMR spectra of each assemblies recorded in CD_2Cl_2 solvent at 293K (solvent viscosity $\eta = 4.3 \times 10^{-3} Pa \cdot s$). r_H : hydrodynamic radius, D : Diffusion coefficient*

5.4 Cationic Shape-Persistent Supramolecular Dimer formation

Supramolecular organization of shape-persistent macrocycles in one, two, or three dimensions has recently become a topic of great interest [Moore 97]. The term shape-persistent macrocycle means that the building blocks of the ring are rather rigid and their connection is performed in such a way that the final structure cannot collapse, in contrast to flexible structures like crown ethers or cycloalkanes. A more precise definition of shape-persistent is not based on the molecular building blocks, but on the flexibility of the final structure [Ghadiri 95, Höger 04].

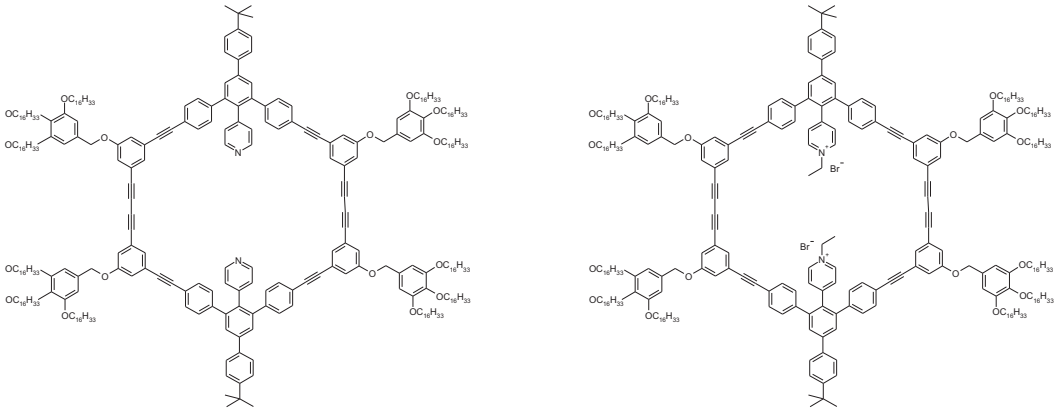

1 2

Figure 5.7: *The structures of compounds.*

Shape-persistent macrocycles with polar groups pointing to the inside play a special role in supramolecular chemistry. The convergent preorganization of the binding sides allows them to act as host molecules for the recognition of appropriate guest molecules according to the lock and key principles. Apart from infinite aggregates, the formation of well defined finite-size assemblies from mesoscale building blocks is currently an attractive goal in supramolecular chemistry.

Recently, Klyatskaya *et al*. showed *via* DLS and X-ray scattering experiments that nanometer-size dicationic shape-persistent macromolecules in nonpolar solvents do not form infinite tubular aggregates, as might be expected from their chemical structure, but dimerize to defined supermolecules [Klyatskaya 06].

The exclusive dimerization in not programmed by synthetic efforts but is a result of the ability of the macrocycles to adopt self-complementary shape during the aggre-

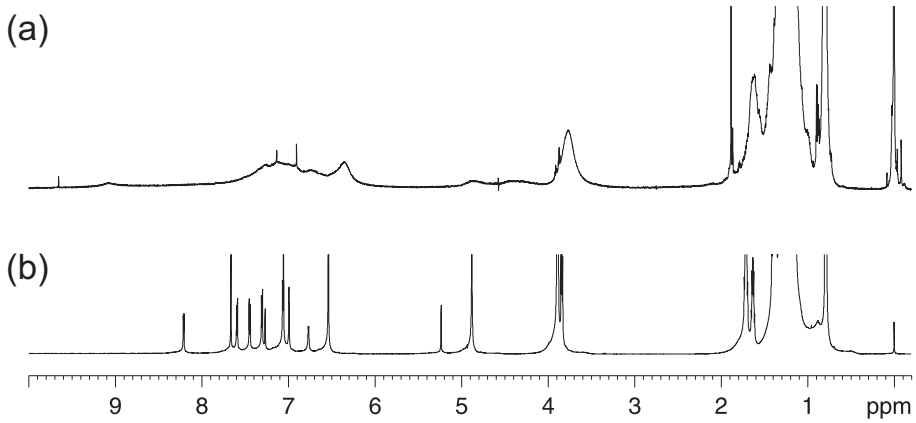

Figure 5.8: *^{1}H NMR spectra of **1** (a) in CD_2Cl_2 and (b) in cyclohexane. D : Diffusion coefficient*

gation that blocks the top and bottom of the supermolecule, thus preventing a further aggregation. During this work, DOSY NMR was also applied to complement the results from DLS and X-ray scattering methods. The first hint of aggregation can be found by comparison of the ^{1}H spectra of in CD_2Cl_2 and in cyclohexane. While the ^{1}H NMR spectrum in CD_2Cl_2 is well resolved, the spectrum in cyclohexane is broadened, which highly implies monomer in CD_2Cl_2 and aggregation forming in cyclehexane.

This was supported by obtaining hydrodynamic radii from 2D DOSY experiments. The diffusion coefficient of **1** (in Fig. 5.7) in CD_2Cl_2 was found to be $2.2 \times 10^{-10} m/s^2$, which results in hydrodynamic radius of $2.1nm$. However in cyclohexane a larger hydrodynamic radius of about $2.6nm$ was measured for **1**. Considering the ratio between the two determined hydrodynamic radii, it is assumed that the aggregated structure is rather dimeric structure than simply a larger scale supramolecule.

In order to enforce the aggregation the (intra-annular) pyridyl groups of the macrocycle were alkylated by treating **1** with ehtylbromide. **2** (Fig. 5.7) is well soluble in chlorinated solvent, THF and even cyclohexane. Again in cyclohexane, broadening of the respective ^{1}H resonances of **2** was observed and similar diffusion coefficients with non-cationized **1** were obtained for the cationized **2**. The diffusion coefficients and corresponding hydrodynamic radii values are summarized in Table 5.1. Conclusively in this chapter it was demonstrated that DOSY NMR can be used to characterize self-assembled supermolecular systems.

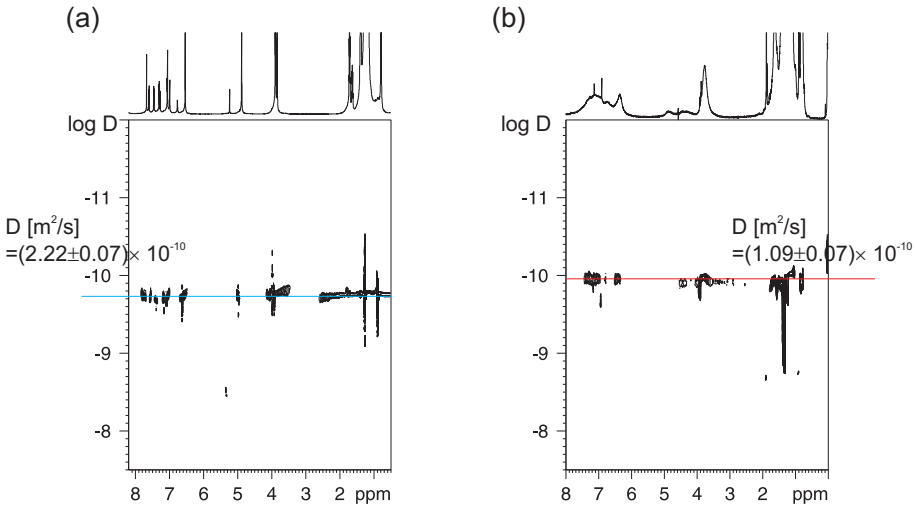

Figure 5.9: *(a) 2D-DOSY NMR spectra of **1** in CD_2Cl_2 at 293K ($\eta = 4.3 \times 10^{-3} Pa \cdot s$) and (b) in cyclohexane at 311K ($\eta = 0.8 \times 10^{-3} Pa \cdot s$).*

	1 in CD_2Cl_2	1 in C_6D_6	2 in CD_2Cl_2	2 in C_6D_6
Diffusion coefficient$[m/s^2]$	2.2×10^{-10}	1.1×10^{-10}	2.1×10^{-10}	1.0×10^{-10}
Hydrodynamic radius$[m]$	2.1×10^{-9}	2.6×10^{-9}	2.2×10^{-9}	2.7×10^{-9}

Table 5.1: *Diffusion coefficients and corresponding hydrodynamic radii of **1** and **2**.(in CD_2Cl_2 at 293K and in cyclohexane at 311K)*

5.5 Conclusions

The work presented in this Chapter demonstrates that DOSY NMR can be a valuable technique for determining the hydrodynamic radius of supermolecules in solution.

The well established preparative chemistry of calix[4]arenes allows the synthesis of specific derivatives which are not only able to self-assemble, but also to take part in self-sorting processes. In constructing a dendrimer, which is uniform in size and structure using these properties of calix[4]arenes, DOSY NMR was applied in combination with light scattering to prove the formation of the desired assemblies [Rudzevich 05b]. For the individual component **4b** and **3x**, diffusion coefficient were 8.6×10^{-11} and $6.2 \times 10^{-11} m/s^2$ respectively. However, the diffusion coefficient of $\mathbf{3}_2 \cdot \mathbf{4b}_6$ was $5.4 \times 10^{-11} m/s^2$ for all ^{1}H signals, proving the existence of a uniform dendritic assembly as well as the absence of both larger aggregates and smaller components (Fig. 5.6).

Recently, Klyatskaya *et al*. showed *via* DLS and X-ray scattering experiments that nanometer-size dicationic shape-persistent macromolecules in nonpolar solvents do not form infinite tubular aggregates, as might be expected from their chemical structure, but dimerize to defined supermolecules [Klyatskaya 06]. This result was supported by obtaining hydrodynamic radii from 2D DOSY experiments. The diffusion coefficient of **1** in CD_2Cl_2 was found to be $2.2 \times 10^{-10} m/s^2$, which results in a hydrodynamic radius of 2.1*nm* (Fig. 5.9). However in cyclohexane a larger hydrodynamic radius of about 2.6*nm* was measured for **1**. Considering the ratio between the two determined hydrodynamic radii it is assumed that the aggregate is a *dimeric* structure rather than a larger scale supramolecule.

Chapter 6

Guest Dynamics in Tetratolyl Urea Calix[4]arenes

6.1 Introduction

Self-organization is a topic of ongoing interest in supramolecular chemistry. A wide variety of biological systems consists of rather simple subunits that are held together via non-covalent interactions. Indeed, self-assembly provides some advantages in comparison to the construction of larger molecules by covalent connection of appropriate building blocks: reversibility of hydrogen bonds, facile formation of end products and synthetic economy constitute important features of self-assembly. Various examples of self-complementary molecules, which are able to form dimers, oligomers or large well-defined aggregates have been described.

Calix[n]arenes are macrocyclic compounds built of *n* phenol units linked *via* alkylidene groups forming cavities of molecular dimensions [Vicens 91, Gutsche 98]. The bowl-like structure allows them to host a variety of species, and the resulting complexes in the solid-state are classified as inter- (endo) or intramolecular (exo) depending on the orientation of the guest relative to the bowl. Facilitated by their rather simple accessibility, (model) compounds based on *p-tert*-butylcalix[4]arene have been extensively characterized in the solid-state by both X-ray diffraction and solid-state NMR. It was found that the basic host prevalently forms 1:1 complexes with the guest moiety exhibiting fairly similar structural arrangements [Brouwer 97]. In rare cases, however, 1: 2 complexes have also been reported. Available information on local order derived from NMR data has been in general crucial for obtaining correct structural models, where the symmetry of the respective host lattice reflects guest symmetry and dynamics.

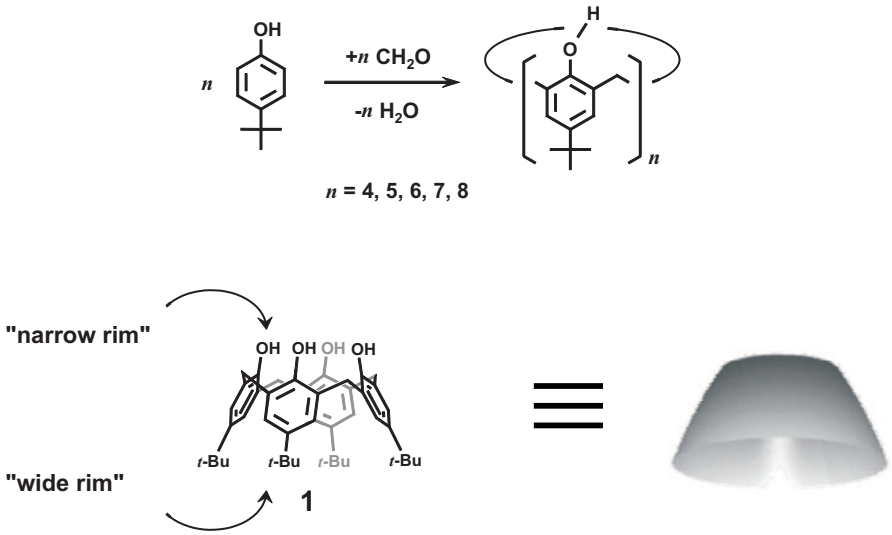

Figure 6.1: *Synthesis and sketchy drawing of calix[4]arenes*

In contrast, calix[4]arenes, substituted on their wide rim by four urea residues, reliably form dimeric capsules in aprotic, apolar solvents that are stabilized by a seam of hydrogen bonds between the urea functions [Hamann 96, Rudzevich 05a]. Since the suitable guest induces the dimerization of such an architecture, dimerization may be used to build up linear polymers from building blocks, in which two tetraurea units are covalently linked via their narrow rims. Though the dynamic nature and reversibility of capture, storage and preferably transport of guest species in their respective host materials has been comprehensively studied in solution, rather little is known about dimeric compounds **in the solid state**. In case of single crystals or powdered materials, the respective host structure may be determined by X-ray diffraction, but commonly mobile guest species are poorly refined, if at all. However, local dynamics and ordering phenomena which are not accessible by X-ray analysis can be conveniently addressed by solid-state NMR, thus providing complementary structural information.

The isotropic chemical shift constitutes a major source of information and thus, may be regarded as fingerprint of a particular structural arrangement. Notably, the chemical shift of guest species is known to significantly change upon (reversible) encapsulation within the host. Possibly observed chemical shift differences of entrapped guest moieties with respect to the "free" solvent shift are commonly referred to as complexation induced shifts (CIS) that not only strongly depend on local geometries of the hosts but also on the presence of characteristic moieties (e.g. aromatic rings)

that constitute the host. In that respect, the recently introduced concept of nucleus-independent chemical shift (NICS) maps may provide rather qualitative means to both facilitate an interpretation of experimental chemical shifts and locate guest molecules within the respective host.

6.2 Complexes in Solution

A dimerization of tetraurea calix[4]arene was first realized when comparing liquid-state ^{1}H NMR spectra of **1** in DMSO (polar solvent) and in the non-polar solvent benzene. Most notably, the former singlet at 6.8 ppm assigned to aromatic protons in DMSO changed into two strongly separated doublets in benzene (6.4 and 8.2 ppm, respectively) with a *J*-coupling constant of 2.1 Hz typically observed for protons in meta-position (Fig. 6.2). Additionally, two close NH proton singlets in DMSO (8.35 ppm and 8.21 ppm) were separated by 2.4 ppm in benzene [Mogck 96a, Shimizu 95]. This experimental observation was explained by dimerization via selective head-to-tail interactions forming a robust seam of hydrogen bonds between the four urea groups in each of the calix[4]arene upper rims. An additional X-ray structure later revealed that this arrangement is persistent in the solid compound, thus confirming the dimerization [Mogck 96b].

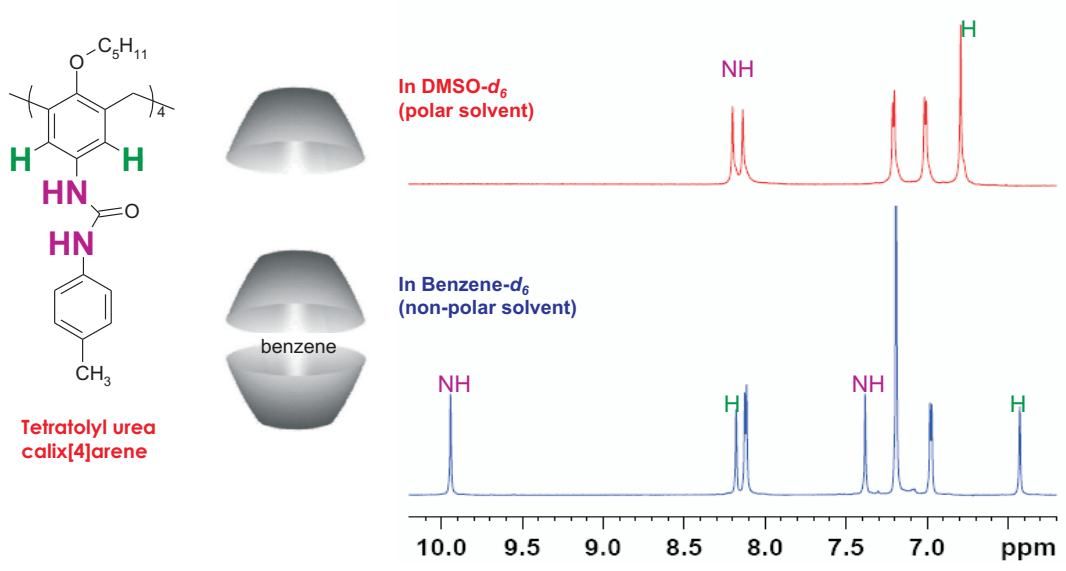

Figure 6.2: *Comparison of* ^{1}*H NMR spectra in DMSO and benzene-*d_6

The mobility of molecules in solution gives rise to a characteristic diffusion coefficient that can be measured via ^{1}H -DOSY NMR. Assuming a suitable model shape of the mobile species (e.g. spheres) then allows for an estimation of hydrodynamic radii using the Stokes-Einstein equation. For monomer **1** in DMSO, the obtained translational diffusion coefficient was $(1.3) \times 10^{-10} m^2/s$ (corresponding to a hydrodynamic radius of $0.7nm$), while in the non-polar solvent benzene-d_6, DOSY NMR yield a hydrodynamic radius of $0.96nm$, thus reflecting the formation of a dimer **1**·$\mathbf{C_6H_6}$·**1**(Fig.

6.3). Both hydrodynamic radii obtained via ^{1}H DOSY NMR are in good agreement with data extracted from light scattering experiments.

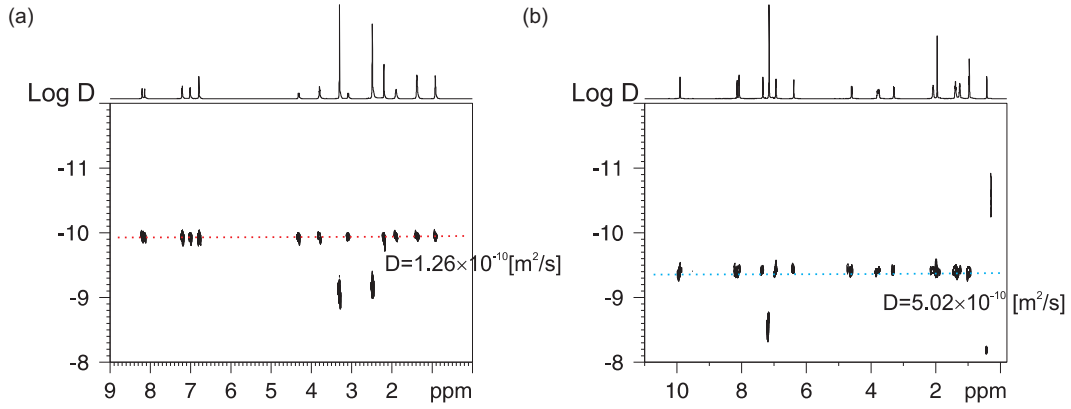

Figure 6.3: *^{1}H 2D-DOSY spectra of (a) **1** in DMSO at 298K and (b) **1**·$\boldsymbol{C_6H_6}$·**1** in benzene-d_6 at 308K.*

Use of an external NMR tube allowed to reliably distinguish reversibly encapsulated benzene from benzene-d_6 locking solvent. Here, protons of included benzene-d_6 were observed at 4.3 ppm, thus revealing a CIS of 2.8 ppm with respect to pure benzene solvent (7.1 ppm), while the obtained signal intensities indicate a 2:1 host:guest stoichiometry (Fig. 6.4 (a)). This refers to a *single* guest molecule being trapped inside the cavity of the tetra urea calix[4]arene dimer. Proton DOSY NMR on this sample consistently revealed *identical* translational diffusion coefficients of both the calix[4]arene host and its benzene guest, hence illustrating the potential of DOSY NMR (Fig. 6.4(b)).

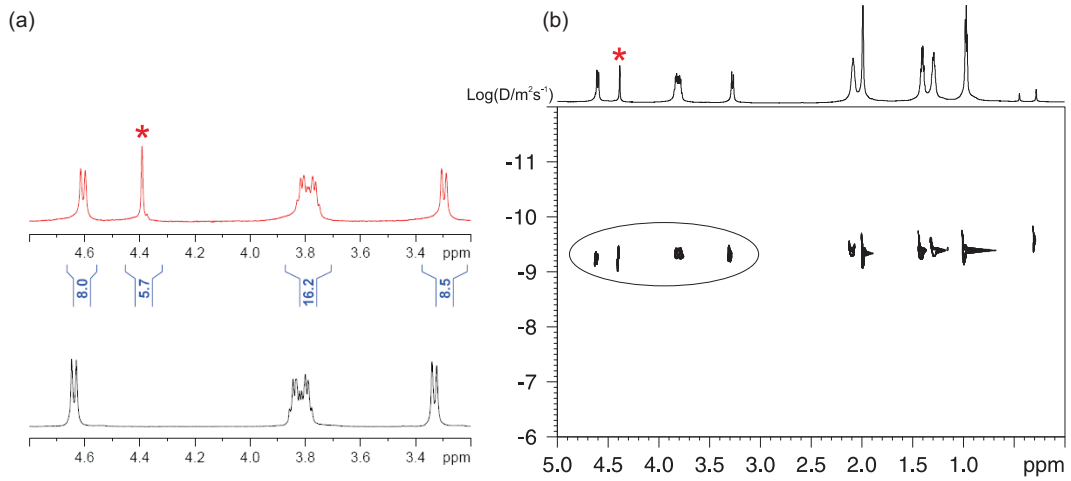

Figure 6.4: *(a) Comparison of* ^1H *spectra of* ***1*** *in benzene-*D_6 *and benzene-*H_6 *using external lock NMR tube. (b) 2D-DOSY spectra of* ***1***$\cdot C_6H_6\cdot$***1*** *using external lock NMR tube. *: trapped benzene-guest peak.*

6.3 Complexes in the Solid State

In this section, solid state NMR investigations of various capsular contents (benzene, benzene-d_6, fluorobenzene, fluorobenzene-d_5, 1,4-difluorobenzene, and cobaltocenium) will be presented.

6.3.1 Benzene capsule

The proton MAS spectra of both monomer **1** and dimer **1**·$\mathbf{C_6H_6}$·**1** are given in Figure 6.5. While for dimeric **1**·$\mathbf{C_6H_6}$·**1**, the observed peak at 9.2 ppm is easily assigned to -NH protons that comprise the hydrogen bonding belt, the peak at 9.2 ppm for monomer can be explained by solid state packing effect. Since in solution, the latter (monomer) exhibits a NH proton peak at about 8.2 ppm, this strongly suggests the presence of packing effects in the solid monomer **1**. In monomeric **1**, there are *inter* molecular hydrogen bonds due to the solid state structure, which was also proved by X-ray experiment. Upon dimerization former peak splittings in the ^{1}H MAS spectrum are obscured by line broadening, however, the shoulder around 7.7 ppm might be attributed to benzene guest.

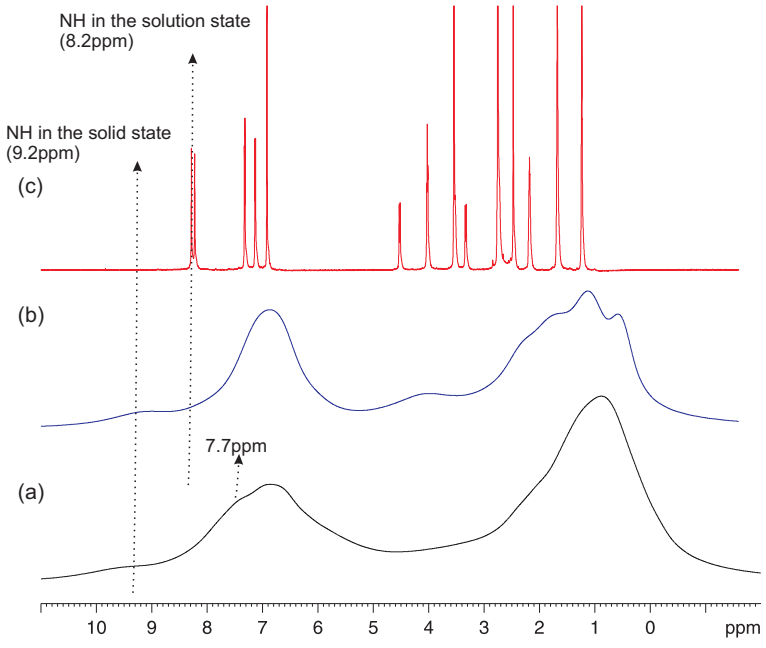

Figure 6.5: *(a) ^{1}H MAS of dimer **1**·$\mathbf{C_6H_6}$·**1** in the solid state (b) ^{1}H MAS of monomer **1** in the solid state (c) ^{1}H of monomer **1** in solution (DMSO-d_6).*

Figure 6.6 shows ^{1}H DQ MAS spectra of monomer **1** and dimer **1**·$\mathbf{C_6H_6}$·**1**, respec-

tively. Notably, the two DQ spectra are fairly similar rendering a distinction between monomer **1** and dimer **1**·$\mathbf{C_6H_6}$·**1** rather impossible. For the latter (dimer), the stabilizing belt of hydrogen bonds among the urea NH protons is anticipated to give rise to so-called *auto*-correlation peaks in the DQ spectrum, which are not observed clearly. The DQ *cross*-peak at about 16.2 ppm in double quantum dimension may be either regarded as contact between two -NH protons or a trivial contact among NH and aromatic protons, and hence does not provide clear indication of the dimerization.

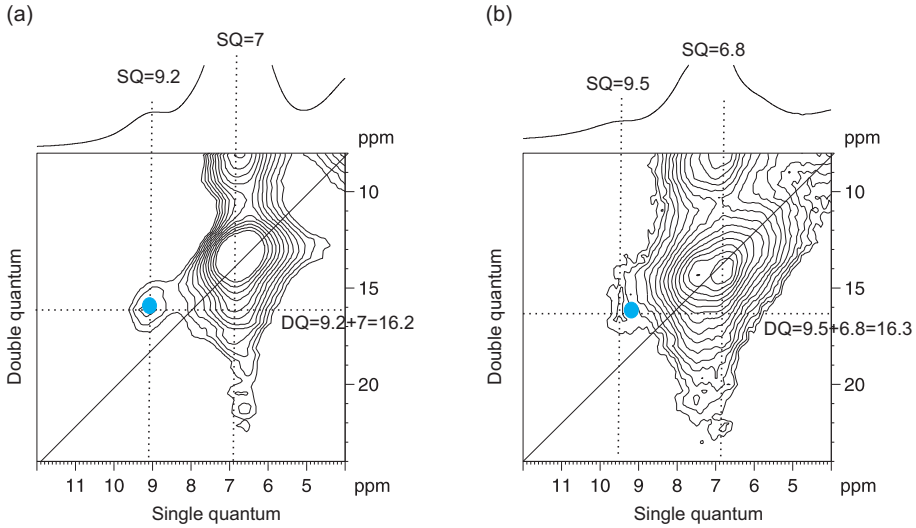

Figure 6.6: *(a)* ^{1}*H DQ MAS of monomer* ***1*** *and (b)* ^{1}*H DQ MAS of dimer* ***1***·$\boldsymbol{C_6H_6}$·***1*** *in the solid state*

Complementary data may be obtained from a ^{13}C CPMAS experiment that in principle is also quite sensitive to dynamic effects when a short delay is inserted prior to proton decoupling (dipolar dephasing spectrum). Moreover, representative guest carbons could be affected by ring currents of the aromatics "walls" of the calixarene host yielding characteristic peak shifts (CIS). Indeed, the corresponding ^{13}C CPMAS spectra of monomer **1** and dimer **1**·$\mathbf{C_6H_6}$·**1** show significant differences: changes in local order are reflected by linebroadening of most carbon peaks. Nevertheless, a representative peak of the guest benzene could not be identified.

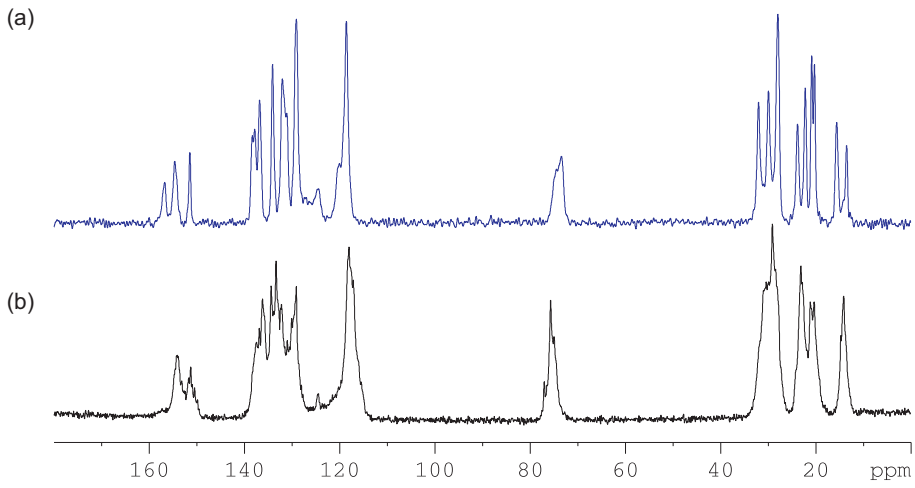

Figure 6.7: *Comparison of* ^{13}C *CPMAS of (a)monomer* ***1*** *and (b) dimer* ***1***$\cdot \boldsymbol{C_6H_6} \cdot$***1***

6.3.2 Benzene-d_6 capsule

An inclusion of benzene-d_6 allows for probing guest dynamics inside the calix[4]arene host. Since ^{2}H is a spin-1 quadrupolar nucleus, the interaction of the nuclear quadrupole moment with the local electric field gradient around the ^{2}H nucleus is very sensitive to molecular motions, thus providing orientation-dependent splittings of the lineshape. The rate and geometry of underlying motions may be extracted *via* matching of experimental lineshapes with simulated lineshapes that result from a given ("jump") model. Though in difficult cases experimental lineshapes may be reproduced by several distinct models, ^{2}H NMR still provide an easy access to local geometries of mobile species. In cases where structural details are not considered, ^{2}H MAS NMR may identify (or confirm) the respective nature of guest molecules.

In excellent agreement with solution ^{1}H NMR data, the corresponding MAS ^{2}H spectrum of **1**·$\mathbf{C_6D_6}$·**1** displays a single peak at 4.3 ppm suggesting that the local order of the benzene guest inside the cavity is retained even *without* dynamic exchange with a solvent reservoir.

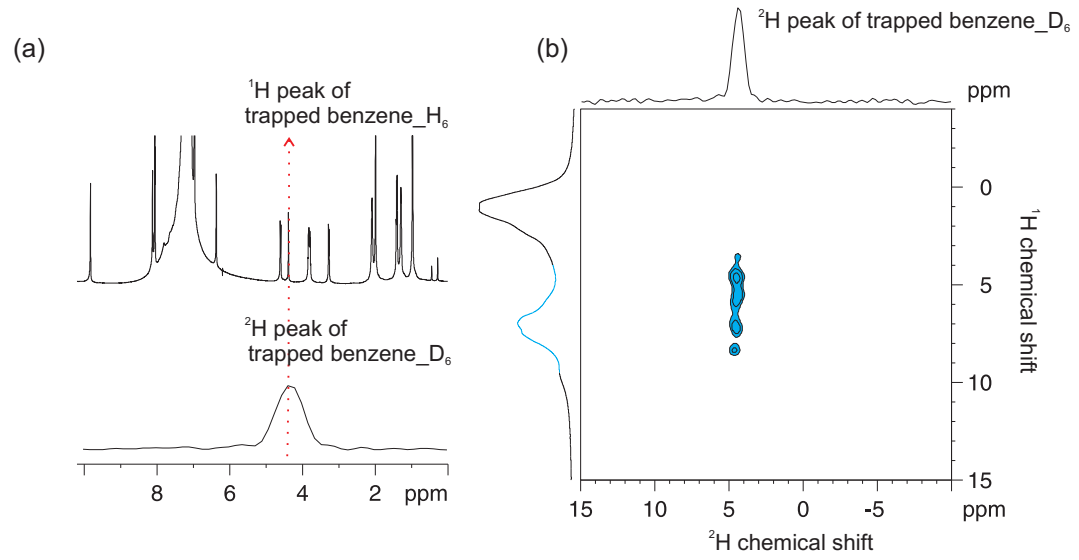

Figure 6.8: *(a) Comparison of ^{1}H in the solution state of* ***1***·$\boldsymbol{C_6H_6}$·***1*** *and ^{2}H MAS of* ***1***·$\boldsymbol{C_6D_6}$·***1*** *in the solids state. (b)^{1}H -^{2}H REPT-HSQC spectrum of* ***1***·$\boldsymbol{C_6D_6}$·***1*** *at 220K (30kHz, 8τ_R)*

Consequently, a solid-state ^{1}H -^{2}H heteronuclear correlation spectrum reveals only *cross*-peaks of deuterons with protons pointing *inside* the cavity (Fig. 6.8(b)), which also emphasizes that there are no benzene-filled voids present in the structure.

It is noteworthy to mention that in (single crystal) X-ray analysis, it is quite dif-

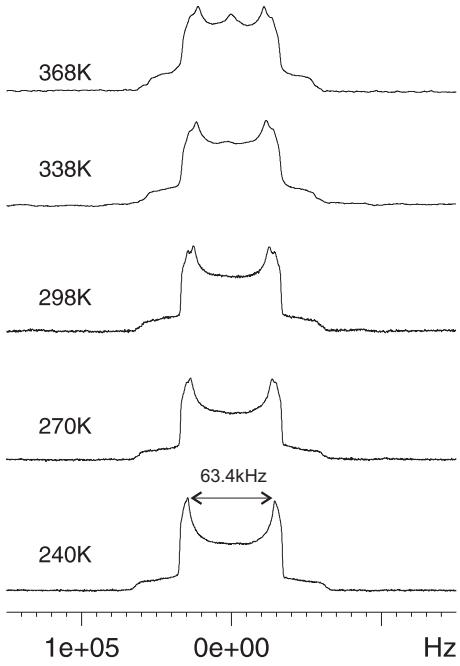

Figure 6.9: ^{2}*H temperature variable static spectra of* ***1***·$\boldsymbol{C_6D_6}$·***1***.

ficult to locate highly disordered guest molecules. Therefore, to study the guest dynamics of benzene-d_6 inside the host temperature-dependent static ^{2}H NMR was employed. At 240 K, a quadrupolar frequency of ω_Q = 63.4 kHz was determined, which is about ω_Q /2 of rigid benzene. This is readily explained by a rapid in-plane rotation around the molecular C_6-axis of the included benzene-d_6 molecule, which is known to persist even at 77 K [Ok 89]. Further elevation of the temperature (up to 400 K) well above the boiling point of benzene did *not* result in a loss of benzene but rather revealed an onset of additional motions (e.g. out-of-plane motions) or rotations around the S_8-symmetry axis of the host. The latter was found to cause a gradual decrease of the observed quadrupolar frequency to ω_Q = 53.8 kHz at 368 K. This not only suggests a dynamic order parameter of 0.84 (53.8 kHz/63.4 kHz), but also demonstrates that a remarkable level of guest stabilization can be obtained. Indeed, the above findings are supported by a recent study based on MD simulations that not only suggest that the motion of the guest is hampered by the host moiety but also report rapid reorientations around both the molecular C_6-axis and the S_8-symmetry axis of the host [Broda 06].

6.3.3 Fluorobenzene capsule

As an independent probe, fluorobenzene was encapsulate into tetra urea calix[4]arene. Here, advantage originates from superior selectivity of ^{19}F NMR, thus avoiding severe signal overlap. In principle, the ^{19}F chemical shift tensor could also provide valuable information on local orientations, but the study was restricted to ^{19}F MAS NMR. The corresponding ^{19}F MAS NMR spectra of both "free" fluorobenzene solvent and the dimeric assembly with an encapsulated guest, **1**·$\mathbf{C_6H_5F}$·**1**, are given in Fig. 6.10. The latter exhibits *two* distinct peaks at -117.7 and -118.3 ppm, respectively, with an integrated area ratio of ≈ 4:1, yielding an averaged CIS of ≈ 4.8 ppm.

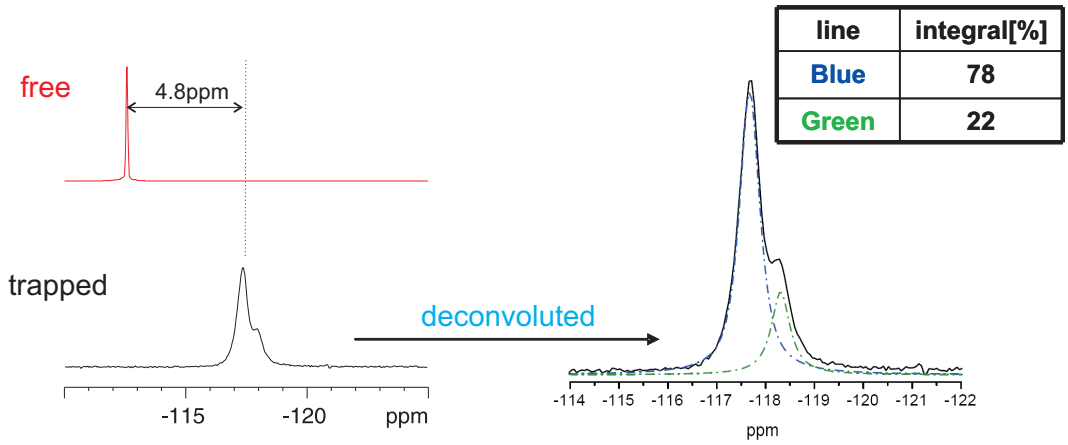

Figure 6.10: ^{19}*F MAS spectra of free 1-fluorobenzene and* ***1***·$\boldsymbol{C_6H_5F}$·***1***.

Though the exact nature of the two peaks observed in the ^{19}F-MAS spectrum is not yet clear, it either suggests the presence of slightly *distinct* orientations of fluorobenzene guests within their respective hosts or a minor fraction of hosts possibly accommodate *two* guest molecules. In an additional solution-state ^{19}F NMR experiment, it was noted that the appearance of an isotropic peak at an exactly averaged chemical shift of the two resonances observed in the solid compound ((-118.2 ppm) + (-117.4 ppm)/2 = -117.8 ppm) reflecting a solvent guest exchange that establishes an equilibrium position of a single guest molecule within the host (Fig. 6.11). Moreover, a ^{19}F NOESY-MAS experiment, performed at 240K using a rather long mixing time of 100 ms does *not* reveal polarization exchange between these two peaks, thus excluding the assumption of *two* guest molecules possibly accommodated per host (Fig. 6.12). Various batches of the host-guest assembly **1**·$\mathbf{C_6H_5F}$·**1** were prepared revealing *different* peak ratios in the corresponding ^{19}F MAS spectra: while the first two samples consistently showed a ratio of 4:1, a 1:1 ratio was found for the third batch

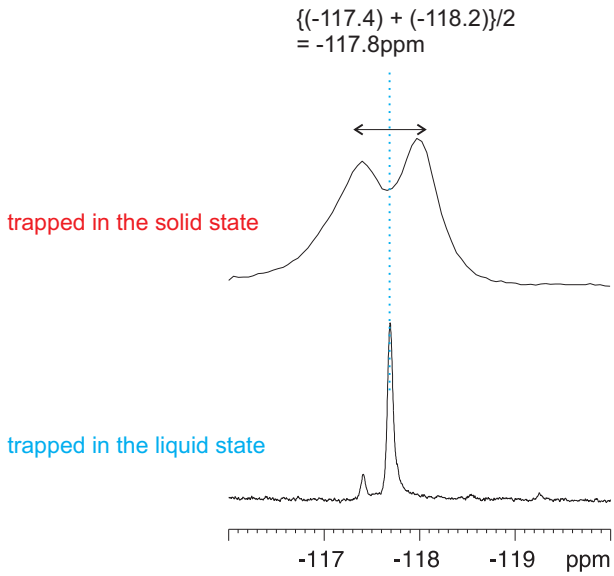

Figure 6.11: *Comparison of solid state and liquid state* ^{19}*F NMR of* ***1***·$\boldsymbol{C_6H_5F}$·***1***

(Fig. 6.13). However, this dependence on sample preparation conditions may be explained by polymorphisms or by simple distortion of the host structures governed by crystallization kinetics.

Variable temperature ^{19}F-MAS spectra up to 400 K clearly show that the observed ratio of the two peaks is maintained, while the chemical shifts apparently move towards the chemical shift of the "free" solvent at room temperature (Fig. 6.14). This is consistent with a fairly stable local structural arrangement like previously observed for benzene-d_6, but also suggest that an increasing mobility at elevated temperatures tends to reduce the effects of the host's aromatic ring currents.

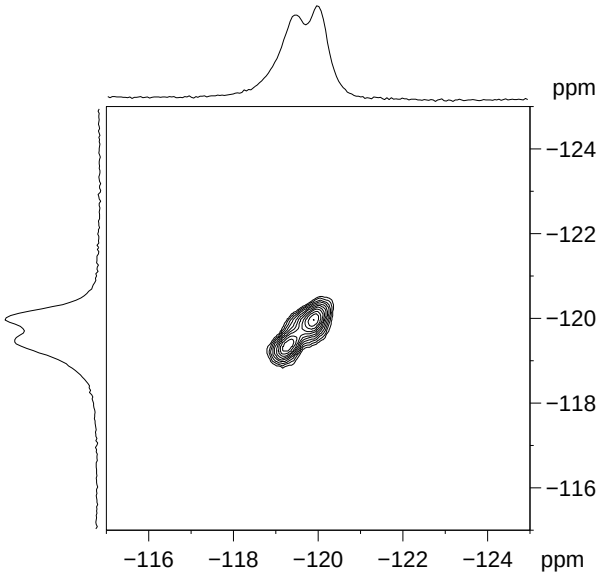

Figure 6.12: ^{19}*F 2D-NOESY spectrum of* ***1***·$\boldsymbol{C_6H_5F}$·***1*** *recorded at 240K, mixing time=100ms.*

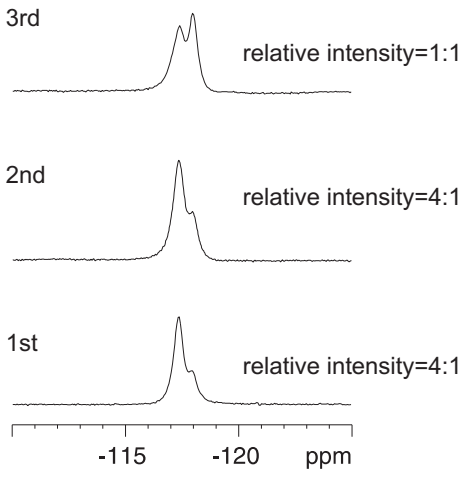

Figure 6.13: ^{19}*F MAS spectra of* ***1***·$\boldsymbol{C_6H_5F}$·***1*** *of three different batches.*

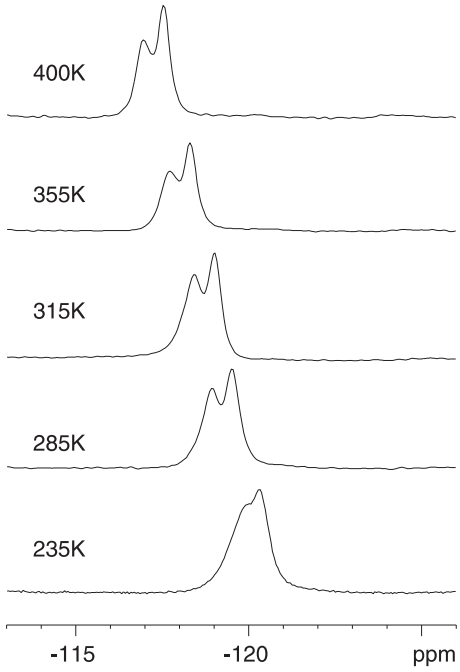

Figure 6.14: ^{19}*F temperature variable MAS spectra of* ***1***$\cdot C_6H_5F\cdot$***1***

6.3.4 Fluorobenzene-d_5 capsule

For comparison, fluorobenzene-d_5 was also encapsulated into tetra urea calix[4]arene allowing to monitor the respective guest dynamics via both ^{19}F and ^{2}H NMR. The corresponding ^{19}F and ^{2}H MAS spectra are shown in Fig. 6.15. Again, two peaks at -117.9 and -118.3 ppm, respectively, are observed in the ^{19}F MAS spectrum, thus resulting in a CIS of 4.8 ppm. The integrated area ratio of the two peaks amounts to 4:1, which is quite similar to that previously found for 1-fluorobenzene.

The ^{2}H MAS NMR spectrum of **1**·$\mathbf{C_6D_5F}$·**1** displays three peaks at 3.17, 5.03, and 6.5 ppm. Clearly, the latter can be assigned to "free" residual solvent that has not yet been removed completely upon drying. The other two peaks most likely result from splitting due to the presence of *ortho*−, *meta*−, and *para*−deuterons, respectively.

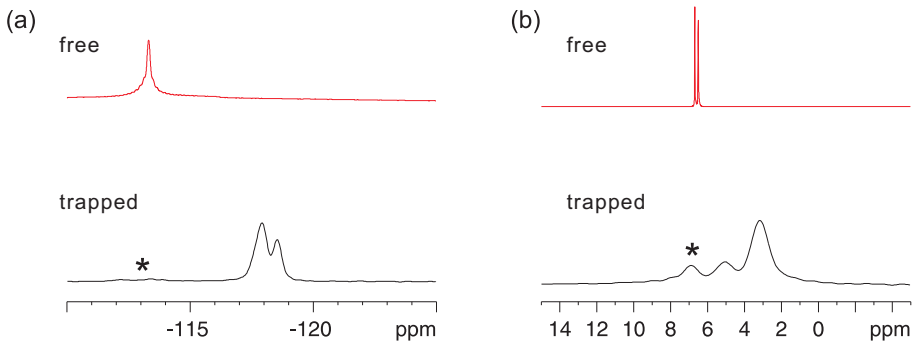

Figure 6.15: *(a) ^{19}F-spectra and (b) ^{2}H -spectra of* ***1***·$\boldsymbol{C_6D_5F}$·***1****. * : remaining free guest*

In an attempt to further remove any residual solvent and to possibly cure structural distortions, the sample was annealed at 100°C for two days. Indeed, distinct changes of the spectra were observed: the linewidth in the corresponding ^{19}F MAS NMR spectra was narrowed (FWHH: from 280 to 207Hz) while the contribution of the small peak at -118.3 ppm was reduced to approximately 4 percent (Fig. 6.16). Also, the ^{2}H MAS NMR spectrum indicated that all residual "free" solvent molecules were successfully removed leaving only included guests. Annealing the sample for 10 days does not show significant difference with the 2-day annealed sample. (data not shown).

The ^{2}H static NMR spectrum of **1**·$\mathbf{C_6D_5F}$·**1** (Fig. 6.17 (a)) exhibits almost a full width Pake pattern with an observed quadrupolar splitting of 121 kHz and an ill-defined inner Pake-like pattern with about 28 kHz splitting. While the outer Pake spectrum is clearly due to static phenyl groups, an inner Pake-like pattern with reduced width of $\omega_Q/4$ indicates large amplitude motion. In-plane motion leads at most to a

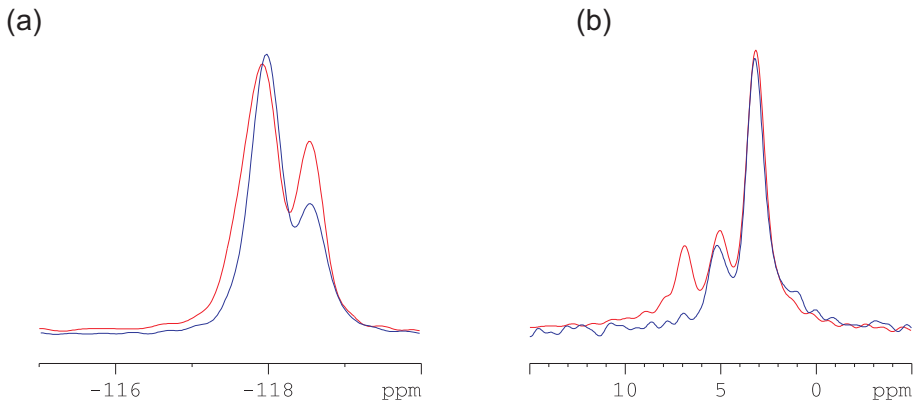

Figure 6.16: *Comparison of annealed sample with original sample(without annealing (a)* ^{19}*F-spectra and (b)* ^{2}*H spectra of* ***1***$\cdot\boldsymbol{C_6D_5F}\cdot$***1****. red one: before annealing, blue one: after annealing for 2 days.*

reduction of the splitting down to $\omega_Q/2$. Therefore, this spectral feature is attributed to phenyl rings undergoing an ill-defined 180° flip motion about the C-F axis. In contrast to pure 180° two-site jumps, where the molecules reside only in two well-defined orientations, ill-defined 180° flips are dynamic processes between two-site jumps and full rotation with a preferential orientation of the phenyl plane. Whereas full phenyl rotation around its C-F axis leads to an axially symmetric tensor with $\omega_Q/8$, ill-defined 180° flips with a broad rotational angle distribution can indeed lead to Pake-like patterns with a width of $\omega_Q/4$. Calculations of the averaged tensors show that for Gaussian distributions with 2σ between 50° and 60°, while the asymmetry parameter η stays below 0.11. Computed ^{2}H NMR line-shapes of the corresponding dynamic processes of the fluorobenzene in the calix[4]arene host are given in Fig. 6.17 (b). In fact, the superposition of a static Pake pattern and the simulated Pake-like line-shape due to an ill-defined out-of plane two-site jump motion is in good agreement with the experimental spectrum, apart from the inner rather sharp signal, which results most likely from some tumbling of "free" molecules. The large flip angle distribution needed to account for the inner spectrum, indicates that the plane of phenyl rings in the cavities is not at all well-defined but the experimental quadrupolar splitting excludes full axial rotation.[Albunia 05]

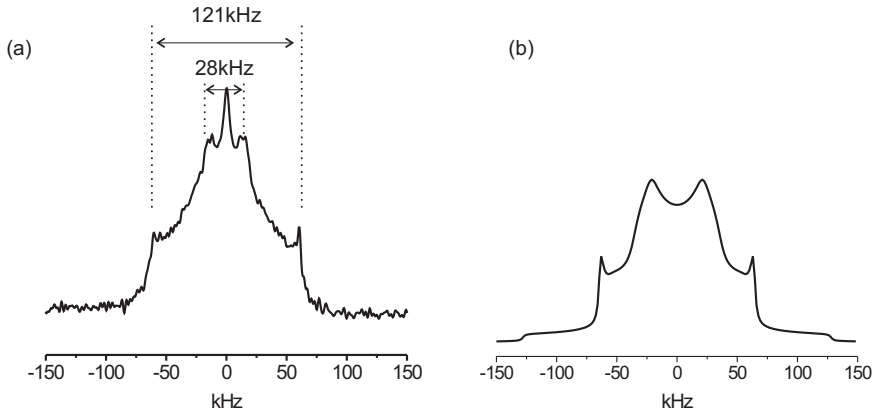

Figure 6.17: *(a)*^{2}*H static spectrum at 298K of* ***1***$\cdot\boldsymbol{C}_6\boldsymbol{D}_5\boldsymbol{F}\cdot$***1*** *and (b)simulated spectrum.*

6.3.5 1,4-difluorobenzene capsule

In order to possibly distinguish structural distortions from orientational preferences, *symmetric* guest 1,4-difluorobenzene was also included into the host cavity. The respective ^{19}F MAS NMR spectrum of $\mathbf{1}\cdot\mathbf{C_6H_4F_2}\cdot\mathbf{1}$ shows one resonance at -123.5 ppm with a FWHH of 415 Hz indicating a rather uniform orientation of 1,4-difluorobenzene guests. The complexation-induced chemical shift change of 1,4-diflurobenzene upon inclusion amounts to 4.2 ppm, and is thus comparable to that of flurobenzene suggesting a similar local ordering, e.g. proximity to the aromatic rings of the host structure. This finding is also consistent with the assumption that an *up*− or *down*− orientation of the fluorobenzene guest with respect the S_8-axis of the host result in similar CIS.

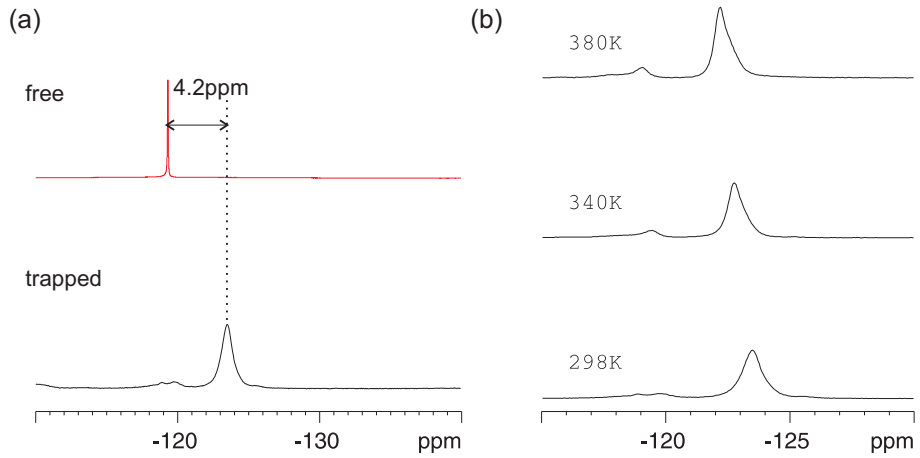

Figure 6.18: *(a) Comparison of ^{19}F-NMR spectra of 1,4-difluorobenzene free one and* $\mathbf{1}\cdot\mathbf{C_6H_4F_2}\cdot\mathbf{1}$. *(b) ^{19}F temperature variable MAS spectra of* $\mathbf{1}\cdot\mathbf{C_6H_4F_2}\cdot\mathbf{1}$

6.3.6 Cobaltocenium capsule

Considering the fact that the calix[4]arene cavity is quite sensitive with respect to the molecular size of included guests, finally the bulky cobaltocenium cation $Co(Cp)_2^+$ was incorporated into the dimeric assembly. It was already demonstrated that $Co(Cp)_2^+$ shows a high affinity towards encapsulation into the dimer driven by so-called cation-π interactions (in $C_2D_2Cl_4$ solution), but no solid-state characterization of the complex **[1·Co(Cp)$_2^+$·1](PF$_6^-$)** is known.

The corresponding ^{1}H MAS and ^{13}C CPMAS NMR spectra of pristine cobaltocenium and **[1·Co(Cp)$_2^+$·1](PF$_6^-$)** are given in Fig. 6.19.

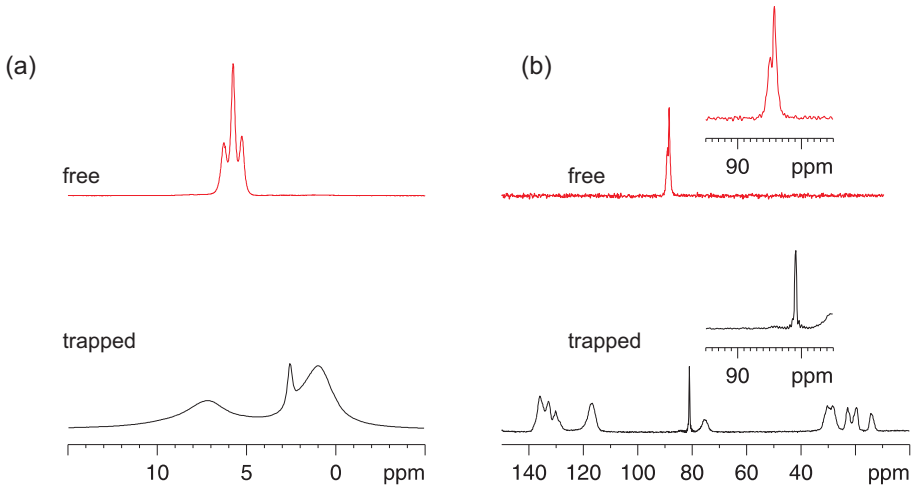

Figure 6.19: *Comparison of (a) ^{1}H MAS NMR spectra of* ***[Co(Cp)$_2^+$](PF$_6^-$)*** *and the dimer* ***[1·Co(Cp)$_2^+$·1](PF$_6^-$)*** *and (b) ^{13}C CPMAS NMR spectra of* ***[Co(Cp)$_2^+$](PF$_6^-$)*** *and the dimer* ***[1·Co(Cp)$_2^+$·1](PF$_6^-$)*** *at 500MHz (11.7T)*

Notably, signal splittings in both ^{1}H MAS and ^{13}C CPMAS spectra of pristine cobaltocenium salt at 11.7 T revealed the presence of *residual* dipolar couplings. The latter originate from a large ^{59}Co quadrupolar coupling that not only exceeds the Zeeman interaction but also prevents an efficient cancellation of dipolar couplings between ^{59}Co and the nucleus detected under fast MAS conditions. However, upon inclusion *no* splitting was observed in ^{1}H MAS and ^{13}C CPMAS spectra of the dimer **[1·Co(Cp)$_2^+$·1](PF$_6^-$)** indicating so-called "*self-decoupling*".

The effect of self-decoupling on the solid-state line shapes of spin 1/2 nucleus neighboring quadrupolar nucleus has been extensively described previously by Spiess *et al*. and Harris *et al*.[Spiess 77, Harris 89]. A more recent example is given by

Heise *et al*.[Heise 99] reporting effect of ^{59}cobalt self-decoupling on the solid state ^{13}C CPMAS spectra of the cobaltocenium salts.

They discussed effects of counterion, the temperature, rotor spinning rate, and the substituent of the cyclopentadienyl ligands on coupling patterns. Notably, it was observed that on heating to 370K, the coupling patterns collapse and the signals are narrowed. This phenomenon can result from two mechanisms: either the dipolar coupling tensor is completely averaged to zero by fast isotropic motion of the molecule, or dynamic processes induce fast T_1 relaxation of the quadrupolar nucleus, leading to self-decoupling of the ^{13}C nuclei. However, as the axially symmetric cation in $[Cp^*CpCo]^+[PF_6]^-$ is not likely to perform isotropic motions as well as the ring rotations, the observed phenomenon is more likely due to self-decoupling than to motional averaging.

Hence it can be concluded that the disappearance of the couplings in the ^{1}H and ^{13}C spectra of **[1·Co(Cp)$_2^+$·1](PF$_6^-$)** may be attributed to self-decoupling of the dipolar interactions between ^{59}Co and ^{1}H (^{13}C) due to the decrease of the T_1 (^{59}Co) upon inclusion. In this case, not only the observed chemical shifts but also the lineshapes changes upon inclusion reflect the successful inclusion of the Co(Cp)$_2^+$ moiety. At our highest available magnetic field (850 MHz, 20 T), the ^{59}Co Zeeman interaction slightly exceeds the quadrupolar coupling leading to a successful suppression of the previously noted *residual* dipolar couplings yielding isotropic peaks for both protons and carbons of Cp. This shows that the dipole-dipole coupling involving ^{59}Co can only be observed under rather special conditions and only slight changes in T_1 are required to achieve self-decoupling. Indeed, Heise *et al*.[Heise 99] observed self-decoupling upon changes of only the counter ion.

In addition, the ^{59}Co MAS NMR spectrum of "free" **[Co(Cp)$_2^+$](PF$_6^-$)** was measured. Under the fast MAS condition (30kHz), the isotropic chemical shift of -2430 ppm (Fig. 6.21) was obtained, which is in good agreement with the results reported by Spiess *et al*. and Ooms *et al*. independently [Spiess 69, Ooms 07]. However, it was not successful to observe cobalt NMR signal for inclusion compound **[1·Co(Cp)$_2^+$·1](PF$_6^-$)** which might also be due to shortening of T_1 upon inclusion.

Upon inclusion of Co(Cp)2$^+$, the obtained CIS amount to 3 ppm for ^{1}H and 3.4 ppm for ^{13}C , respectively. The CIS difference of 0.4 ppm most likely results from the C-H bond length of about 1.1 Å, however, it is reported that CIS(^{1}H) may exceed CIS(^{13}C). Notably, the CIS(^{1}H) of 3 ppm in the solid compound is identical to the reported proton CIS in $C_2D_4Cl_2$ solution, suggesting comparable local order within the cavity.

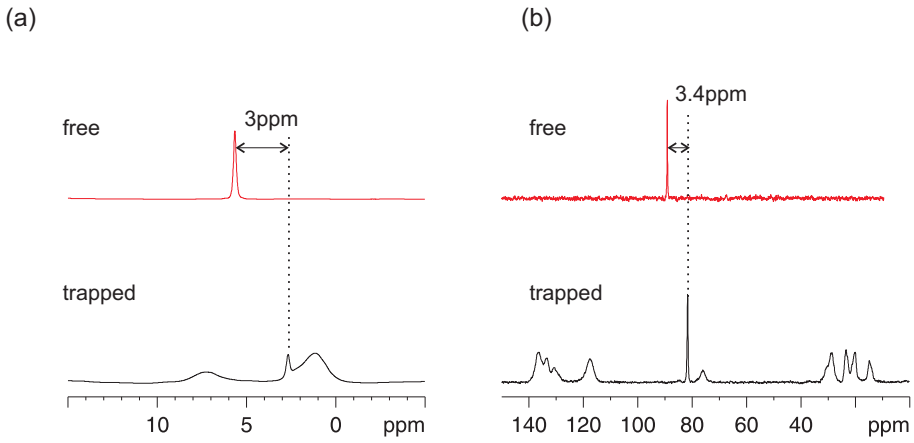

Figure 6.20: *Comparison of (a) ^{1}H MAS NMR spectra of* ***[Co(Cp)$_2^+$](PF$_6^-$)*** *and the dimer* ***[1·Co(Cp)$_2^+$·1](PF$_6^-$)*** *and (b) ^{13}C CPMAS NMR spectra of* ***[Co(Cp)$_2^+$](PF$_6^-$)*** *and the dimer* ***[1·Co(Cp)$_2^+$·1](PF$_6^-$)*** *at 850MHz (20T)*

The ^{1}H DQ MAS spectrum of **[1·Co(Cp)$_2^+$·1](PF$_6^-$)** is shown in Fig. 6.22. The sharp proton peak assigned to the Co(Cp)$_2^+$ ring protons shows a cross-peak with both aromatic protons and -CH$_2$ protons of the calix[4]arene host, which is consistent with Co(Cp)$_2^+$ cations captured inside the cavity. In contrast, the (PF$_6^-$) counterion has no observable influence on the inclusion and rests outside the host, as is indeed evidenced by both the ^{31}P chemical shift of the anion that did not change upon inclusion (Fig. 6.23(a)) and a characteristic cross-peak among (PF$_6^-$) and alkyl-chain protons obtained in a hetero-nuclear ^{1}H -^{31}P correlation experiment. Here, the alkyl chains are located outside the calix[4]arene cavity (Fig. 6.23(b)).

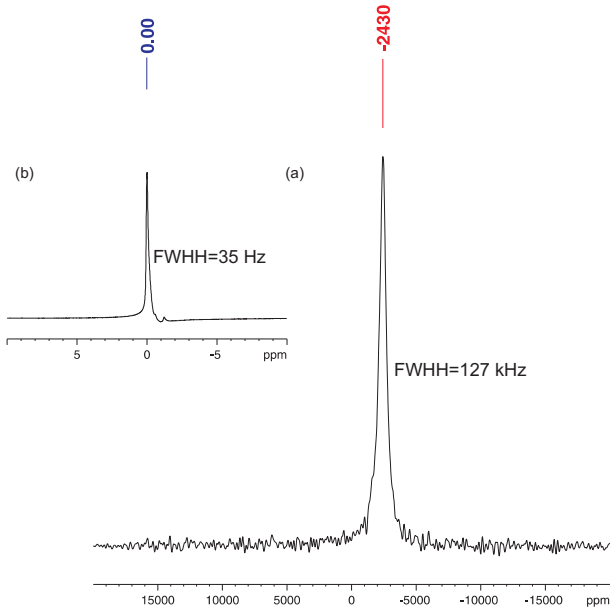

Figure 6.21: *(a)*^{59}*Co spectrum of* ***[Co(Cp)$_2^+$](PF$_6^-$)*** *referenced by (b)* $K_3(CoCN_6)$ *at 0ppm at 850MHz(20T).*

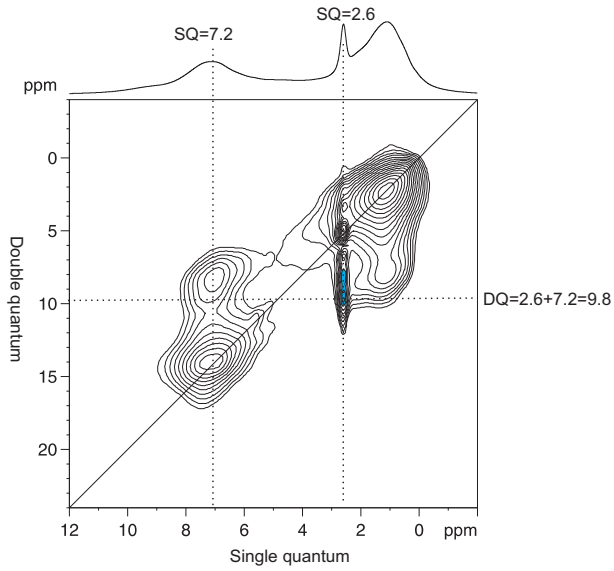

Figure 6.22: ^{1}*H DQ MAS spectrum of* ***[1·Co(Cp)$_2^+$·1](PF$_6^-$)*** *at 30kHz*

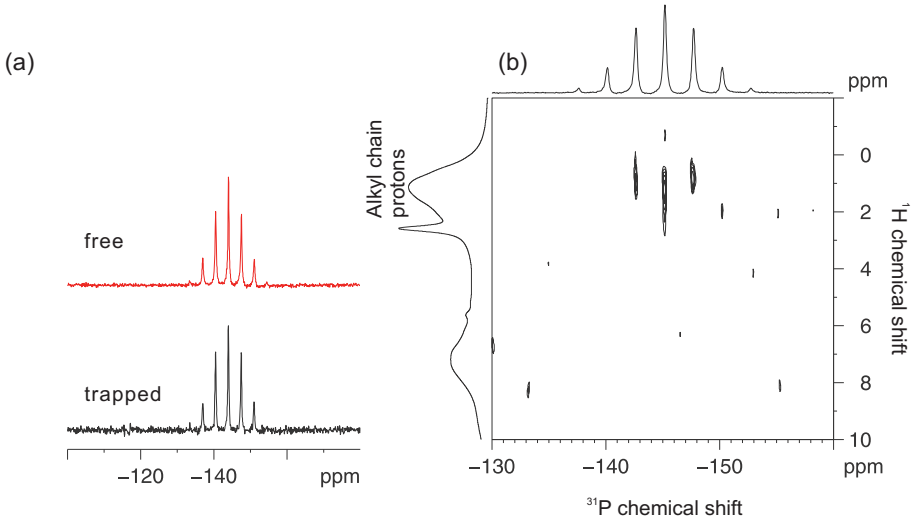

Figure 6.23: *(a) Comparison of* ^{31}*P-MAS spectra of* ***[Co(Cp)$_2^+$](PF$_6^-$)*** *and* ***[1·Co(Cp)$_2^+$·1](PF$_6^-$)*** *and (b)* ^{1}*H -*^{31}*P REPT-HSQC of* ***[1·Co(Cp)$_2^+$·1](PF$_6^-$)***

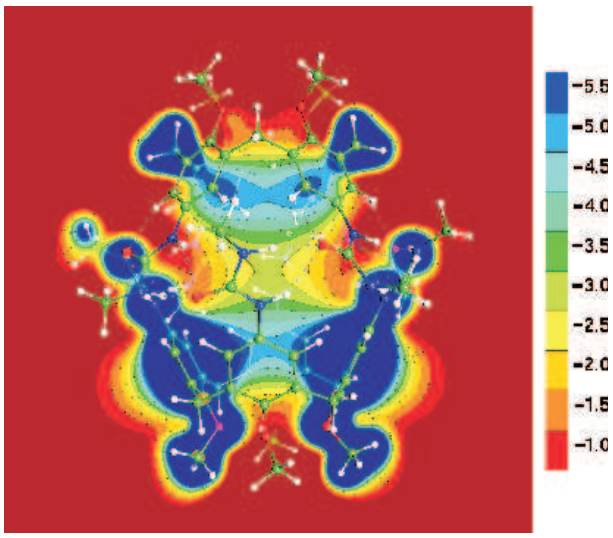

Figure 6.24: *The NICS map illustrates the spatially inhomogeneous magnetic susceptibility around an electron density distribution. Positive values NICS correspond to locally increased magnetic fields. Done by D.Sebastiani*

6.3.7 NICS map and MD simulation

To rationalize the observed complexation-induced chemical shifts, we computed a Nuclear Independent Chemical Shift (NICS) map of the calix[4]arene host. The NICS map of tetra urea calix[4]arene is computed based on the reported crystal structure [Mogck 96b]. In short, this map displays how much the local magnetic fields are changed due to the proximity of a particular host moiety, thereby providing a qualitative approach to experimentally observed CIS. This allows for an estimation of possible guest locations *inside* the calix[4]arene cavity even in the absence of refined X-ray data. The obtained NICS map is shown in Fig. 6.24. The orientation is chosen such that the plane comprised of the belt of stabilizing hydrogen-bonds is perpendicular to the paper plane, thus facilitating a comparison with idealized orientations depicted in Fig. 6.25.

In principle, an aromatic guest inside the tetra urea capsule can adopt three extreme orientations (Fig. 6.25). In the first case, the plane of the aromatic ring coincides with the equatorial plane and all substituents point to the seam of the hydrogen bonds(equ). In the other two cases, the S_8-axis of the host capsule (the long axis connecting the poles) bisects the plane of the aromatic ring. With the aromatic plane perpendicular to the equatorial plane, two opposing substituents either lie in the equatorial plane $\pi_{(equ)}$ or face the "poles" of the capsule $\pi_{(ax)}$ [Broda 06].

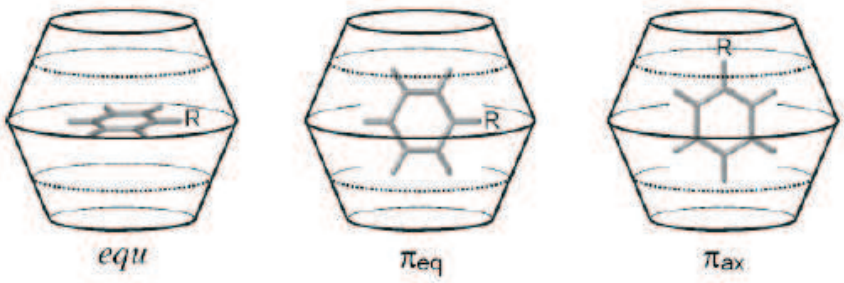

Figure 6.25: *Idealized orientations of aromatic guests within the host. Dashed lines denote the border region of the aromatic rings of the host. The middle circle represents the equatorial plane defined by the carbonyl carbon atoms of the urea functions [Broda 06].*

Based on the NICS map, we may conclude that benzene-d_6 guests with a CIS of 2.8 ppm (yellow-greenish region) are most likely located at the center of the cavity, with the molecular C_6-axis of motion perpendicular to the equatorial plane, but rather parallel to an additional S_8-axis defined by the host structure (equ). In case of fluorobenzene (CIS = 4.8 ppm) as well as 1,4-difluorobenzene (CIS = 4.2 ppm), however, the fluoro-atoms rather point to the "poles" of the capsule ((π_{ax}), turquoise region). This is in contrast to reported data on the supramolecular model complex *p-tert-butyl-* calix[4]arene-fluorobenzene suggesting that the fluorine substituent rather avoids contact with aromatic rings [Brouwer 99].

Since the NICS approach is strictly valid only in the complete absence of electron-electron interactions among the host structure and guest molecules, we have explicitly computed the ^{19}F and ^{2}H NMR chemical shifts for cavities with *one* as well as *two* either mono- or difluorobenzene molecules placed inside the host. For each system, a trial geometry was set up by hand, and the system was subsequently relaxed within density functional theory (DFT) using Car-Parrinello molecular dynamics (CPMD) simulations with a weak annealing of the atomic velocities.

The set of computed ^{19}F NMR chemical shifts with respect to a "free" 1,4-difluorobenzene molecule is shown in table 6.1. While there are considerable uncertainties in the precise determination of these shifts, certain trends can be recognized nevertheless. Except for a single centered guest, all doubly fluorinated benzenes are deshielded compared to the free molecule, which is an unexpected effect because of the nearby presence of aromatic moieties. However, we could reproduce a similar deshielding effect also at a higher level of theory in a model system, which was a difluorobenzene placed near an isolated benzene molecule.

This effect is most likely due to direct electronic interactions between the electron clouds of fluorine and the aromatic calix[4]arene moieties. The effect is particularly strong when the 1,4-difluorobenzene is located in an off-centered position, i.e. when it sticks to only one of the two calix[4]arene molecules. The centered difluorobenzene instead, whose fluorines are 3.1 Å away from the nearest host carbon, displays the expected additional shielding due to the surrounding aromatic cage structure. The same deshielding effect is observed when two monofluorobenzene molecules are contained in the host structure. In this case, the proximity of the fluorine atoms to the cage molecules lead to direct electronic interactions, which overcompensate the shielding effect of the aromatic moieties. If only a single guest is placed at a centered position in the cage, a shielding of 3-5 ppm is obtained with respect to an isolated monofluorobenzene, both for an axial or an equatorial orientation of the CF-bond. Instead, an attachment of the monofluorobenzene to one of the calix[4]arenes would lead to a ^{19}F chemical shift almost identical to that of a free molecule.

When comparing the computed ^{19}F chemical shifts with experimental shifts, it appears highly unlikely that *two* guest molecules can be hosted inside the calix[4]arene cages, since they would yield deshielded resonances, in contradiction to the shielding observed in experiment. Also, off-centered configurations exhibit this incorrect trend, so that only rather well-centered orientations remain consistent with the experimental findings. *Axial* and *equatorial* orientations of the fluorobenzenes can in principle result in chemical shift resonances differing by several ppm, which is indeed consistent with experimental data, but the uncertainties of the computed ^{19}F chemical shifts render an unambiguous assignment of the respective guest orientation impossible.

At this point, we may consider the computed ^{2}H chemical shifts. Since all off-centered guest locations as well as multiple guest molecules per host are safely ruled out based on the ^{19}F shifts, a single guest may be centered at an axial or equatorial position. The peak assignment is hampered due to the presence of *ortho*−, *meta*− and *para*− deuterons with respect to the ^{19}F substituent. The computed ^{2}H chemical shifts strongly suggest that the *para*-deuteron may indicate the respective orientation, as the predicted complexation-induced shifts of both *ortho*− and *para*− deuterons are rather similar (including an approximate error of $\pm$0.5 ppm).

Experimentally, two resonances are observed in the ^{2}H MAS spectrum, with a CIS of 3.4 ppm and 1.6 ppm respectively with relative intensity of 4:1(major:minor). If we assume that the minor peak can be attributed to the para-deuterons, then the CIS of 1.6 ppm rather suggest an equatorial position for the fluorobenzene-d_5 molecule. In fact, the computed ^{2}H CISs of the *para*-deuteron amounts to either 1.0 ppm (equ.) or 4.4 ppm (axial), respectively. Since the *para*-deuteron cannot be the major signal

fraction, an axial orientation appears unlikely, though contradicting the conclusion based on fluorine shifts. In an equatorial orientation, the *ortho*− and *meta*− deuterons have predicted CISs of 3.6 ppm and 3.4 ppm, which is in rather good agreement with experimental data. Upon comparison with the NICS map, we finally arrive at an (π_{equ}) orientation of fluorobenzene-d_5 inside the host.

Recently, a chemical molecular dynamics simulation study of tetra urea calix[4]arene host with a variety of aromatic guest molecules including fluorobenzenes suggested a pronounced preference for the (π_{equ}) orientation on the MD timescale (9-18 ns simulation time), but did not provide explicit chemical shifts of the guest molecules in their respective orientation [Broda 06]. Nevertheless, it appears difficult to explain why the guest molecules should retain their orientations during the relatively long timescale (μs-ms)) of the NMR measurement. A possible explanation could be a self-consistent rearrangement of the host structures, in response to one or another guest orientation, which would then lead to a self-consistent stabilization of a once-attained orientation.

	Single guest, centered	Single guest, off-centered	Two guests	Free molecule
F_1-Benzene $^{19F}(\delta)$	3.6^{eq} 1.9^{ax}	6.1^{op} 6.2^{HB}	7.5^{op}	6.6
F_2-Benzene $^{19F}(\delta)$	-2.7^{ax}	11.5^{op} 4.1^{HB}	-2.7^{op}, 3.0^{op} 0.3^{HB},4.7^{HB}	0.0 (by def.)
F_1-Benzene $^{2H}(\delta)$	$[3.6^{ax}$; $2.4^{eq}]^{ortho}$ $[3.5^{ax}$; $2.9^{eq}]^{meta}$ $[1.6^{ax}$; $5.0^{eq}]^{para}$	$[3.3^{op}$; $4.6^{HB}]^{ortho}$ $[5.1^{op}$; $2.8^{HB}]^{meta}$ $[4.2^{op}$; $1.5^{HB}]^{para}$	$2.8^{ortho,op}$ $4.5^{meta,op}$ $4.4^{para,op}$	$6.0^{para,ortho}$ 6.3^{meta}

Table 6.1: *Fluorine and deuteron NMR chemical shifts of fluorobenzene molecules confined inside a calix[4]arene host structure, computed from DFT calculations. All shifts are in ppm and referenced to the computed shieldings of a free difluorobenzene molecule (for ^{19}F) and of TMS (for ^{2}H). The superscript* ***op*** *indicates an orientation towards the "opening" of the cages where the ethylene oxide is located,* ***HB*** *means an orientation towards the H-bond ring of the calix[4]arene dimer,* ***ax*** *refers to an axial orientation of a centered molecule (the CF bond being parallel to the connection between the two openings), and* ***eq*** *represents an equatorial orientation (the CF being in the plane of the H-bond ring). In some cases, two independent calculations have been performed at two different geometries, illustrating the variance of the computed values. Done by D.Sebastiani*

6.4 Conclusions

Based on ^{1}H DOSY NMR, the hydrodynamic radius (R_H=0.7nm) of the tetraurea calix[4]arene in DMSO was obtained, while in the non-polar solvent benzene-d_6, an R_H of 0.96nm was found, reflecting the formation of a dimer. Use of an external locking NMR tube allowed to observe the encapsulated benzene solvent resonance at 4.3ppm, which DOSY NMR consistently revealed identical translational diffusion coefficients of both the calix[4]arenes host and its entrapped benzene guest.

Furthermore, several different types of capsular contents of tetraurea calix[4]arene (benzene, benzene-d_6, fluorobenzene, fluorobenzene-d_5, 1,4-difluorobenzene, and cobaltocenium) **in the solid state** were studied. Upon inclusion all the entrapped guest moieties showed CIS(complexation induced shifts) varying from 2.7ppm-4.8ppm. The ^{1}H -^{2}H heteronuclear correlation spectrum of **1**·$\mathbf{C_6D_6}$·**1** reveals only *cross*-peaks of deuterons with protons pointing *inside* the cavity, which also emphasizes that there are no benzene-filled voids present in the structure. Evidences that the local order of guests within the dimeric assembly is maintained were collected in the solid state applying multinuclear solid state NMR techniques. All guest molecules were shown to undergo distinct motions, ranging from mere C_6-rotations (benzene) to ill-defined 180 °C phenyl flips (fluorobenzene-d_5).

In the solid state, two peaks were observed in the ^{19}F-MAS spectra for both **1**·$\mathbf{C_6D_5F}$·**1** and **1**·$\mathbf{C_6H_5F}$·**1** capsules. Though the exact nature of the two peaks is not perfectly clear, the presence of slightly distinct orientation of fluorobenzene was suggested. The calix[4]arene host cavity even accommodates the bulky cobaltocenium cation, while the counterion stays outside, as demonstrated by ^{31}P MAS and ^{1}H -^{31}P correlation experiment.

Using the combined approach of a Nuclear Independent Chemical Shift (NICS) map and ^{19}F and ^{2}H ab-initio DFT chemical shift calculations, it was possible to locate the guests inside the host cavity qualitatively based on complexation-induced shifts. Benzene-d_6, for example, populates the center plane (so-called (equ)) comprised of the stabilizing seam of hydrogen-bonds of the urea units, while fluorobenzene-d_5 prefers an (π_{equ}) position. All off-centered orientations towards the "walls" of the host can be ruled out.

Chapter 7

Summary

Supramolecular aggregate systems in both solution and solid state were investigated by advanced NMR methods. In particular, ^{1}H fast MAS and dipolar recoupling experiments proved to be very powerful in studying local structure and dynamics of complex supramolecular architectures. In this work, particularly materials lacking long-range order were considered, where established scattering techniques are limited, hence solid state NMR was of indispensable help. Moreover, where applicable, the interpretation of experimental results was facilitated by computational methods, such as DFT-based ab-initio chemical shift calculation, Nucleus-Independent Chemical Shift(NICS) maps.

The solid state structures of three barbituric acid derivatives **(1-*n*-butyl-5-phenyl barbituric acid(Bu)**, **1-*n*-butyl-5-(4-nitrophenyl)-barbituric acid(NiBu)**, **1,3-dimethyl-5-(4-nitrophenyl)-barbituric acid(NiDMe))** and their assembled complexes with bases of varying basicity **(2,6-diacetamidopyridine(DAC)**, **2,6-diaminopyridine(DAP)**, **Proton Sponge(PS: 1,8-bis(dimethylamino)-naphthalene))** were derived. The novel enolizable chromophor, **1-n-butyl-5-(4-nitrophenyl)-barbituric acid (NiBu)** preferably adopts an *enol*1 form with vicinal NH and OH protons. In the presence of strong bases like the so-called proton sponge **(PS)**, a simple acid-base reaction occurred where the OH proton of NiBu was stripped. The corresponding enolate anion of **NiBu** revealed a dimeric structure, reflecting the stability of this arrangement. The enolic dimer can be broken upon addition of adenine-mimetic base **2,6-diacetamidopyridine (DAC)**, which offers a complementary hydrogen-bonding pattern. However, if that pattern is offered to pristine **NiBu**, as in the case of **NiBu+DAC**, complex formation competes with self-aggregation of **NiBu** in the solid-state. A similar competition was observed upon

addition of **2,6-diaminopyridine (DAP)** to **NiBu**. In the latter case, the salt formation due to proton transfer is preferred contrary to hydrogen-bonded complexation. It has been shown that both the prototropic tautomerism and the acidity of the enolizable barbituric acids in the solid compounds is strongly influenced by ordering or packing effects, which are absent in solution.

In addition, DOSY NMR provided deep insights into the size of different supramolecular entities in solution. NMR experiments employing pulsed field gradients (PFGs) have been used for many years to measure the diffusion coefficients of species in solution. PFG NMR experiments directly measure the net displacement of nuclear spins during a defined delay, and such displacements can be related to the translational diffusion coefficients of the spins that give rise to the resonances in question. Since diffusion coefficients are related to the effective radius of the molecular species, DOSY NMR could be applied to determine the size of different supramolecular entities in solutions. The well established preparative chemistry of calix[4]arenes allows the synthesis of specific derivatives which are not only able to self-assemble, but also to take part in self-sorting processes. For the individual components **4b** and **3x**, diffusion coefficients were 8.6×10^{-11} and $6.2 \times 10^{-11} m/s^2$ respectively. However, the diffusion coefficient of $\mathbf{3}_2 \cdot \mathbf{4b}_6$ was $5.4 \times 10^{-11} m/s^2$ for all ^{1}H signals, proving the existence of a uniform dendritic assembly as well as the absence of both larger aggregates and smaller components (Fig. 5.6).

Recently, Klyatskaya *et al*. showed *via* DLS and X-ray scattering experiments that nanometer-size dicationic shape-persistent macromolecules in nonpolar solvents do not form infinite tubular aggregates, as might be expected from their chemical structure, but dimerize to defined supermolecules [Klyatskaya 06]. This result was supported by hydrodynamic radii obtained from 2D DOSY experiments. The diffusion coefficient of **1** in CD_2Cl_2 was found to be $2.2 \times 10^{-10} m/s^2$, which results in hydrodynamic radius of $2.1nm$ (Fig. 5.9). However in cyclohexane a larger hydrodynamic radius of about $2.6nm$ was measured for **1**. Considering the ratio between the two determined hydrodynamic radii it is assumed that the aggregated structure is *dimeric* rather than a larger scale supramolecule.

Several different capsular contents of tetra urea calix[4]arenes (benzene, benzene-d_6, fluorobenzene, fluorobenzene-d_5, 1,4-difluorobenzene, and the cobaltocenium ion) **in the solid state** are studied by advanced NMR techniques. First based on ^{1}H DOSY NMR, the hydrodynamic radii of both the tetra urea calix[4]arene monomer($R_H = 0.7nm$) and dimer($R_H = 0.96nm$) in solution were determined. Upon

inclusion all the entrapped guest moieties showed CIS (complexation induced shifts) varying from 2.7ppm-4.8ppm. The ^{1}H -^{2}H heteronuclear correlation spectrum of **1**·$\mathbf{C_6D_6}$·**1** reveals only *cross*-peaks of deuterons with protons pointing *inside* the cavity, which also emphasizes that there are no benzene-filled voids present in the structure. Evidences that the local order of guests within the dimeric assembly is maintained were collected in the solid state applying multinuclear solid state NMR techniques. All guest molecules were shown to undergo distinct motions, ranging from mere C_6-rotations (benzene) to ill-defined 180°C phenyl flips (fluorobenzene-d_5). In the solid state, two peaks were observed in the ^{19}F-MAS spectra for both **1**·$\mathbf{C_6D_5F}$·**1** and **1**·$\mathbf{C_6H_5F}$·**1** capsules. Though the exact nature of the two peaks is not perfectly clear, the presence of slightly distinct orientation of fluorobenzene was suggested. The calix[4]arene host cavity even accommodates the bulky cobaltocenium cation, while the counterion stays outside, as demonstrated by ^{31}P MAS and ^{1}H -^{31}P correlation experiment. Using the combined approach of a Nuclear Independent Chemical Shift (NICS) map and ab-initio DFT chemical shift predictions for ^{19}F and ^{2}H nuclei, it was possible to locate the guests inside the host cavity qualitatively based on their respective complexation-induced shifts. Benzene-d_6, for example, populates the center plane (so-called (*equ*)) comprised of the stabilizing seam of hydrogen-bonds of the urea units, while fluorobenzene-d_5 prefers an (π_{equ}) position, where off-centered orientations towards the "walls" of the host were safely ruled out.

In summary, the results of this work contributed to the understanding of structural and dynamical properties of complex supramolecular systems.

Bibliography

[Abragam 61] A. Abragam. The Principles of Nuclear Magnetism. Oxford Univ. Press, Oxford (1961).

[Alam 07] T. M. Alam, M. Nyman, S. K. McIntyre. Double Quantum ^{1}H MAS NMR Studies of Hydrogen-Bonded Protons and Water Dynamics in Materials . *J. Phys. Chem. A* **111**, 1792–1799 (2007).

[Albunia 05] Alexandra R. Albunia, Robert Graf, Gaetano Guerra, Han Wolfgang Spiess. ^{2}H NMR Study of Aromatic Guest Dynamics in Clathrate Phases of Syndiotatic Polystyrene. *Macromol. Chem. Phys.* **206**, 715–724 (2005).

[Alder 89] R. W. Alder. Strain effects on amine basicities . *Chem. Rev.* **89**, 1215–1223 (1989).

[Allen 02] F. H. Allen. . *Acta Crystallogr.*pp. 380–388 (2002).

[Andrew 58] E. R. Andrew, A. Bradbury, R. G. Eades. Nuclear Magnetic Resonance Spectra from a Crystal Rotated at High Speed. *Nature* **182**, 1659 (1958).

[Antalek 02] Brian Antalek. Using Pulsed Gradient Spin echo NMR for Chemical Mixture Analysis: How to Obtain Optimum Results. *Concepts in Magnetic Resonance* **14**, 225–258 (2002).

[Benedicte 05] E. Benedicte, L. Emsley. Powder Crystallography by Proton Solid-State NMR Spectroscopy. *J. Am. Chem. Soc.* **127**, 9140–9146 (2005).

[Benedicte 06] E. Benedicte, G. Pintacuda, N. Mifsud, L. Emsley. Molecular Structure Determination in Powders by NMR Crystallography from Proton Spin Diffusion. *J. Am. Chem. Soc.* **128**, 9555–9560 (2006).

[Bennett 95] A. E. Bennett, C. M. Rienstra, M. Auger, K. V. Lakshmi, R. G. Griffin. Heteronuclear Decoupling in Rotating Solids. *J. Chem. Phys.* **103**, 6951–6958 (1995).

[Bloch 46] F. Bloch. Nuclear Induction. *Phys. Rev.* **70**, 460–474 (1946).

[Bohanon 95] T. M. Bohanon, S. Denzinger, R. Fink, W. Paulus, H. Ringsdorf, M. Weck. Barbituric Acid/2,4,6-Triaminopyrimidine Aggregates in Water and Their Competitive Interaction with a Monolayer of Barbituric Acid Lipids at the Gas-Water Interface. *Angew. Chem. Int. Ed.* **34**, 58–60 (1995).

[Bohanon 99] T. M. Bohanon, P.-L. Caruso, S. Denzinger, R. Fink, D. Möbius, W. Paulus, J. A. Preece, H. Ringsdorf, D. Schollmeyer. Molecular Recognition-Induced Function and Competitive Replacement by Hydrogen-Bonding Interactions: Amphiphilic Barbituric Acid Derivatives, 2,4,6-Triaminopyrimidine, and Related Structures at the Air-Water Interface . *Langmuir* **15**, 174–184 (1999).

[Bolz 06] I. Bolz, S. Spange (2006). unpublished results.

[Breitmaier 93] E. Breitmaier. Structure Elucidation by NMR in Organic Chemistry. J. Wiley & Sons Ltd., Chichester (1993).

[Broda 06] Frank Broda, Myroslav O. Vysotsky, Volker Böhmer, Iris Thondorf. Orientational preferences of aromatic guests in dimeric capsules of tetraurea calix[4]arenes-MD and NMR studies. *Org. Biomol. Chem.* **4**, 2424–2432 (2006).

[Brouwer 97] E. B. Brouwer, G. D. Enright, J. A. Ripmeester. Solid-State NMR and Diffraction Studies of a Tunable *p-tert*-Butylcalix[4]arene $\cdots$ Guest Structure. *J. Am. Chem. Soc.* **119**, 5404–5412 (1997).

[Brouwer 99] E. B. Brouwer, R. D. M. Gougeon, J. Hirschinger, K. A. Udachin, R. K. Harris, J. A. Ripmeester. Intermolecular distance measurements in supramolecular solids: ^{13}C-^{19}F REDOR NMR spectroscopy of *p-tert*-butylcalix[4]arene fluorobenzene . *Phys. Chem. Chem. Phys.* **1**, 4043–4050 (1999).

[Brown 00] S. P. Brown, I. Schnell, J. D. Brand, K. Müllen, H. W. Spiess. A ^1H Double-quantum Magic-angle Spinning Solid-state NMR Investigation of Packing and Dynamics in Triphenylene and Hexabenzocoronene Derivatives. *J. Mol. Struc.* **521**, 179–195 (2000).

[Brown 01] S. P. Brown, H. W. Spiess. Advanced Solid-state NMR Methods for the Elucidation of Structure and Dynamics of Molecular, Macromolecular and Supramolecular systems. *Chem. Rev.* **101**, 4125–4155 (2001).

[Brown 07] S. P. Brown. Probing proton-proton proximities in the solid state. *Progr. NMR Spectrosc.* **101**, 199–251 (2007).

[Carravetta 00] M. Carravetta, M. Edén, X. Zhao, A. Brinkmann, M. H. Levitt. Symmetry Principles for the Design of Radiofrequency Pulse Sequences in the Nuclear Magnetic Resonance of Rotating Solids. *Chem. Phys. Lett.* **321**, 205–215 (2000).

[Castellano 98] R. K. Castellano, Rebek J. Jr. Formation of Discrete, Functional Assemblies and informational Polymers through the Hydorgen-Bonding Preferences of Calixarene Aryl and Sulfonyl Tetraureas. *J. Am. Chem. Soc.* **120**, 3657–3663 (1998).

[Cavanagh 96] J. Cavanagh, W. J. Fairbrother, A. G. Palmer III, N. J. Skelton. Protein NMR Spectroscopy - Principles and Practise. Academic Press, San Diego, CA (1996).

[Claridge 99] Timothy D W Claridge. High-Resolution NMR techniques in Organic Chemistry. Elsevier Science, Oxford (1999).

[Cohen 05] Yoram Cohen, Liat Avram, Limor Frish. Diffusion NMR Spectroscopy in Supramolecular and Combinatorial Chemistry: An Old Parameter-New Insights. *Angew. Chem. Int. Ed.* **44**, 520–554 (2005).

[Crank 97] J. Crank. The Mathematics of Diffusion, 2nd ed. Claxendon, Oxford (1997).

[Cussler 84] E. L. Cussler. Diffusion: Mass Transfer in Fluid Systems. Cambridge University, Cambridge (1984).

[Davis 76] J. H. Davis, K. R. Jeffrey, M. Bloom, M. I. Valic, T. P. Higgs. Quadrupolar Echo Deuteron Magnetic Resonance Spectroscopy in Ordered Hydrocarbon Chains. *Chem. Phys. Lett.* **42**, 390–394 (1976).

[deAzevedo 99] E. R. deAzevedo, W.-G. Hu, T. J. Bonagamba, K. Schmidt-Rohr. Centerband-Only Detection of Exchange: Efficient Analysis of Dynamics in Solids by NMR. *J. Am. Chem. Soc.* **121**, 8411–8412 (1999).

[Dehner 05] A. Dehner. Diffusion NMR Spectroscopy: Folding and Aggregation of Domains in p53. *ChemBioChem* **6**, 1550–1565 (2005).

[Demeunynck 03] M. Demeunynck, C. Bailly, W. D. Wilson. DNA and RNA binders. Wiley, Weinheim (2003).

[Densmore 05] C. G. Densmore, P. G. Rasmussen, G. R. Goward. Probing Hydrogen Bonding and Proton Mobility in Dicyanoimidazole Monomers and Polymers . *Macromolecules* **38**, 416–421 (2005).

[Detken 02] A. Detken, E. H. Hardy, M. Ernst, B. H. Meier. Simple and Efficient Decoupling in Magic-angle Spinning Solid-state NMR: the XiX Scheme. *Chem. Phys. Lett.* **356**, 298–304 (2002).

[Duer 04] M. J. Duer. Solid-State NMR Spectroscopy. Blackwell Publishing, Oxford (2004).

[Dusold 00] S. Dusold, A. Sebald. Dipolar Recoupling under Magic-Angle Spinning Conditions. In Annual reports on NMR spectroscopy, Volume 41, pp. 185–264. Academic Press (2000).

[Eckert 05] H. Eckert, S. Elbers, J. D. Epping, M. Janssen, M. Kalwei, W. Strojek, U. Voigt. Dipolar Solid State NMR Approaches Towards Medium-Range Structure in Oxide Glasses. *Topics in Current Chemistry* **246**, 195–233 (2005).

[Emsley 85] J. W. Emsley. Nuclear Magnetic Resonance of Liquid Crystals, Nato ASI Series. D. Reidel Publishing Company, Dordrecht (1985).

[Ernst 03] M. Ernst. Heteronuclear Spin Decoupling in Solid-state NMR under Magic-angle Sample Spinning. *J. Magn. Reson.* **162**, 1–34 (2003).

[Evans 95] J. N. S. Evans. Biomolecular NMR Spectroscopy. Oxford University Press, Oxford (1995).

[Feike 96] M. Feike, D. E. Demco, R. Graf, J. Gottwald, S. Hafner, H. W. Spiess. Broadband Multiple-Quantum NMR Spectroscopy. *J. Magn. Reson. A* **122**, 214–221 (1996).

[Fischbach 03] I. Fischbach. *Supramolecular Order and Dynamics of Discotic Materials Studied by Solid-State NMR Recoupling Methods*. Dissertation, Universität Mainz (2003).

[Gan 97] Z. Gan, R. R. Ernst. Frequency- and Phase-modulated Heteronuclear Decoupling in Rotating Solids. *Solid State Nucl. Magn. Res.* **8**, 153–159 (1997).

[Gerstein 85] B.C. Gerstein, C.R. Dybowski. Transient Techniques in NMR of Solids. Academic Press, London (1985).

[Ghadiri 95] M. R. Ghadiri, K. Kobayashi, J. R. Granja, R. K. Chalha, D. E. McRee. The Structural and Thermodynamic Basis for the Formation of Self-Assembled Peptide Nanotubes . *Angew. Chem., Int. Ed. Engl.* **34**, 93–95 (1995).

[Gullion 89a] T. Gullion, J. Schaefer. Detection of Weak Heteronuclear Dipolar Coupling by Rotational-Echo Double-Resonance Nuclear Magnetic Resonance. *Adv. Magn. Reson.* **13**, 57–83 (1989).

[Gullion 89b] T. Gullion, J. Schaefer. Rotational-Echo Double-Resonance NMR. *J. Magn. Reson.* **81**, 196–200 (1989).

[Gullion 97] T. Gullion. Measurement of Heteronuclear Dipolar Interactions by Rotational-Echo, Double-Resonance Nuclear Magnetic Resonance. *Magn. Reson. Rev.* **17**, 83–131 (1997).

[Gutsche 98] C. D. Gutsche. Calixarenes Revised. RSC, Cambridge (1998).

[Haeberlen 68] U. Haeberlen, J. S. Waugh. Coherent Averaging Effects in Magnetic Resonance. *Phys. Rev.* **175**, 453–467 (1968).

[Hahn 50] E. L. Hahn. Spin Echoes. *Phys. Rev.* **80**, 580–594 (1950).

[Haitao 99] H. Haitao, AJ. Shaka. Composite pulsed gradients with refocued chemical shifts and short recovery times. *J. Magn. Reson.* **136**, 54–62 (1999).

[Hamann 96] B. C. Hamann, K. D. Shimizu, Jr J. Rebek. test. *Angew. Chem. Int. Ed.* **108**, 1425– (1996).

[Harris 89] R. K. Harris, A. Root. High-resolution phosphorus-31 N.M.R. studies of solid phosphorus pentachloride. *Mol. Phys.* **66**, 993–1013 (1989).

[Heise 99] Henrike Heise, Frank H. Köhler, Eric B. Brouwer, Robin K. Harris, Stefan Steuernage. ^{59}Co second-order quadrupolar effects in the ^{13}C cross-polarization magic angle spinning NMR spectra of the cobaltocenium salts $[CP^*_2Co]^+[PF_6^-]$ and $[CP^*CpCo]^+[PF_6^-]$. *Magn. Reson. Chem.* **37**, 573–578 (1999).

[Höger 04] Sigurd Höger. Shape-Persistent Macrocycles: From Molecules to Materials. *Chem. Eur. J.* **10**, 1320–1329 (2004).

[Hughes 04] C. E. Hughes. test. *Prog. Nucl. Magn. Reson. Spectrosc.* **45**, 301 (2004).

[Huo 03] R. Huo, R. Wehrens, J. van Duynhoven, L.M.C. Buydens. Assessment of techniques for DOSY NMR data processing. *Analytica Chimica acta* **490**, 231–251 (2003).

[Jeener 71] J. Jeener (1971). Ampere International Summer School, Basko Polje, Yogoslavia.

[Jehenson 90] P. Jehenson, M. Westphal, N. Schuff. Analytical Method for the compensation of eddy-current effets induced by pulsed magnetic field gradeints in NMR systems. *J. Magn. Reson.* **90**, 264–278 (1990).

[Johnson 99] C. S. Johnson. Diffusion ordered nuclear magnetic resonance spectroscopy: principles and applications. *Progress in Nuclear Magnetic Resonance Spectrosocpy* **34**, 203–256 (1999).

[Kaljurand 05] I. Kaljurand, A. Kütt, L. Sooväli, T. Rodima, V. Mäemets, I. Leito, I. A. Koppel. Extension of the Self-Consistent Spectrophotometric Basicity Scale in Acetonitrile to a Full Span of 28 pKa Units: Unification of Different Basicity Scales . *J. Org. Chem.* **70**, 1019–1028 (2005).

[Khitrin 03] A. K. Khitrin, Toshimichi Fujiwara, Hideo Akutsu. Phase-modulated Heteronuclear Decoupling in NMR of Solids. *J. Magn. Reson.* **162**, 46–53 (2003).

[Klyatskaya 06] Svetlana Klyatskaya, Nico Digenouts, Christine Rosenauer, Beate Müller, Sigurd Höger. Cationic Shape-Persistent Macrocycles: The Unexpected Formation of a Nano-Size Supramolecular Dimer. *J. Am. Chem. Soc.* **128**, 3150–3151 (2006).

[Kyogoku 68] Y. Kyogoku, R. C. Lord, A. Rich. Specific Hydrogen Bonding of Barbiturates to Adenine Derivatives. *Nature* **218**, 69–72 (1968).

[Lee 95] Y. K. Lee, N. D. Kurur, M. Helmle, O. G. Johannessen, N. C. Nielsen, M. H. Levitt. Efficient Dipolar Recoupling in the NMR of Rotating Solids. A Sevenfold Symmetric Radiofrequency Pulse Sequence. *Chem. Phys. Lett.* **242**, 304–309 (1995).

[Lehn 02] J.-M. Lehn. Supramolecular polymer chemistry -scope and perspectives. *Polymer International* **51**, 825–839 (2002).

[Lesage 01] A. Lesage, L. Duma, D. Sakellariou, L. Emsley. Improved Resolution in Proton NMR Spectroscopy of Powdered Solids. *J. Am. Chem. Soc.* **123**, 5747–5752 (2001).

[Levitt 01] M. Levitt. Spin Dynamics. Wiley, Weinheim (2001).

[Llamas-Saiz 94] A. L. Llamas-Saiz, C. Foces-Foces, J. Elguero. Proton sponges . *J. Mol. Struct* **328**, 297–323 (1994).

[Lowe 59] I. J. Lowe. Free Induction Decays of Rotating Solids. *Phys. Rev. Lett.* **2**, 285–287 (1959).

[Macho 01] V. Macho, L. Brombacher, H. W. Spiess. The NMR-WEBLAB: an Internet Approach to NMR Lineshape Analysis. *Appl. Magn. Res.* **20**, 405–432 (2001).

[Malinowski 91] ER Malinowski, DG Howery. Factor analysis in chemistry. Wiley, New York (1991).

[Marion 83] D. Marion, K. Wüthrich. Application of Phase Sensitive Two-dimensional Correlated Spectroscopy (COSY) for Measurements of H-1 H-1 Spin-spin Coupling-constants in Proteins. *Biochem. Biophys. Res. Commun.* **113**, 967–974 (1983).

[Marion 89] D. Marion, M. Ikura, R. Tschudin, A. Bax. Rapid Recording of 2D NMR-Spectra without Phase Cycling- Application to the Study of Hydrogen-Exchange in Proteins. *J. Magn. Res.* **85**, 393–399 (1989).

[Mehring 83] M. Mehring. High Resolution NMR of Solids. Springer-Verlag, Berlin (1983).

[Merrill 93] MR. Merrill. NMR diffusion measurements using a composite gradeint PGSE sequence. *J. Magn. Reson. Ser A* **103**, 223–225 (1993).

[Metz 94] G. Metz, X. Wu, S. O. Smith. Ramped-Amplitude Cross Polarization in Magic-Angle-Spinning NMR. *J. Magn. Reson. A* **110**, 219–227 (1994).

[Mogck 96a] Oliver Mogck, Volker Böhmer, Walter Vogt. Hydrogen bonded homo- and heterodimers of tetra urea derivatives of calix[4]arenes . *Tetrahedron* **52**, 8489–8496 (1996).

[Mogck 96b] Oliver Mogck, Erich F. Paulus, Volker Böhmer, Iris Thondorf, Walter Vogt. Hydrogen-bonded dimers of tetraurea calix[4]arenes: unambiguous proof by single crystal X-ray analysis. *Chem. Commun.* **12**, 2523–2534 (1996).

[Moore 97] J. S. Moore. Shape-Persistent Molecular Architectures of Nanoscale Dimension . *Acc. Chem. Res.* **30**, 402–413 (1997).

[Morcombe 05] C. R. Morcombe, E K. Paulson, V. Gaponenko, R. A. Byrd, K. W. Zilm. ^{1}H-^{15}N correlation spectroscopy of nanocrystalline proteins . *J. Biomol. NMR* **31**, 217 (2005).

[Morris 92] Kevin F. Morris, Charles S. Johnson Jr. Diffusion-Ordered Two-dimensional Nuclear Magnetic Resonance Spectroscopy. *J. Am. Chem. Soc.* **114**, 3139–3141 (1992).

[Morris 93] Kevin F. Morris, Jr. Charles S. Johnson. Resolution of Discrete and Continuous Molecular size Distribution by Means of Diffusion-Ordered 2D NMR Spectrosocpy. *J. Am. Chem. Soc.* **115**, 4291–4299 (1993).

[Munowitz 87] M. Munowitz, A. Pines. Principles and Applications of Multiple-Quantum NMR. *Adv. Chem. Phys.* **66**, 1–152 (1987).

[Ok 89] Jong Hoa Ok, Regitze R. Vold, robert L. Vold. Deuterium Nuclear Magnetic Resonance Measurements of Rotation and Libration of Benzene in a Soild-State Cyclamer. *J. Phys. Chem.* **93**, 7618–7624 (1989).

[Okamoto 05] A. Okamoto, K. Tainaka, K.-i, N. I. Saito. Monitoring DNA Structures by Dual Fluorescence of Pyrene Derivatives. *J. Am. Chem. Soc.* **127**, 13128–13129 (2005).

[Ooms 07] Kristopher J. Ooms, Victor V. Terskikh, Roderick E. Wasylishen. Ultrahigh-Field Solid-State ^{59}Co NMR Studeis of $Co(C_2B_9H_{11})_2^-$ and $Co(C_5H_5)_2^+$ Salts. *J. Am. Chem. Soc.* **129**, 6704–6705 (2007).

[Pake 48] G. E. Pake. Nuclear Resonance Absorption in Hydrated Crystals: Fine Structure of the Proton Line. *J. Chem. Phys.* **16**, 327–336 (1948).

[Paulini 05] R. Paulini, K. Müller, F. Diederich. Orthogonal Multipolar Interactions in Structural Chemistry and Biology. *Angew. Chem. Int. Ed.* **44**, 1788–1805 (2005).

[Paulson 03] E K. Paulson, C. R. Morcombe, V. Gaponenko, B. Dancheck, R. A. Byrd, K. W. Zilm. Sensitive High Resolution Inverse Detection NMR Spectroscopy of Proteins in the Solid State. *J. Am. Chem. Soc.* **125**, 15831–15836 (2003).

[Pawsey 03] S. Pawsey, M. McCormick, S. DePaul, R. Graf, Y. S. Lee, L. Reven, H. W. Spiess. ^{1}H Fast MAS NMR Studies of Hydrogen-Bonding Interactions in Self-Assembled Monolayers . *J. Am. Chem. Soc.* **125**, 4174–4184 (2003).

[Percec 02] V. Percec, M. Glodde, T. K. Bera, Y. Miura, I. Shiyanovskaya, K. D. Singer, V. S. K. Balagurusamy, P. A. Heiney, I. Schnell, A. Rapp, H. W. Spiess, S. D. Hudson, H. Duan. Self-organisation of Supramolecular Helical Dendrimers into Complex Electronic Materials. *Nature* **419**, 384–387 (2002).

[Pines 72] A. Pines, W.-K. Rhim, J. S. Waugh. Homogeneous and Inhomogeneous Nuclear Spin Echos in Solids. *J. Magn. Reson.* **6**, 457–465 (1972).

[Pines 73] A. Pines, M. G. Gibby, J. S. Waugh. Proton-enhanced NMR of Dilute Spins in Solids. *J. Chem. Phys.* **59**, 569–590 (1973).

[Powles 63] J. G. Powles, J. H. Strange. Zero Time Resolution Nuclear Magnetic Transients in Solids. *Proc. Phys. Soc. Lond.* **82**, 60 (1963).

[Price 91] WS Price, PW Kuchel. Effect of nonrectangular field gradient pulses in the Stejskal and Tanner (diffusion) pulse sequence. *J. Magn. Reson.* **94**, 133–139 (1991).

[Purcell 46] E. M. Purcell, H. C. Torrey, R. V. Pound. Resonance Absorption by Nuclear Magnetic Moments in Solids. *Phys. Rev.* **69**, 37–38 (1946).

[Rudzevich 05a] Yuliya Rudzevich. *Synthesis and Characterization of Tetraurea Derivatives of Calix[4]arenes*. Dissertation, Universität Mainz (2005).

[Rudzevich 05b] Yuliya Rudzevich, Valentyn Rudzevich, Chulsoon Moon, Ingo Schnell, Karl Fischer, Volker Böhmer. Self-Assembly of Programmed Building Blocks into Structurally Uniform Dendrimers. *J. Am. Chem. Soc.* **127**, 14168–14169 (2005).

[Saalwächter 01a] K. Saalwächter, R. Graf, H. W. Spiess. Recoupled Polarization-Transfer Methods for Solid-State ^{1}H-^{13}C Heteronuclear Correlation in the Limit of Fast MAS. *J. Magn. Reson.* **148**, 398–418 (2001).

[Saalwächter 01b] K. Saalwächter, H. W. Spiess. Heteronuclear ^{1}H-^{13}C Multiple-spin Correlation in Solid-state Nuclear Magnetic Resonance: Combining Rotational-echo Double-resonance Recoupling and Multiple-quantum Spectroscopy. *J. Chem. Phys.* **114**, 5707–5728 (2001).

[Saalwächter 02] K. Saalwächter. Methyl Groups as Local Probes for Polymer Dynamics as Investigated by ^{1}H Double-Quantum Magic-Angle Spinning NMR Spectroscopy. *Chem. Phys. Lett.* **362**, 331–340 (2002).

[Sando 04] S. Sando, H. Abe, E. T. Kool. Quenched Auto-Ligating DNAs: Multicolor Identification of Nucleic Acids at Single Nucleotide Resolution . *J. Am. Chem. Soc.* **126**, 1081–1087 (2004).

[Scarminio 93] I. Scarminio, M. Kubista. Analysis of corrected spectral data. *Anal. Chem.* **65**, 409–416 (1993).

[Schmidt-Rohr 94] K. Schmidt-Rohr, H. W. Spiess. Multidimensional Solid-State NMR and Polymers. Academic Press, London (1994).

[Schnell 01] I. Schnell, H. W. Spiess. ADVANCES IN MAGNETIC RESONANCE High-resolution ^{1}H NMR Spectroscopy in the Solid State: Very Fast Sample Rotation and Multiple-quantum Coherences. *J. Magn. Reson.* **151**, 153–227 (2001).

[Shimizu 95] K. D. Shimizu, *Jr*. J. Rebek. . *Proc. Nat. Acad, Sci.* **92**, 12403–12407 (1995).

[Silva 97] A. P. De Silva, H. Q. N. Gunaratne, T. Gunnlaugsson, A. J. M. Huxley, C. P. McCoy, J. T. Rademacher, T. E. Rice. Signaling Recognition Events with Fluorescent Sensors and Switches . *Chem. Rev.* **97**, 1515–1566 (1997).

[Slichter 96] C. P. Slichter. Principles of Magnetic Resonance. Springer-Verlag, Berlin (1996).

[Spiess 69] H. W. Spiess, H. Haas, H. Hartmann. Anisotropic Chemical Shifts in Coblat (III) Complexes. *J. Chem. Phys.* **50**, 3057–3064 (1969).

[Spiess 77] H. W. Spiess, U. Haeberlen, H. Zimmermann. ^{1}H Multiple-pulse study of a single crystal of trans-diiodoethylene: Example of self-decoupling . *J. Magn. Reson.* **25**, 55–66 (1977).

[Spiess 81] H. W. Spiess, H. Sillescu. Solid Echoes in the Slow-Motion Region. *J. Magn. Res.* **42**, 381–389 (1981).

[Staab 88] H. A. Staab, T. Saupe. "Proton Sponges" and the Geometry of Hydrogen Bonds: Aromatic Nitrogen Bases with Exceptional Basicities . *Angew. Chem. Int. Ed.* **27**, 865–879 (1988).

[Steed 00] Jonathan W. Steed, Jerry L. Atwood. Supramolecular Chemistry. Wiley, West Sussex (2000).

[Stejskal 65] O. E. Stejskal, J. E. Tanner. Spin Diffusion Measurements: Spin Echoes in the Presence of a Time-Dependent Field Gradient . *J. Chem. Phys.* **42**, 288–292 (1965).

[Stilbs 87] Peter Stilbs. Fourier transform pulsed-gradient spin-echo studies of molecular diffusion. *Prog. Nucl. Magn. Reson. Spectrosc.* **19**, 1–45 (1987).

[Stilbs 96] Peter Stilbs, K. Paulsen, Griffiths PC. Global least-squares analysis of large, correlated spectral data sets: Application to compoenent-resolved FT-PGSE NMR spectroscopy. *J. Phys. Chem.* **100**, 8180–8189 (1996).

[Tanner 70] J.E. Tanner. Use of the Stimulated Echo in NMR Diffusion Studies. *J. Chem. Phys.* **52**, 2523–2526 (1970).

[Thompson 05] K. C. Thompson, N. Miyake. Properties of a New Fluorescent Cytosine Analogue, Pyrrolocytosine . *J. Phys. Chem. B* **109**, 6012–6019 (2005).

[Torrey 56] C. Torrey. Bloch Equations with Diffusion Terms. *Phys. Rev.* **104**, 563–565 (1956).

[Vicens 91] J. Vicens, V. Böhmer. Calixarenes: A Versatile Class of Macrocyclic Compounds. Kluwer Academic, Dordrecht (1991).

[Vinogradov 99] E. Vinogradov, P. K. Madhu, S. Vega. High-resolution proton solid-state NMR spectroscopy by phase-modulated Lee-Goldburg experiment. *Chem. Phys. Lett.* **314**, 443–450 (1999).

[Vinogradov 00] E. Vinogradov, P. K. Madhu, S. Vega. A bimodal Floquet analysis of phase-modulated Lee-Goldburg high resolution proton magic angle spinning NMR experiments. *Chem. Phys. Lett.* **329**, 207–214 (2000).

[Voet 72] D. Voet, A. Rich. Barbiturates and adenine derivatives. Molecular structure of a hydrogen-bonded complex . *J. Am. Chem. Soc.* **94**, 5888–5891 (1972).

[Vysotsky 03] M. O. Vysotsky, M. Bolte, I. Thondorf, Volker Böhmer. New Moleccular Topologies by Fourfold Metathesis Reacions within a Hydrogen-Bonded Calix[4]arene Dimer. *Chem.-Eur. J.* **9**, 3375–3382 (2003).

[Waldeck 97] A. Reginald Waldeck, Philip W. Kuchel, Alison J. Lennon, Bogdan E. Chapman. NMR diffusion measurements to characterise membrane transport and solute binding . *Prog. Nucl. Magn. Reson. Spectrosc.* **30**, 39–68 (1997).

[Wasserfallen 05] D. Wasserfallen, I. Fischbach, N. Chebotavera, M. Kastler, W. Pisula, F. Jäckel, M. D. Watson, I. Schnell, J. P. Rabe, H. W. Spiess, K. Müllen. Influence of Hydrogen Bonds on the Supramolecular Order of Hexa-perihexabenzocoronenes . *Adv. Funct. Mater.* **15**, 1585–1594 (2005).

[Waugh 68] J. S. Waugh, L. M. Huber, U. Haeberlen. Approach to High-Resolution NMR in Solids. *Phys. Rev.* **20**, 180 (1968).

[Weitekamp 82] D. P. Weitekamp, J. R. Garbow, A. Pines. Determination of Dipole Coupling Constants Using Heteronuclear Multiple Quantum NMR. *J. Chem. Phys.* **77**, 2870–2883 (1982).

[Wider 94] G. Wider, V. Dötsch, K. Wüthrich. Self-compensating pulsed magnetic-field gradient for short recovery times. *J. Magn. Reson. Ser A* **108**, 255–258 (1994).

[Würthner 03] F. Würthner, S. Yao. Merocyanine Dyes Containing Imide Functional Groups: Synthesis and Studies on Hydrogen Bonding to Melamine Receptors. *J. Org. Chem.* **68**, 8943–8949 (2003).

[Würthner 04] F. Würthner. Perylene bisimide dyes as versatile building blocks for functional supramolecular architectures . *Chem. Comm.* **14**, 1564–1579 (2004).

[Yu 99] L. Yu, H.-J. Schneider. Structural Effects on the Stability of Some Hydrogen-Bonded Complexes with Nucleobases. *Eur. J. Org. Chem.* **7**, 1619–1625 (1999).

[Zhou 06] D. H. Zhou, D. T. Graesser, W. T. Franks, C. M. Rienstra. Sensitivity and resolution in proton solid-state NMR at intermediate deuteration levels: Quantitative linewidth characterization and applications to correlation spectroscopy. *J. Magn. Reson.* **178**, 297–307 (2006).

[Zuccarello 03] F. Zuccarello, G. Buemi, C. Gandolfo, A. Contino. Barbituric and thiobarbituric acids: a conformational and spectroscopic study . *Spectrochim. Acta A* **59**, 139–151 (2003).